

**A study of Pleistocene Lacustrine Sediments at  
the Southern Front of the Tibetan Plateau:  
Dating and Palaeoclimate record**

**Dissertation**

zur Erlangung des Grades eines Doktors der Naturwissenschaften

der Geowissenschaftlichen Fakultät  
der Eberhard-Karls-Universität Tübingen

vorgelegt von  
**Srinivasa Rao Goddu**  
aus Visakhapatnam (India)

2004

Tag der mündlichen Prüfung: **05 - 11 - 2004**

Dekan: **Prof. Dr. Klaus G. Nickel**

1. Berichterstatter: **Prof. Dr. Erwin Appel**

2. Berichterstatter: **Prof. Dr. Jörg Pross**

Dedicated to my parents  
and  
my teachers who taught me up till now

## Acknowledgements

This work was financed by German Science Foundation (DFG) and National Natural Science Foundation of China (NSFC).

First of all I am grateful to Prof. Dr. Erwin Appel for being my supervisor. I thank him for his support and incredible guidance in every step of my research work.

My hearty thanks to Dr. Shouyun Hu and the other Chinese colleagues Wang, S., Yang, X., Li, H., Wu, R., Xia, W., Zhang, Z. of Nanjing Institute of Geography and Limnology, Chinese Academy of Sciences, 73 East Beijing Rd., Nanjing, China, for providing the data set of lake Heqing.

I am thankful to Dr. Yaeko Igarashi, of Hokkaido University, Sapporo, Japan for carrying out pollen analysis on the samples of Kathmandu basin. I am glad of her quick analysis and interpretations.

I thank Dr. Alexander Rocholl and Dr. Rick Oches for dating the samples of Kathmandu section.

I am thankful to the collaborative members of this project (Himlakes) Dr. Nathani Basavaiah, Dr. Gautam Pitamber for their great cooperation in the project especially in the field. I also thank Dr. Binita Phartiyal and Ram Singh for helping me in the fieldwork.

I would like to thank my institute members for their cooperation, comments, and suggestions during my work. Many thanks to Dr. Martin Waldhör for translating my abstract into German. If I would translate, it would have taken one more year to finish my PhD. I thank Andreas Becht for his kindness towards me and helping me with the Reflex program. Thanks to Dr. Peter Dietrich for his suggestions in interpretation of my statistical results. Thanks to Florian Wehland for his suggestions during my work which helped me a lot. Thanks to Ricarda Wagner for reading the first draft of my thesis and finding some errors.

I thank all my teachers who taught me for all these years. I thank my parents, family members and friends for their, love, encouragement and support.

Last but not the least my hearty thanks to Belgin Canbay and my housemates who supported me morally during my presence here in Germany and helped me to regain my normal stage when I was ill.

# Contents

<b>Abstract</b>	1
<b>1 Introduction</b>	6
1.1 Basic background	6
1.1.1 Natural remanent magnetization	6
1.2 Sources of magnetic minerals	7
1.2.1 Natural occurrence	7
1.2.2 Anthropogenic occurrence	8
1.3 Estimation of concentration and grain size	8
1.4 Non-magnetic techniques for analyzing magnetic phases	9
1.5 Present study	9
<b>2. A study of Heqing basin</b>	12
2.1 Geological settings of Heqing basin	12
2.2 Lithology and sampling	12
2.3 Magnetostratigraphy and its orbital tuning	13
2.3.1 Introduction	13
2.3.2 Demagnetization	14
2.3.3 Remanence directions	15
2.3.4 Radiocarbon dating	17
2.3.5 Rock magnetism	17
2.3.6 Milankovitch theory of climate	21
2.3.7 Age calibration	23
2.3.8 Tuned age model	26
2.4 Palaeoclimatic proxies, multivariate statistics and time series analysis	32
2.4.1 Magnetic proxies	32
2.4.2 Non-magnetic proxies	35
2.4.3 Multivariate statistics	37
2.4.4 Time series analysis	43
2.5 Discussion and conclusions	48
<b>3. A study of Kathmandu basin</b>	55
3.1 Geological settings, lithology and sampling of Kathmandu basin	55
3.2 Dating and palaeoclimate at Kathmandu basin	58
3.2.1 Dating	58
3.3 Palaeoclimatic proxies	65
3.3.1 Pollen	65
3.3.2 Total organic carbon	67
3.3.3 Magnetic parameters	68
3.4 Discussion	70
3.5 Conclusions	72
<b>4. General conclusions</b>	73
<b>5. References</b>	75

## Abstract

The rise of the Himalaya and the Tibetan plateau strongly controlled the monsoon system. Lacustrine sediments of long living lakes at the southern margin of the Tibetan plateau are useful archives to study long-term palaeoenvironmental changes with high time resolution. Three sites at the southern hinge of the Tibetan plateau, i.e. Kashmir basin in the west, Kathmandu basin in the central part, and Heqing Basin in the far eastern part were sampled. Detailed studies on Heqing and Kathmandu basins are reported in this thesis. High-resolution magnetostratigraphy, cyclostratigraphy, and AMS radiocarbon dating are integrated to establish an optimum age model for a 168 m long drill core of lacustrine sediments from Heqing Basin, Yunnan Province, southwestern China. A  $^{14}\text{C}$  age of  $51.62 \pm 2.42/-1.85$  kyr BP is obtained at a depth of 7.3 m. Remanent magnetization resides in maghemite and partly magnetite, both showing the same direction. The polarity sequence clearly reveals the Brunhes/Matuyama (B/M) boundary at 141.5 m. The upper boundary of Jaramillo is indicated at 167 m, as well as Blake Event between 16.3 to 17.5 m. Fourier analysis was done on carbonate, magnetic susceptibility and saturation isothermal remanent magnetization (SIRM) in wavelength domain for sliding windows with different window lengths. Almost all spectra within the range of window centers (30-140 m) show a dominant long wavelength, which changes from about 18.5 m in the lower part (>65 m) to about 14.5 m in the upper part (<65 m) of the core. It is assumed that the long wavelength peak represents the 95-kyr Milankovitch cycle (eccentricity). Based on this assumption a wavelength age model is determined using the  $^{14}\text{C}$  age as a tie point. The B/M boundary and Blake Event match very well with this model, but the age of Jaramillo is strongly underestimated. Fourier spectra of sliding windows slightly indicate a drop of the sedimentation rate at the lowermost part of the core. A tuned age model was calculated by cubic spline interpolation using tie points from  $^{14}\text{C}$  dating, magnetostratigraphy ('true' ages of Blake Event, B/M boundary, and Jaramillo), and wavelength model (change in sedimentation rate at 65 m i.e. 15 cm/Kyr above 65 m and 19 cm/Kyr below). With this age model, spectrum of carbonate shows clear Milankovitch cyclicities. Alternative depth to age transfer functions were tested, i.e. a cyclostratigraphic model (using bandpass-filtered carbonate data corresponding to 95 kyr eccentricity cycles) and correlation of carbonate variations to the marine oxygen isotope curve. However non of the approaches lead to a convincing Milankovitch spectrum of whole core carbonate data. According to this result the Heqing core spans almost the complete past 1 Ma (5 to 1,001 ka). Correlation coefficient of sliding windows between susceptibility and carbonate dominantly show negative correlations between 55 m to 155 m and positive for rest of the core. Cluster analysis on selected variables show systematic grouping pattern and confirm the subdivision of the core into three parts, i.e. below about 120m (ca700 ka), 120-65 m and

above 65 m (ca 420 ka). The whole core Fourier spectra of carbonate shows clear Milankovitch cyclicities (95, 41, 23, and 19 kyr), and susceptibility, Anhyseretic Remanent Magnetization (ARM) and SIRM show only Earths eccentricity and obliquity cycles using tuned time series. Localized variations of power within the time series are known using wavelet transform. The highest power is concentrated between 300 – 750 ka. ARM/SIRM ratio represents magnetic mineralogy and also has a strong tie with *Tsuga* (tree pollen). Spectral results as well as a rough correlation of susceptibility and carbonate with the marine oxygen isotope record suggest that the climatic record of this area is tied directly to the global climatic pattern. Pollen data from Heqing indicate alternations between temperate humid and cold-dry climatic conditions, which is typically a regional palaeoclimatic pattern. Maghemite and magnetite dominate the magnetic mineralogy. Maghemite is distributed throughout the whole core, whereas magnetite occurs additionally in samples with higher  $\chi$  in cold dry periods. The magnetic and non-magnetic variations show a strong anomaly at ~ 65 m (corresponding to MIS 11 onset which is ~400 ka) and a change at ~ 55 m indicating a change in depositional system related to a climatic and/or tectonic event.

Katmandu is mainly influenced by the SW India monsoon. A sequence of about 170 m is exposed at the southern part of the basin. The bottom part of the sequence mainly comprises fine-grained sediments whereas gravel beds dominate the upper part. A total of 750 oriented samples were collected all along the accessible sequence in 2 cm<sup>3</sup> plastic boxes with a sampling interval of 10 cm. Additionally 128 samples were collected for pollen analysis with a sampling interval of 50 cm. Magnetostratigraphy was established and four magnetic transitions were observed indicating that the sampled section spans 0.7 to 1.8 Ma. Amino acid dating on a fossil found in one of the intercalated lignite layers yielding an age of ~ 900 ka is in agreement with the magnetostratigraphy. Anisotropy of magnetic susceptibility was measured for 250 samples. The results show good grouping in the bottom part of the section and a scatter in the uppermost part. The lithology and the AMS results indicate a significant change in the depositional system above 50 m depth. Mainly two magnetic components are dominant. One with lower coercivity (identified as magnetite), which is dominant all along the sequence and additionally hematite is associated at layers with lower susceptibility. A rough correlation between pollen and susceptibility is observed. Pollen results show typical regional signal and indicate the coldest driest period at ~ 0.9 Ma.

The Heqing core has revealed interesting new aspects about the palaeoenvironmental evolution in the Indian monsoon region southeast of Tibetan plateau. On the other hand Kathmandu basin overlaps in part with Heqing basin, but the results show clearly the limited use of outcrop studies.

## Zusammenfassung

Das System des Monsoons wurde stark beeinflusst vom Aufstieg des Himalaya und Tibetplateaus. Seen, die am südlichen Rand des Tibetplateaus über längere Zeit hinweg Sedimente aufgenommen haben, stellen nützliche Archive dar, an denen längerfristige Veränderungen der Paläoumwelt mit hoher Auflösung untersucht werden können. An drei Stellen der südlichen Front des Tibetplateaus wurden Proben genommen: Kashmir-Becken im Westen, Kathmandu-Becken im Zentrum und Heqing-Becken im Osten. In der vorliegenden Arbeit werden Untersuchungen an den Heqing und Kathmandu-Becken vorgestellt.

Hochauflösende Magnetostratigraphie, Zyklusstratigraphie und AMS Radiokarbondatierung werden verwendet, um ein optimales Altersmodell für einen 168m langen Bohrkern aus lakustrinen Sedimenten des Heqing-Beckens (Yunnan Province, Südwest-China) zu erarbeiten. In einer Tiefe von 7.3 m ergeben sich  $^{14}\text{C}$ -Alter von  $51.62 \pm 2.42/-1.85$  kyr BP. Die Remanenz in diesem Bereich wird getragen von Maghemit und Magnetit, beide zeigen dabei dieselbe Richtung. Die Polaritätsskala weist mit hoher Sicherheit die Brunhes/Matuyama-Grenze (B/M) bei 141.5 m auf. Die Oberkante von Jaramillo liegt bei 167 m. Ausserdem tritt der Blake Event zwischen 16.3 und 17.5 m auf.

Fourieranalysen wurden angewendet auf Karbonat, magnetische Suszeptibilität und Sättigungs-Isothermale-Remanenz (SIRM) im Wellenlängenbereich, wobei gleitende Fenster mit unterschiedlichen Breiten verwendet wurden. Nahezu alle Spektren innerhalb des Bereiches der Fensterzentren (30-140 m) zeigen eine dominante Wellenlänge, die im unteren Teil (>65 m Tiefe) 18.5 m beträgt und im oberen Teil (<65m) auf 14.5 m abnimmt. Es ist anzunehmen, dass dieser langwelliger Anteil den 95-kyr Milankovitch-Zyklus darstellt (Exzentrizität).

Mit dieser Annahme und der  $^{14}\text{C}$ -Altersreferenz wurde ein Wellenlängen-Alters-Modell entwickelt. Die B/M-Grenze und der Blake Event passen sehr gut dazu, jedoch ergibt sich für das Jaramillo-Alter ein viel zu geringer Wert. Fourierspektren gleitender Fenster weisen leicht auf eine Abnahme der Sedimentationsraten zuunterst im Kern hin. Mittels kubischer Spline-Interpolation liess sich ein angepasstes Altersmodell erstellen, das die  $^{14}\text{C}$ -Datierung, Magnetostratigraphie ('wahre' Alter von Blake Event, B/M-Grenze und Jaramillo) und das Wellenlängenmodell (Veränderung der Sedimentationsrate bei 65m, 15 cm/Kyr oberhalb 65 m und 19 cm/Kyr unterhalb) berücksichtigt.

In diesem Modell zeigen die Karbonatspektren eindeutige Milankovitch-Zyklen. Alternative Tiefen-Alters-Transferfunktionen wurden getestet, u.a. ein zyklusstratigraphisches Modell unter Verwendung bandpassgefilterter Karbonatdaten, die 95 kyr Exzentrizitätszyklen entsprechen, sowie die Korrelation von Karbonatvariationen mit der marinen Sauerstoffisotopenkurve.

Keiner dieser Ansätze führt jedoch zu einem überzeugenden Milankovitch-Spektrum für die Karbonatdaten des gesamten Kerns. Demnach umfasst der Heqing-Kern einen Zeitraum von beinahe 1 Million Jahre (5 bis 1,001 ka). Korrelationskoeffizienten gleitender Fenster zwischen Suszeptibilität und Karbonat weisen überwiegend negative Korrelationen von 55-155 m und positive für den Rest des Kerns. Cluster-Analyse an ausgewählten Variablen ergeben systematische Gruppierungsstrukturen und bestätigen die Unterteilung des Kerns in 3 Abschnitte: unter 120m (ca. 700 ka), 120-65 m und über 65 m (ca. 420 ka). Die Gesamtspektren von Karbonat zeigen dabei klare Milankovitch-Zyklen (95, 41, 23 und 19 ka). Suszeptibilität, Anhysteresische Remanenz und SIRM zeigen nur die Exzentrizität der Erde und Schiefezyklen, wenn angepasste Zeitserien verwendet werden. Lokale Variationen der Potenzen in den Zeitserien werden sichtbar bei der Verwendung einer Wavelet-Transformation.

Die höchsten Potenzen konzentrieren sich bei 300-750 ka. Das ARM/SIRM-Verhältnis zeigt die Magnetomineralogie an und hat ausserdem eine starke Relation zu den Baumpollen, den *Tsuga*. Sowohl die Spektren als auch die insgesamt Korrelation von Suszeptibilität und Karbonat mit der marinen Sauerstoffisotopenkurve weisen darauf hin, dass die dort aufgezeichnete Klimageschichte direkt mit dem globalen Klima in Verbindung steht. Pollen von Heqing zeigen den Wechsel zwischen gemässigt-feuchtem und kalt-trockenem Klima, typischerweise ein regionales Klimamuster. Maghemit und Magnetit dominieren die magnetische Mineralogie. Maghemit kommt im gesamten Kern vor, während Magnetit ausserdem in Proben hoher  $\chi$  und in kalten Abschnitten auftritt. Die magnetischen und nicht-magnetischen Variationen ergeben eine starke Anomalie bei ~ 65 m (entspricht dem Beginn von MIS 11 von ~400 ka) und einen markanten Wechsel bei ~ 55 m, was auf einen Wechsel der Ablagerungsbedingungen aufgrund klimatischer oder tektonischer Ereignisse hinweist.

Katmandu ist hauptsächlich vom SW-Indien-Monsoon beeinflusst. Eine Abfolge von ca. 170 m ist im südlichen Teil des Beckens aufgeschlossen. Im unteren Teil dominieren feinkörnige Sedimente, im oberen Kieslagen. Insgesamt wurden 750 orientierte Proben (2 cm<sup>3</sup> Plastikzylinder, 10 cm Probenabstand) genommen entlang der zugänglichen Abfolge. Weitere 128 Proben im Abstand von 50 cm wurden entnommen für Pollenanalyse. Die Magnetostratigraphie ergibt vier magnetische Übergänge, was einem Altersbereich von 0.7 - 1.8 Ma entspricht. Die Datierung von Aminosäuren an einem Fossil aus einer der Ligniteinschaltungen erbringt übereinstimmend damit ein Alter von ~ 900 ka. Die Anisotropie der magnetischen Suszeptibilität wurde an 250 Proben bestimmt. Die Ergebnisse gruppieren gut im unteren Teil der Abfolge, oben streuen sie jedoch. Lithologie und AMS deuten auf einen signifikanten Wechsel der Ablagerungsverhältnisse über 50 m Tiefe hin. Zwei magnetische Komponenten sind dominierend: Magnetit niedriger Koerzitivkraft, der über die gesamte Abfolge vorherrscht, sowie Hämatit in Schichten

geringerer Suszeptibilität. Zwischen Pollen und Suszeptibilität tritt eine grobe Korrelation auf. Die Pollen zeigen das typische regionale Verhalten mit die kältesten Periode bei ~ 0.9 Ma.

Der Heqing-Bohrkern hat neue, interessante Erkenntnisse über die Entwicklung der Paläoumwelt in der indischen Monsoongegend südöstlich des Tibetplateaus geliefert. Das Kathmandu-Becken hingegen überlappt zwar teilweise mit dem Heqing-Becken, aber die Ergebnisse zeigen klar den begrenzten Nutzen von Aufschlussstudien.

# 1. Introduction

## 1.1 Basic magnetic background

Magnetic properties can be used as a proxy for several environmental processes as they are quite sensitive to grain size variations, concentration and composition (Verosub and Roberts, 1995; Thompson and Oldfield, 1986). Rock magnetic measurements are relatively fast, non-destructive, cheap and can be performed on bulk samples. They have been extensively used in palaeoclimatic and environmental pollution monitoring studies for the last two decades. The basic principles of palaeomagnetism and the origin of magnetic minerals will be first discussed briefly as well as parameters to deduce the magnetic grain size, mineral composition and concentration.

### 1.1.1 Natural remanent magnetization (NRM)

Iron oxides are abundant in almost all rocks. These magnetic minerals can carry a permanent magnetic moment, which is termed as natural remanent magnetization (NRM). Primary remanent magnetization is acquired during the rock formation, which depends on the local geomagnetic field and geological processes. Over geological time the rock may acquire new remanence components, which are added to the existing NRM, referred as secondary remanent component. The secondary remanence alters the primary NRM partially or completely. The sum of primary and secondary components gives the total NRM. The primary remanence plays the central role for palaeomagnetic investigations. The main types of remanent magnetization are 1) thermoremanent magnetization, acquired during cooling from above the Curie temperature in the presence of a magnetic field 2) chemical remanent magnetization, formed by alteration or new formation of ferro(i)magnetic grains below their Curie temperatures and 3) detrital remanent magnetization, acquired during accumulation of sedimentary rocks containing detrital ferro(i)magnetic particles. The primary component can be resolved from total NRM by stepwise demagnetizing of the sample using either increasing alternating field (AF demagnetization) or increasing temperatures (thermal demagnetization) in a magnetic field free space. The distribution of magnetic grains in a sample should be ideally isotropic and the primary magnetization must have long relaxation times in order to record a faithful directional record. Changes in magnetic field with time tend the magnetic grains to align in the new field. The tendency of the magnetic grains aligning to new magnetic field depends on the height of energy barrier. When the process of new alignment occurs in short period they are said to have short relaxation (order of seconds to days) and when the alignment

process occurs slowly or is negligible with respect to geological time scale, the relaxation time is said to be long (could be in the order of age of the Earth). After removal of the magnetizing field the magnetic remanence  $M_r$  decrease exponentially with time i.e.  $M_r(t) = M_r(t_0)e^{-t/\tau}$  where  $\tau$  is the characteristic relaxation time after which  $M_r = M_r(t_0)/e$ . Louis Néel showed that for SD grains the characteristic relaxation time is given by equation

$$\tau = \frac{1}{C} \exp\left(\frac{\mu_0 v h_c M_s}{2kT}\right)$$

Where  $C$  is the frequency factor  $\sim 10^{-8} \text{ s}^{-1}$  (means how quickly the atomic spins can reorient within magnetic material).  $\mu_0, v, h_c, M_s$  are free-space permeability, volume, microscopic coercivity and saturation magnetization,  $k$  is Boltzmann constant and  $T$  is absolute temperature.  $\mu_0 v h_c M_s$  is referred to the energy barrier and  $kT$  is the thermal energy. Relaxation times and magnetic properties steadily change as a function of domain structures. There are four basic types of structures (domain states). The smallest grains with shortest relaxation times ( $\tau < \sim 150 \text{ s}$ ) are superparamagnetic grains. Slightly bigger grains are called single domain (SD). The SD range for magnetite is  $\sim 0.03$  to  $0.5 \mu\text{m}$  for spherical shape and can be bigger for elongated particles. Still larger grains, which contain few domains are called pseudo-single domain (PSD). They are called so because their magnetic properties resemble SD grains. For magnetite the upper threshold of PSD grains is  $\sim 10 \mu\text{m}$ . The largest grains ( $> \sim 10 \mu\text{m}$  for magnetite) are said to be multidomain (MD). The domain state of grains mainly depend on the size of the magnetic particle and its composition. SD grains have extremely high relaxation times (in order of the age of the Earth). The relaxation time decreases with increase of grain size from PSD to MD) grain sizes. The SP grains have the lowest relaxation times. The above-mentioned equation is valid for SP and SD grains.

## 1.2 Sources of magnetic minerals

### 1.2.1. Natural occurrence

There are several ways that magnetic particles occur in rocks. In igneous rocks the magnetic minerals are crystallized from lavas. In sediments the magnetic material stems from several sources. Metamorphic rocks contain initial and newly formed magnetic minerals.

Detrital particles are physically and/or chemically eroded and transported to the depositional site. Some diagenetic process take place during or shortly after deposition. Bacteria and intercellular magnetosomes that use iron in their metabolism and poor

crystalline magnetite are known to occur outside of the cell referred as extracellular magnetite (Biogenic particles). Authigenic particles, which are formed in-situ due to chemical processes. Iron sulfides are known to be the most commonly occurring in this process.

### **1.2.2. Anthropogenic occurrence**

The increase of industries especially during the last four decades has produced considerable amount of environmental pollution. Especially the iron bearing processes are mainly responsible for input of magnetic particles into environment. Especially magnetite containing spherules are the most common constituents in fly ash and bottom ash, which result from combustion of coal and oil. Road and rail transport also play a role in input of magnetic particles (mainly by abrasion) into the environment. The magnetic properties of anthropogenic origin differ from the ones of natural origin (Oldfield et al., 1985).

## **1.3 Estimation of concentration and grain-size**

The different process and origins of magnetic particles has an influence on the magnetic concentration, particle-size distribution and mineralogy of the magnetic component. The rock magnetic parameters (such as susceptibility ( $\chi$ ), anhysteretic remanent magnetization (ARM), saturation isothermal remanent magnetization (SIRM), isothermal remanent magnetization (IRM), saturation magnetization ( $M_s$ )) and their ratios can be used to characterize the magnetic components of sediments and soils.

Rock magnetic parameters,  $\chi$ , ARM, SIRM and  $M_s$  indicate mainly magnetic concentration. They increase with increasing magnetic concentration and are also dependent on magnetic mineralogy. ARM and SIRM are grain size dependent and they show an increase in presence of higher proportion of fine grain (single domain) magnetic particles.  $\chi$  is also dependent on grain sizes; it is dominant in presence of larger and very fine grain sizes (multi-domain and superparamagnetic).  $M_s$  is independent of grain sizes and show maximum values for magnetite and maghemite. SIRM shows relatively low values in presence of lower magnetization minerals (e.g. hematite). Especially in sediments, the remanence bearing minerals occur in low proportions and the para and diamagnetic components can extensively control  $\chi$ . In this case the laboratory induced remanences ARM and SIRM would be extensively useful to determine concentration of ferro(i)magnetic phases.

The interparameter ratios ARM/ $\chi$  and ARM/SIRM signify primarily the grain size variations and are also dependent on magnetic mineral content. These ratios vary inversely with

magnetic grain size. Both ratios primarily reflect the presence of finer grain sizes (single domain) and also can be used to detect the relative changes in concentration of finer magnetic grain sizes. The S-ratio ( $-IRM/SIRM$ ) and HIRM ( $(-IRM+SIRM)/2$ ) indicate the concentration of hard magnetic phase. Values of S ratio close to 1 indicate softer magnetic components and lower values indicate higher concentrations of harder components like hematite and goethite. Values of HIRM are proportional to the content of high coercivity minerals (hematite and goethite).

## **1.4 Non-magnetic techniques for analyzing magnetic phases**

Mineral magnetic changes depend on different climatic processes. Identifying magnetic mineralogy is of primary importance for any palaeoclimatic interpretation. Apart from the identification of mineralogy through magnetic techniques, it is always necessary to substantiate them using independent analysis. To examine the magnetic minerals, they need to be extracted from the bulk samples and analyzed by standard methods like Mößbauer spectroscopy, X-ray diffraction (XRD), scanning electron microscopy (SEM) and transmission electron microscopy (TEM). However, these analyses are strongly influenced by strongly magnetic minerals as they are more inclined to be separated during extraction from the soils or sediment matrix.

The rock magnetic parameters are ambiguous and do not represent a palaeoclimatic proxy per se. The magnetic variations are to be verified with other direct palaeoclimatic proxies like pollen, carbonate, Total organic carbon (TOC), etc. Once they are verified for a certain case (e.g. a lake) they can be used as a tool for high resolution studies of palaeoclimatic changes.

## **1.5 Present study**

The study of the past climate gives awareness of the natural climatic fluctuations and is a key to understand the present climatic changes due to human impact. During the past few decades a good amount of work has been carried out for both continental and marine environments. In the continental realm loess-palaeosol sequences, ice cores, tree rings and lake sediments were investigated. However the distribution of ice cores and loess is limited and tree rings provide only short-term climatic fluctuations.

Lakes are quite sensitive to climatic variations and have an advantage of high rates of sedimentation, continuous deposition, and wide distribution. These favorable factors serve as the initial impetus for environmental magnetism studies (Oldfield, 1991). Excellent correlation of palaeoclimatic records obtained from lacustrine sequences and marine sediments, loess and ice cores demonstrate that the lakes could provide invaluable information of global climatic changes. The studies of Williams et al. (1997) from lake Baikal show that the lake has responded to orbital insolation during the last five million years. Thouveny et al., (1994) obtained a 140,000 years palaeoclimatic record using magnetic parameters, pollen and total organic carbon from maar sediments in France. Magnetic variations of the lake show good correlation with ice cores from Greenland demonstrating that magnetic parameters are reliable proxies of palaeoclimatic changes.

It is hypothesized that the uplift of the Himalaya and Tibetan plateau (HTP) gave rise to monsoon climate in Asia and resulted in the global cooling during late Cenozoic (Ruddimann and Kutzbach, 1989, Prell and Kutzbach, 1992, Prell et al., 1992; Ruddiman, 1997, Hahn and Manabe, 1975). The mineralogic and biologic evidences suggest that the rate of upliftment of Himalayas and Tibetan Plateau increased substantially since early Pliocene. Radiometric ages of siwalik formation and other molasses deposits along the southern margin of the Himalayan range indicate that progressively faster rates of uplift, erosion and sedimentation have occurred during this interval (Saini et al., 1979, Burbank and Johnson, 1983). Pollen studies indicate that, over the past 5 Ma the uplift rates were twice the rates as those of previous (Hsu, 1978). This drastic upliftment during Plio-Pleistocene might have played a major role in strengthening of the Asian monsoon (Ruddiman, 1997, Kukla and Clerk 1996). It is also hypothesized that uplift of HTP and the consequent increase in chemical weathering rate was the cause of Cenozoic global cooling through a decrease of atmospheric CO<sub>2</sub> (Raymo et al., 1988, Raymo, 1991). Higher CO<sub>2</sub> levels might indicate strengthening of monsoon through increased land-sea temperature contrasts. Superposed on the tectonic and CO<sub>2</sub> trends are orbitally induced periodic variations of solar radiation over the Earth's surface. All the variance in the distribution of solar radiation is associated with obliquity and precession parameters alone (Hays, et al., 1976, Berger, 1978, Ruddiman et al 1986) and can change in order of +/- 12.5% (Laskar et al., 1993; Berger and Loutre, 1991). The variations of monsoon indicators (sea surface temperatures, upwelling fauna, dust grain size, and vegetation types) at Indian Ocean and western Pacific (monsoon indicators) vary coherently with these orbital periodicities i.e. strong coherence with precession and moderate coherence with obliquity (Clemens and Prell, 1990, 1991a, 1991b; Clemens et al., 1991, 1996; Prell, 1984a, 1984b; Bloemendal and Menocal, 1989, Morley and Heusser, 1997; Schultz et al., 1998). However these variations are not always in phase with the solar radiation. These phase differences influence the timing and amplitude of the monsoon.

The modern Asian monsoon is driven by two major heat sources, i.e. sensible heating of the Asian land mass and the latent heating within the troposphere over the Asian plateau. The latent heat source originates from the moisture collected from the southern sub-tropics of Indian Ocean, carried through the equator and released during precipitation over Asia. Both these heat mechanisms contribute to the land-sea temperature contrast and pressure differences that ultimately drive the summer monsoon circulation (Fig. 1.1). Recent studies point to the southern subtropical Indian ocean as the source of 70% of the latent heat released over the Asian plateau during summer monsoon (Cadet, 1981a, 1981b, Hastenrath, 1985).

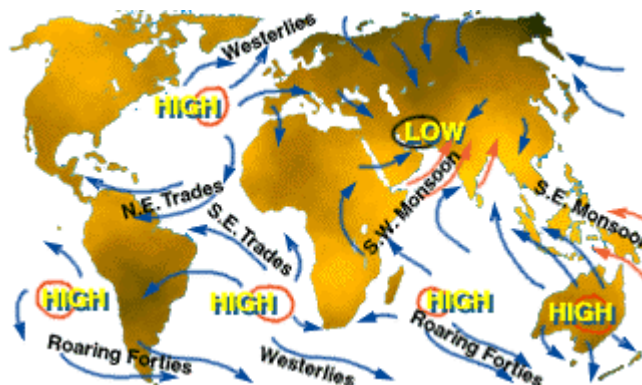


**Fig. 1.1 Global monsoon system. Source:**  
<http://snrs.unl.edu/amet351/ogren/monsoons.html>

Despite of several advances in climatic studies, the long-term evolution of Asian climate is not well understood due to lack of proper dating resolution in most Asian records. In addition, strong influence of the Himalayas and the Tibetan plateau at various times added more complexity. At SE Tibetan plateau and south of Chinese loess plateau very few palaeoclimatic records are obtained up till now. In order to understand the regional palaeoclimatic change and its relationship to global change, three long living lake sediment deposits Kashmir basin (India), Kathmandu basin (Central Nepal) and Heqing basin (SW China) at the southern hinge of the Tibetan plateau were chosen for our study. An age frame was established for Heqing and Kathmandu lacustrine sections using mainly magnetostratigraphy in combination with other absolute dating methods. Palaeoclimatic reconstruction was done based on rock magnetic proxies combined with non-magnetic proxies, such as pollen contents, carbonate records, total organic carbon etc. As the records of Heqing basin were continuous they were further used for multivariate statistics and time series analysis. For both lakes, palaeoenvironmental changes and tectonic (uplift?) phases are discussed respectively.

## 2. A study on Heqing basin

### 2.1 Geological Settings of Heqing basin

Heqing Basin (100°06'-100°29' E, 25°51' -26°46' N) is situated in northwestern Heqing County, Yunnan Province, China (Fig. 2.1). The basin is located at the southeastern margin of the Tibetan Plateau, and its structure is controlled by a nearly north-south striking fault. Limestone and partly granite are exposed in the surrounding mountains which are the main detrital sources of the lake (Yang et al., 2000). Since the late Cenozoic, a 700 m thick sedimentary sequence (unpublished geophysical data from exploration industry) has been deposited in the basin, and this sequence serves, in principle, as a potential archive of palaeoclimatic history. In 1997, Core HQ with a length of 168 m was recovered from the center of the ancient lake.

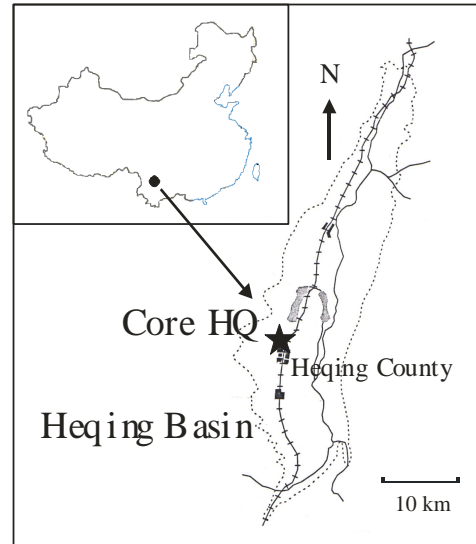


**Fig. 2.1** Location of Heqing basin (solid circle in the inset upper figure). The star in the center of the basin shows the position of the Heqing core.

### 2.2 Lithology and sampling

Initially drilling was done only up to the depth of 110 m and later it was continued up to 168 m from the same borehole. The complete core was recovered mainly comprising of fine-grained lacustrine sediments with only slight color changes downcore. Lithologically the core can be divided into four units:

1. 0-4 m, green-grey mud containing charcoal fragments; Above 2.2 m, sediments gradually change to brown-yellow, yellow mud;
2. 4-78 m, mainly dark grey, grey-green and green-grey mud;
3. 78-135 m, mainly blue-grey, grey and grey-green mud;
4. 135-168 m, mainly grey-green, green-grey and grey mud.

The core was divided into 10 cm cores for transportation. 1656 palaeomagnetic samples (cubic shape 2 x 2 x 2 cm) were collected at a sampling interval of about 10 cm. Also, 1096 samples were taken for carbonate analysis, and 769 samples for pollen and spores studies.

## 2.3 Magnetostratigraphy and its orbital tuning

### 2.3.1 Introduction

Magnetic stratigraphy was initially used to organize young igneous rock strata based on stratigraphic intervals and similar magnetic characteristics. It was consecutively developed and was extended to older geomagnetic polarity time scales using sedimentary environments. The magnetic characteristic most often used is the polarity of magnetic remanence. The pattern of polarity zones is determined by measuring the magnetic remanence vectors of samples taken from the stratigraphic section. The polarity is said to be normal when the north seeking magnetization gives the northern hemisphere pole (as today) and reverse when the north seeking magnetization gives the southern hemisphere pole. The systematic change in geomagnetic polarity along long sequences has set a fundamental application of dating. Studies have shown that the oceanic crustal record only goes back to the late Callovian (latest Middle Jurassic) anywhere on Earth (Ogg, 1995), whereas the older polarity time scales are confined to volcanic and sedimentary sequences on land. The magnetostratigraphic studies on land have proven that they are accurate and resolved some of the short polarity events, which were not clear in marine sequences (Lowrie et al., 1980b). Recent studies of Cande and Kent (1995) have given a more detailed polarity timescale of the last 120 million years which intensified the precision of geomagnetic polarity dating.

In sediments the primary remanence is acquired by alignment of ferro(i)magnetic particles in the ambient magnetic field during or shortly after the deposition, termed as depositional or post depositional remanence magnetization (pDRM). The recording is efficient in calm environment depositional systems particularly in fine-grained homogenous sediments. However the exact mechanism of remanence acquisition process is still not completely understood (Kent, 1973, Verosub, 1977). Resolving the primary remanence (remanence acquired during deposition) along the stratigraphy is the fundamental requirement of magnetostratigraphy. Enormous amount of magnetostratigraphy work was done on Quaternary deposits and their dates were well established around the globe.

Lacustrine sediments are a suitable archive for records of palaeoenvironmental changes on different time scales (e.g. Thouveny et al., 1994; Williams et al., 1997; Wang et al., 1999). A reliable and accurate age frame is a fundamental requirement for any such interpretation. Radiocarbon dating provides a powerful tool for periods younger than about 60 ka. Beyond the range of  $^{14}\text{C}$  lifetime absolute dating methods are very limited.

Magnetostratigraphy has been particularly successful for long sequences (e.g. Kashmir basin; Burbank and Johnson, 1982).

### 2.3.2 Demagnetization

In sedimentary rocks fine ferrimagnetic magnetic particles in the SD and PSD have relatively strong and stable magnetization and align efficiently along the geomagnetic field

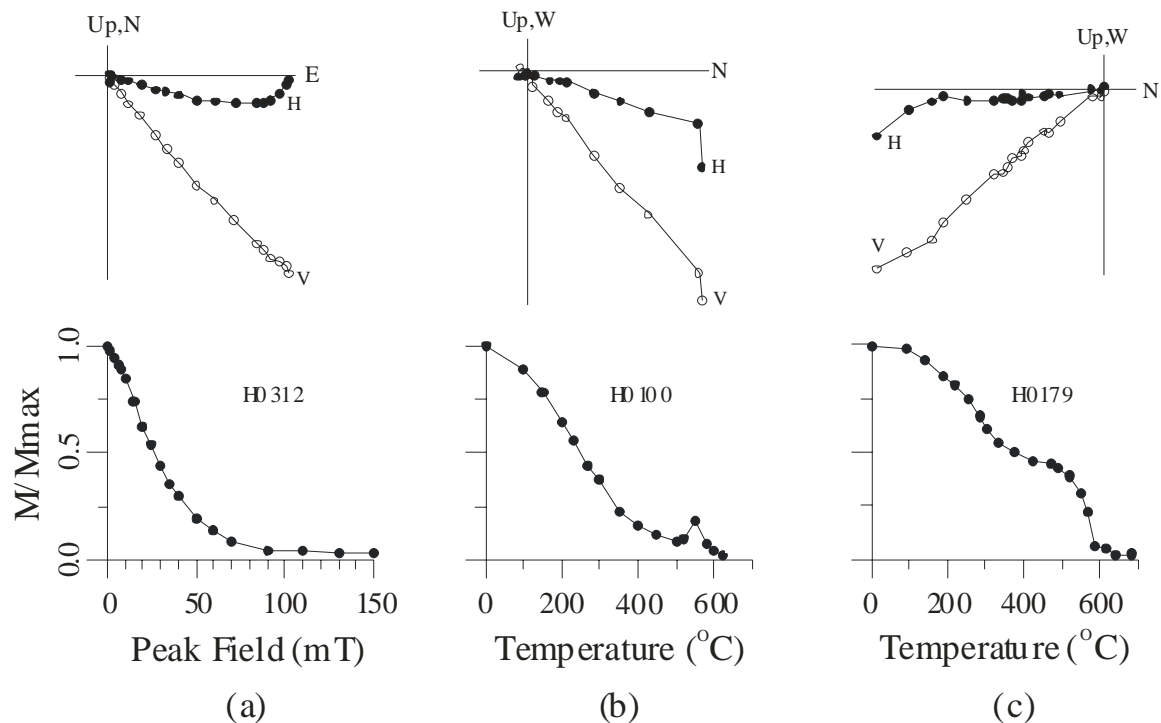


**Fig 2.2 Demagnetization behavior of representative samples. (a) Stepwise AF demagnetization showing a predominance of soft remanence components. (b,c) Stepwise thermal demagnetization of representative samples with only LTC (b) and LTC+HTC (c). Data provided by Hu. S**

carrying the Characteristic Remanent Magnetization (ChRM). The larger MD grains have low intensity of magnetization and they tend to attain the present geomagnetic field, which is a secondary remanence. To isolate the ChRM, demagnetization experiments alternating field demagnetization (AF) and thermal demagnetization were carried out.

AF demagnetization discriminates in between higher and lower coercive phases which can be either related to SD/PSD - MD particles or different magnetomineralogy. Because of instrumental limitation where maximum fields of 200 mT can be applied Usually MD grains have low coercivity and SD and PSD grains have higher coercivity, thus it is capable of

removing the soft magnetic component which is carried by lower coercive grains leaving the ChRM unaffected.

Pilot samples were chosen for stepwise AF demagnetization (98 samples) and thermal demagnetization (90 samples) based on criteria of lithology and color. Remanence measurements were made with a 2G SQUID magnetometer. AF demagnetization was carried out in a 2G degausser attached to the magnetometer, while for thermal demagnetization a MMTD18 furnace was used. Susceptibility was measured using a Bartington MS2B instrument. All demagnetization and susceptibility measurements were conducted in the palaeomagnetic laboratory at Tübingen University, Germany.

AF demagnetization for pilot samples were conducted with 2 mT interval up to 10 mT, 5 mT up to 30 mT, 10 mT up to 60 mT and later with 20 mT up to 140 mT (sometimes even 150 mT field was also applied). The decay curve shows a two-component behaviour from orthogonal vector projections. The intensity of NRM was reduced to less than 10% by a field of 60 mT. The median destructive field (MDF) is about 25 mT, which indicates that a relatively soft magnetic component is predominant in the samples. After a softer component was removed at around 10 mT, the demagnetization paths show an univectorial behaviour pointing towards the origin. A typical AF demagnetization behaviour can be seen in Figure 2.2a. The ChRM was revealed between 10 mT to 60 mT demagnetization steps.

When the secondary remanence is carried by harder component, it cannot be erased by AF demagnetization as their coercive force can easily exceed the maximum available AF field. This property is common in hematite bearing rocks. To overcome this the only alternative and efficient method is thermal demagnetization. Moreover thermal demagnetization is believed to separate the remanences better and it can give the picture of remanence carrying mineral.

Pilot samples were subjected to detailed stepwise thermal demagnetization. After every heating step magnetic susceptibility was monitored to detect possible mineral alterations during heating. The demagnetization curves are quite smooth and reveal two types of behaviour. For the first type, remanence intensity decreases mainly between 100-400 °C (Fig. 2.2b). In the following we call this component the low temperature component (LTC). For the second type, another component (HTC) with higher unblocking temperature close to the Curie temperature of magnetite (about 580 °C) appears in addition to the LTC (Fig. 2.2c). Within the second type of samples, both magnetic minerals were deposited and/or were authigenically produced at (nearly) the same time as they show almost the same characteristic remanent magnetization (ChRM) directions.

Both methods, AF and thermal demagnetization, effectively reveal the ChRM. For the pilot samples, remanence components after AF cleaning of the soft component and after heating above 200 °C show similar directions. However, since stepwise AF demagnetization is less time-consuming, and more suitable for fragile samples, it was used for demagnetization of the bulk of samples.

### 2.3.3 Remanence directions

Magnetostratigraphy is based only on magnetic inclination data, because the core lacks azimuthal orientation. The drill cores were cut into pieces of a few 10 cm length for transportation; therefore, it is not possible to use declination data. Also anisotropy of magnetic susceptibility (AMS) does not allow to fit different core parts because AMS shows a sedimentary fabric (minimum axis perpendicular to the bedding plane and randomly distributed maximum and intermediate axes).

Magnetic inclination is plotted against their stratigraphic position in Figure 2.3. The Brunhes Chron is clearly indicated by predominantly positive inclinations from the top core down to 141.5 m depth. There are some negative inclinations within the Brunhes Chron, based on at least

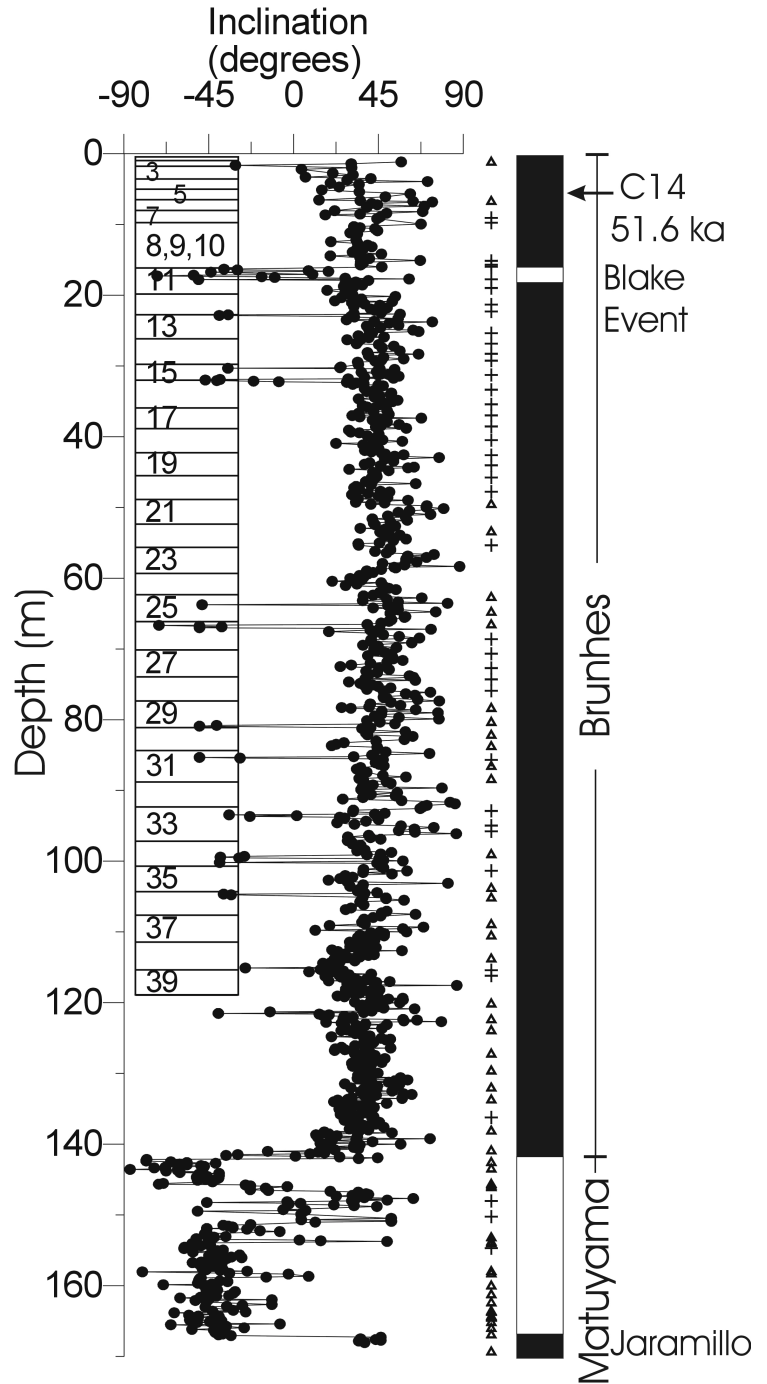


Fig. 2.3 Results of magnetostratigraphy (inclination) with interpreted polarity sequence. Position of the sample giving a radiocarbon age is marked. Samples analysed in more detail for magnetic mineralogy are indicated: ( $\Delta$ : maghemite only; +: maghemite and magnetite). Drilling turns (above 120 m) are plotted next to the depth scale. The results are provided by S.Hu.

3 consecutive samples with negative inclinations i.e. around depths of 16.3-17.5 m, 31.9-32.2 m, 66.7-67.0 m and 99.3-99.5 m. Without a better age control it is difficult to decide whether or not these may represent geomagnetic excursions during the Brunhes Chron. It is found that many such negative inclinations are located at either the top or/and the bottom of drilling turns, such as turns 13, 15, 25, 30, 32, 34, 40 (Fig. 2.3) and therefore could be artifacts caused by the drilling process.

One possible excursion may exist between 16.3-17.5 m defined by 11 successive samples (8 with negative and 3 with shallow positive inclinations). Although this part is close to the top of turn 11, it seems to be unlikely that so many samples are affected by the drilling process.

Indication that this represents a record of the Blake Event comes from interpolation of the  $^{14}\text{C}$ -age and B/M boundary. In the upper Matuyama Chron, at 146-151 m, samples with positive and intermediate inclinations frequently appear. They are related to high susceptibility values and may be artifacts of the recording process rather than a record of geomagnetic field behaviour (Verosub and Banerjee, 1977; Hu et al., 1999). At the bottom of the core, eight consecutive samples also show positive inclinations. This could represent the top of the Jaramillo Subchron.

### **2.3.4 Radiocarbon dating**

The  $^{14}\text{C}$  measurements by means of accelerator mass spectrometry have been carried out at the Leibniz Labor für Altersbestimmung und Isotopenforschung of the Christian-Albrechts-Universität in Kiel. The samples analysed were snail shells taken from a drill core. In order to increase the accuracy of the data, a correction for possible "matrix effects" was performed by concurrent analysis of a "dead" (i.e. no life  $^{14}\text{C}$  present) reference snail shell (sample # 208, 24.45 m depth). Sample 63 (7.3 m depth) yielded a radiocarbon age of 51620  $\pm$ 2420/-1850 BP and sample #108 (12.9 m depth) yielded a minimum radiocarbon age of > 51930 BP. These ages are consistent with their relative stratigraphic position within the lake sediment.

### **2.3.5 Rock magnetism**

It is essential to identify the magnetic mineralogy for knowing the mineral carrying remanence. Rock magnetic experiments enable us to understand the geologic, limnologic, climatic and remanence acquisition processes involved during sedimentation. The presence or absence of some minerals can be a good indicator of certain diagenetic

process of environment (Geiss and Banerjee, 1997). However identifying important minerals which are in less concentrations (< 150 ppm) is always a difficult task. Thermal demagnetization of NRM indicates two blocking temperatures and the challenge lies in identifying these remanence-carrying components.

**IRM acquisition and its thermal demagnetization**

The shape of the IRM acquisition curve with increasing magnetizing field is a measure of coercivity spectra of the magnetic minerals present in the sample (Dunlop, 1972). Due to low coercivity of ferrimagnetic magnetite, it is saturated at relatively low magnetic fields

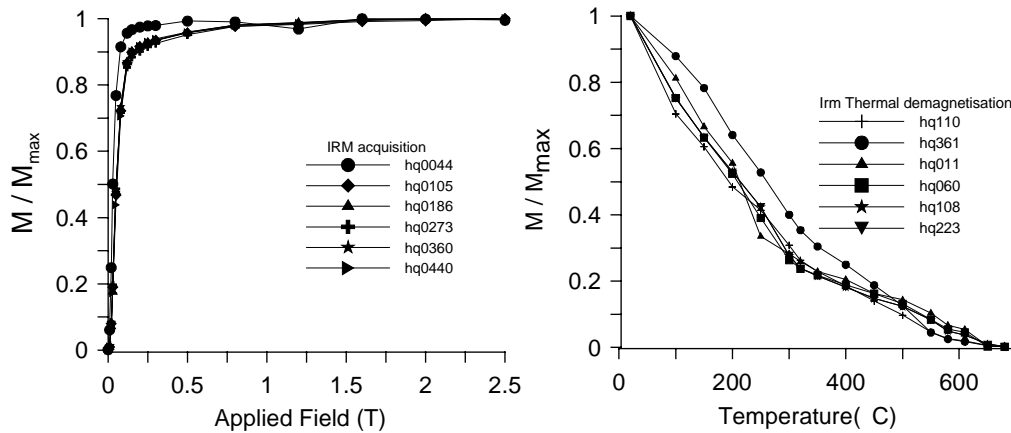


Fig.2.4 Stepwise IRM acquisition and its thermal demagnetization

while weakly antiferrimagnetic hematite is still unsaturated after application of maximum field of 1.5 T. Stepwise IRM acquisition results show 95% of saturation remanence below 300 mT demonstrating that the soft magnetic minerals mainly dominates the magnetic mineralogy (Fig. 2.4). After IRM acquisition the samples were stepwise thermally demagnetized. The results show similar behaviour as the curves of NRM thermal demagnetization, < 5% of the residual remanence remains after 600 °C, which could be an indication for hematite phase (Fig 2.4).

**Thermomagnetic susceptibility measurements**

Thermomagnetic runs of susceptibility were performed (using a CS-3 heating

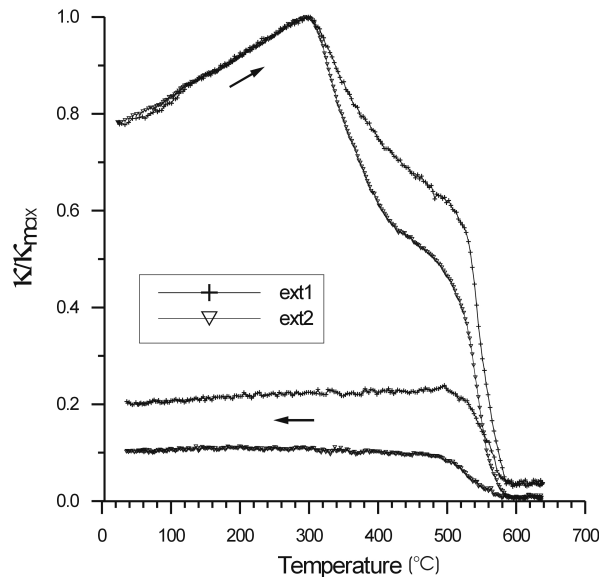
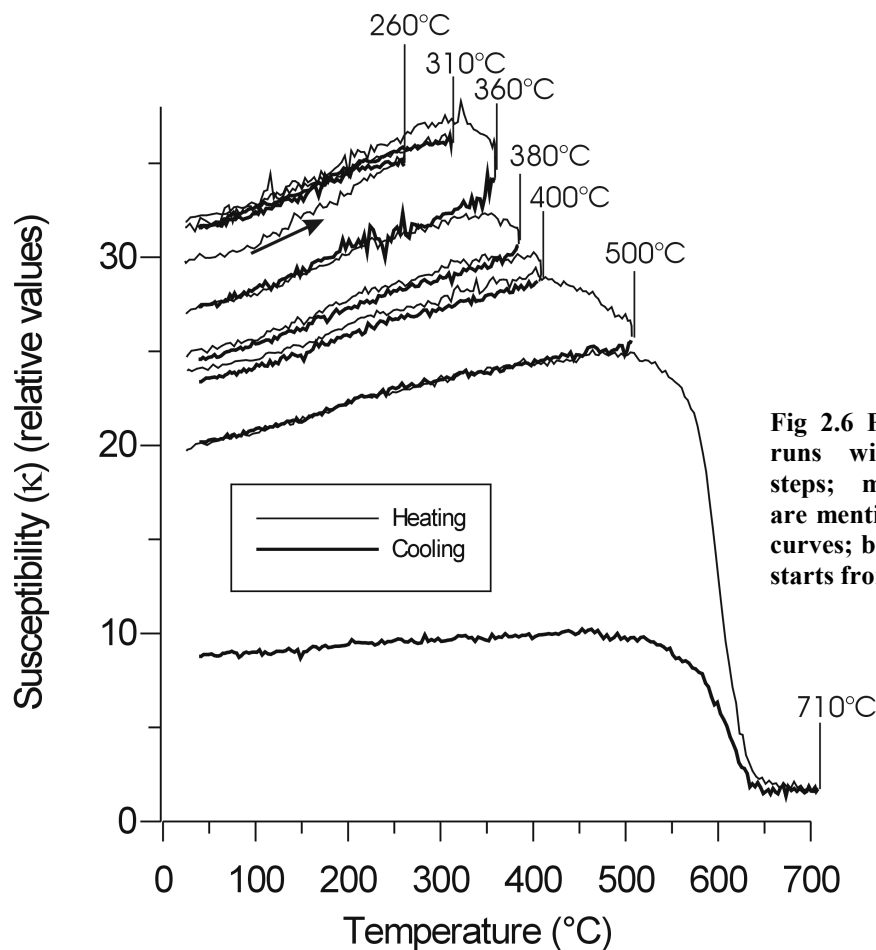


Fig. 2.5 Thermo-magnetic susceptibility runs on magnetic extracts; arrows represent heating and cooling curves.

device attached to a KLY-3 susceptibility bridge). More than 40 samples of raw material, distributed along the whole core, were investigated. However, almost all curves show a sharp magnetic increase above  $\sim 350^{\circ}\text{C}$  due to secondary formation of magnetite and cannot be interpreted in terms of the original magnetic mineralogy. Additionally two magnetic extracts were prepared, a first one (ext1) from samples at depths of 21.69 m and 28.44 m, representing the upper part of the core, and a second one (ext2) from samples at depths of 135.35 m and 146.44 m, representing sediments with higher susceptibility. Both samples show a similar behaviour (Fig. 2.5). During heating,  $\kappa$  increases steadily towards a peak at about  $300^{\circ}\text{C}$ . At higher temperatures, a decrease is observed up to the Curie temperature of magnetite. A second phase is indicated by deflection of the curves at around  $400^{\circ}\text{C}$ . During cooling, there is only evidence for magnetite. Non-reversibility indicates that the second phase has been destroyed during heating. This let us assume maghemite or greigite to be responsible for the LTC.

### ***Partial Thermomagnetic susceptibility measurements***

To identify the mineral carrying the LTC, two additional magnetic extracts were prepared for partial thermomagnetic runs from samples at depths of 21 m (which show relatively



**Fig 2.6** Partial thermo-magnetic runs with successive heating steps; maximum temperatures are mentioned at their respective curves; breakdown of maghemite starts from  $320^{\circ}\text{C}$ .

lower  $\chi$ ) and 92.2 m (which have relatively higher  $\chi$ ). Both the samples revealed a similar behaviour (Fig. 2.6). No major magnetic mineral magnetic changes occur up to a temperature of 310°C; the slight increase after first heating is likely related to stress release by annealing. After subsequent heating the LTC phase is gradually destroyed from ~320 to ~500°C and probably converted to hematite which is a typical behaviour of maghemite. Greigite can be ruled out because it has a Curie temperature of around 300°C and is usually destroyed below 300°C (Hoffmann, 1992).

### ***X-ray diffraction measurements***

Even though magnetic mineralogy is clearly identified with the magnetic methods, it is common to confirm it by using a straightforward method. Magnetic extracts (used for partial thermomagnetic runs) were prepared for X-Ray diffraction analysis. The extracts were prepared with out any external pressure to avoid mineralogical changes

The diffractogram was collected between 5° to 90° (2 $\theta$ ) with Cu-K  $\alpha$  radiation on a Philips Bragg-Brentano

diffractometer equipped with a secondary

monochromator Only magnetite could be identified. The second ferrimagnetic phase (maghemite) is probably below the detection limit (5%) due to less efficient extraction (Fig. 2.7).

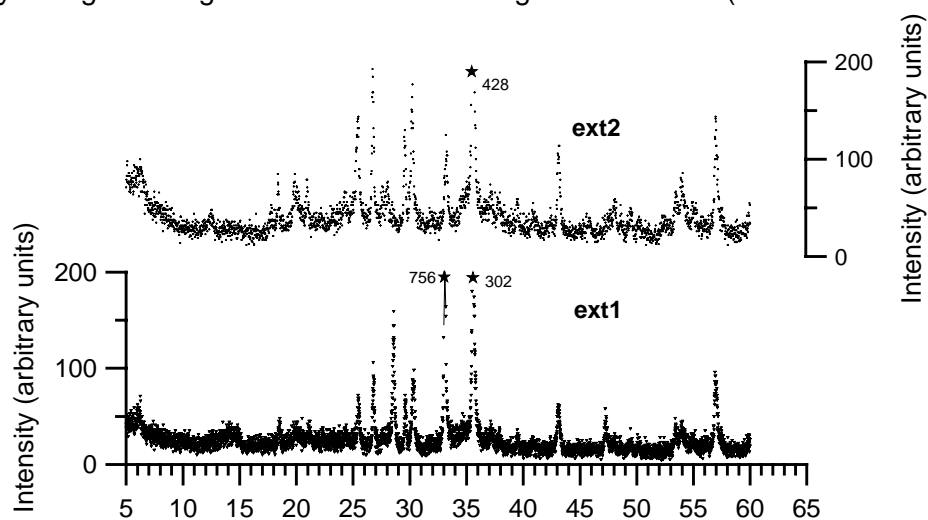


**Fig. 2.7 X-Ray diffraction analysis showing the presence magnetite among other non-magnetic minerals**

### 2.3.6 Milankovitch theory of climate

Adhemar first linked climate to astronomy in 1842. He explained the glacial climate with the Earth's precession. Later in 1875 James Croll approached the problem theoretically taking into account the combined effects of three of the major astronomical factors on seasonal insolation during perihelion and aphelion. He accomplished that the precession of the equinoxes should play a significant role and how effective the precessional wobble in changing the intensity of the seasons. However in 1924 Milutin Milankovitch a Yugoslavian astronomer developed a complete mathematical theory of orbital patterns to be regular and predictable. The complete theory proposes the forcing mechanism of glaciations due to Earth's orbital pattern during revolution. The elements of Earth-Sun geometry combine to produce variations in the amount of solar energy that reaches Earth (Imbrie and Imbrie, 1979). The three main astronomical factors are: eccentricity or changes in shape of the Earth's orbit, obliquity or changes in the tilt of Earth's rotational axis and precession or wobble of the Earth's rotational axis (Fig. 3.7).

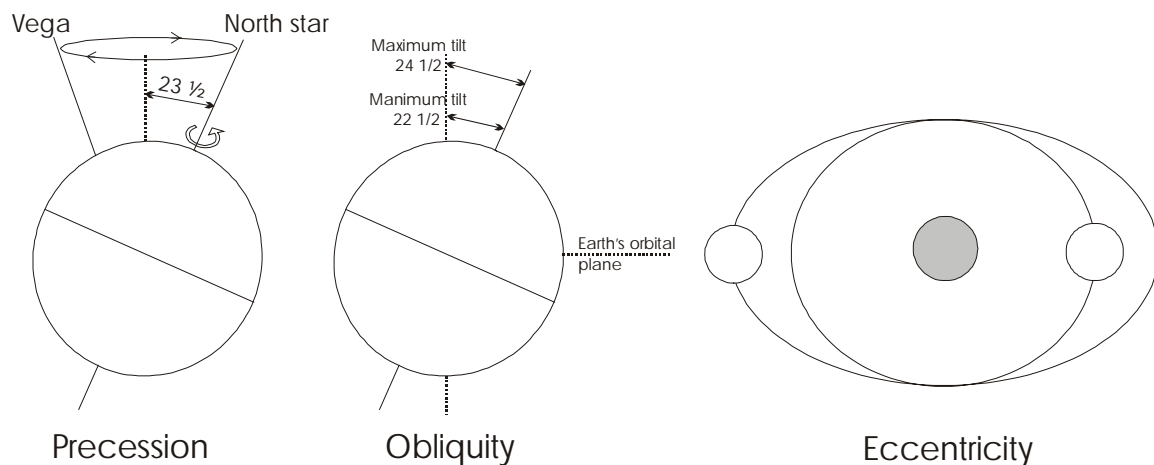


**Fig. 2-8. Schematic representation of the astronomical variables influencing the climate on Earth**

Due to lack of proper correlations and dating techniques, the theory was not accepted for many years. Another reason is that the eccentricity affects mainly in altering the precession cycle, its direct contribution to energy changes is too small ( $<0.1\%$ ) to force large climatic variations like shift from glacial to interglacial events. However during the 1970's a quick development of dating methods and oxygen isotope techniques has brought the Milankovitch hypothesis again into limelight. The pioneering work of Hays et al. (1976) convincingly showed a fit to the estimated astronomical periods from their

oxygen isotope record of deep-sea sediments of Pleistocene. During the recent years the spectral analysis on several ocean and continental drill cores has provided an extensive support to accept the theory. The dominant climatic cycles of particular importance are periods 413 kyr and 95 kyr (eccentricity), 54 kyr and 41 kyr (obliquity), 23 kyr and 19 kyr (precession). The orbital geometry is shown in Figure 2.9. The decrease in Earth-Moon distance and increasing of ellipticity is bound to cause shortening of the periods of obliquity and precession in large geological scales of order >72 Ma. On the other hand the periods of eccentricity have not changed due to this process at any stage (Berger and Loutre, 1994). The theoretical values of Milankovitch periods and ratios of Quaternary period (which is of interest in this study) are shown in Table 1 and 2.

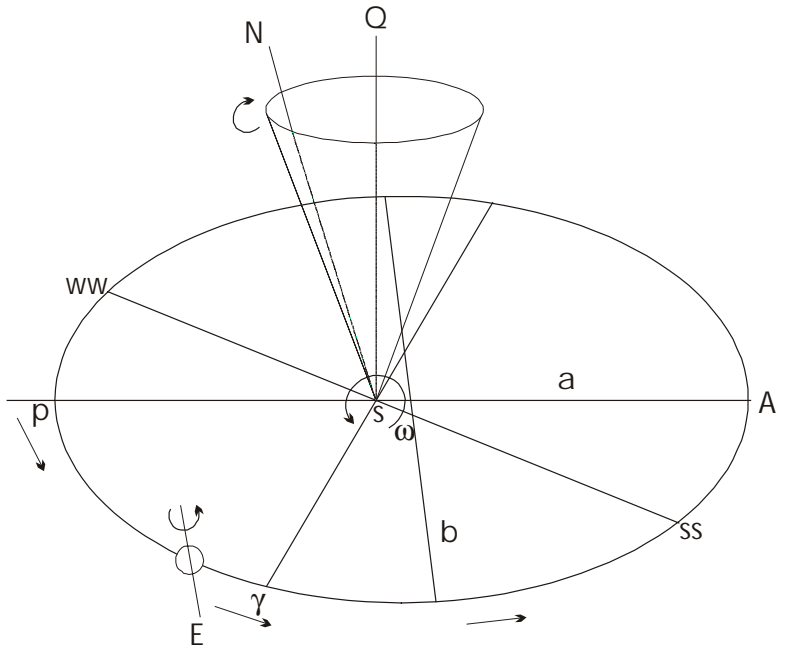


**Fig. 2.9 Elements of Earth's orbit.** The orbit of the Earth, E, around the Sun, S, is represented by ellipse PγEA, P being the perihelion and A the aphelion. It's eccentricity  $e$  is given by  $(a^2-b^2)^{1/2}/a$ ,  $a$  being the semi major axis and  $b$  the semi minor axis. WW, SS are winter and summer solstice. SQ is perpendicular to the ecliptic, and obliquity  $\epsilon$  is equal to the angle between the Earth's axis of rotation SN and SQ. Parameter  $\omega$  is the longitude of the perihelion relative to the moving vernal equinox, and is equal to  $\pi+\phi$ . The annual general precession in longitude,  $\phi$ , describes the absolute motion of the perihelion relative to absolute motion of  $\gamma$  along the Earth's orbit relative to the fixed stars (from Berger, 1988)

**Table 1: Milankovitch periods at present.**

Cycle periods (Kyr)					
Time	Precession 1	Precession 2	Average of p.1 and p.2	Obliquity	Eccentricity
Present	19	23	21	41	95

**Table 2: Ratios of present Milankovitch period.**

Cycle ratios			
Time	Avg prec : obliq	Avg.Prec : Ecce	Obliq : Ecce
Present	0.512	0.221	0.432

The 95 kyr (often listed as ~100 kyr) has been proposed to signify nonlinear response to the relatively weak eccentricity forcing. The non-linearity of the climate system response is suggested as an internal energy of large high latitude ice sheets. The obliquity and precession have a direct linear link (Imbrie et al., 1993) between insolation and climatic fluctuations. The obliquity (41 kyr) has the maximum effects on insolation at regions of higher latitude due to varying seasonality. On the other hand the variations in precessional forcing (~23 kyr) have more effects on insolation in lower latitudes (Ruddiman et al., 1989, Imbrie et al., 1992). Milankovitch cycles are used as an application to access the rates and duration of geological processes and in palaeoclimatic studies. In the following sections the 95 kyr period was used to tune the ages of magnetostratigraphy.

### 2.3.7 Age calibration

Unfortunately only three magnetic polarity transitions, i.e. Blake event, B/M boundary, and Jaramillo are well accepted for the last 1 Ma. Linear interpolation between reversals can be used to establish a first order age model provided that the rate of sedimentation is rather constant throughout the sequence. However, lacustrine sedimentation with a constant rate of deposition rarely exists through longer periods. To overcome this drawback cyclostratigraphy can be employed. The linkage between climate and variances of the Earth's orbital parameters is not only established from ice core and marine records but also it is evidential from spectacular results obtained from long continental records of Quaternary age since last decade (Kukla et al., 1988; Kukla and Clerk, 1996). Milankovitch cycles mark time intervals of tens of thousands to several millions of years (Schwarzacher, 1993) and can be used as a tool for higher resolution dating. (House, 1985; Raymon and McIntyre, 1986; Herbert, 1992; Kent, 1995; Mayer and Appel, 1999).

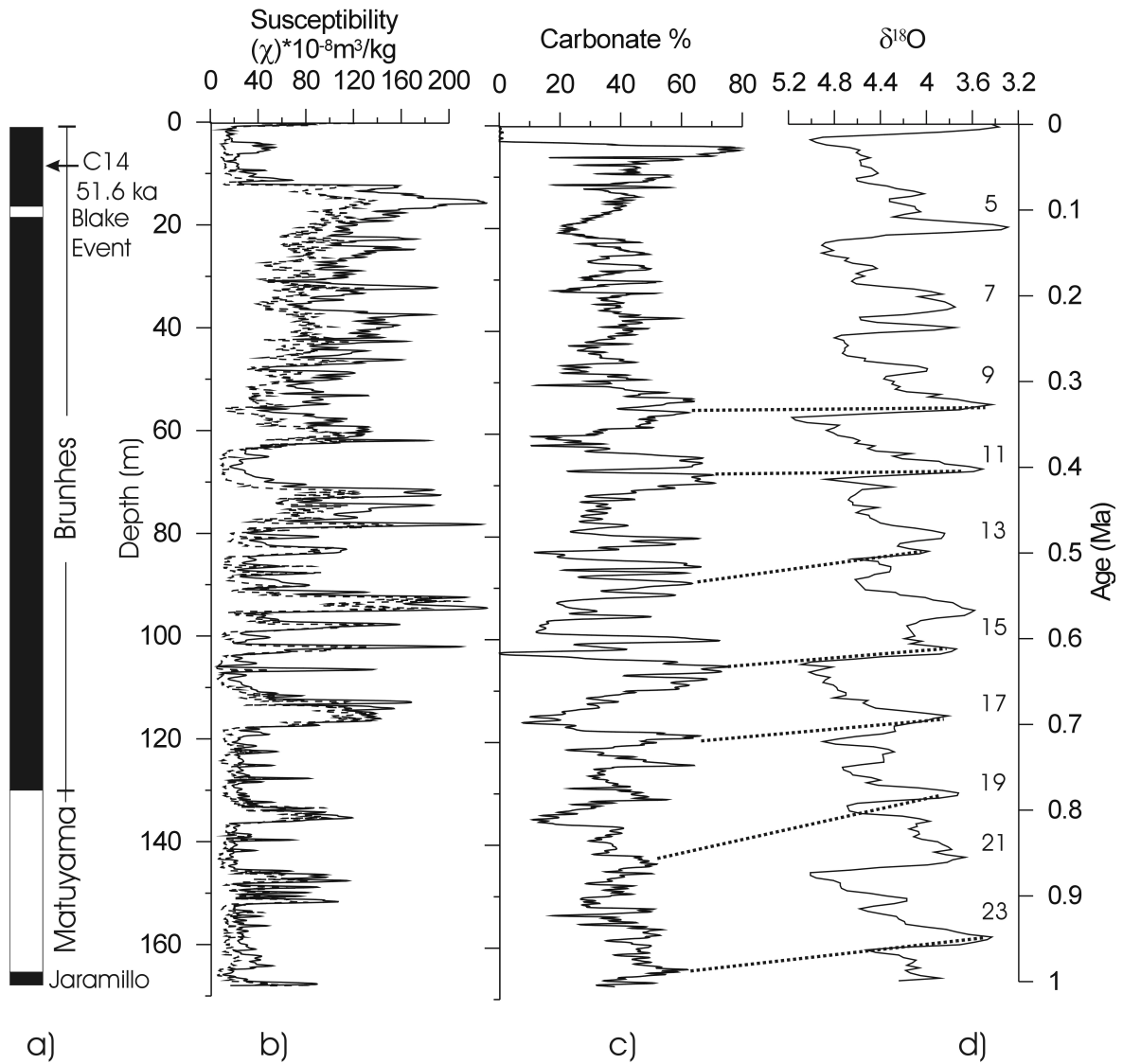


**Fig. 2.10 a) Geomagnetic polarity time scale of Heqing core, b) variations of susceptibility, uncorrected (dashed line) and corrected for carbonate (full line), c,d) variations of carbonate and its tentative correlation with marine oxygen isotope**

Fourier analysis in wavelength domain was performed on susceptibility (corrected for carbonate content) carbonate (Fig. 2.10) and SIRM data for sliding windows with different window lengths of 40 m, 60 m, and 80 m (sliding intervals 2.5 m) using STATISTICA

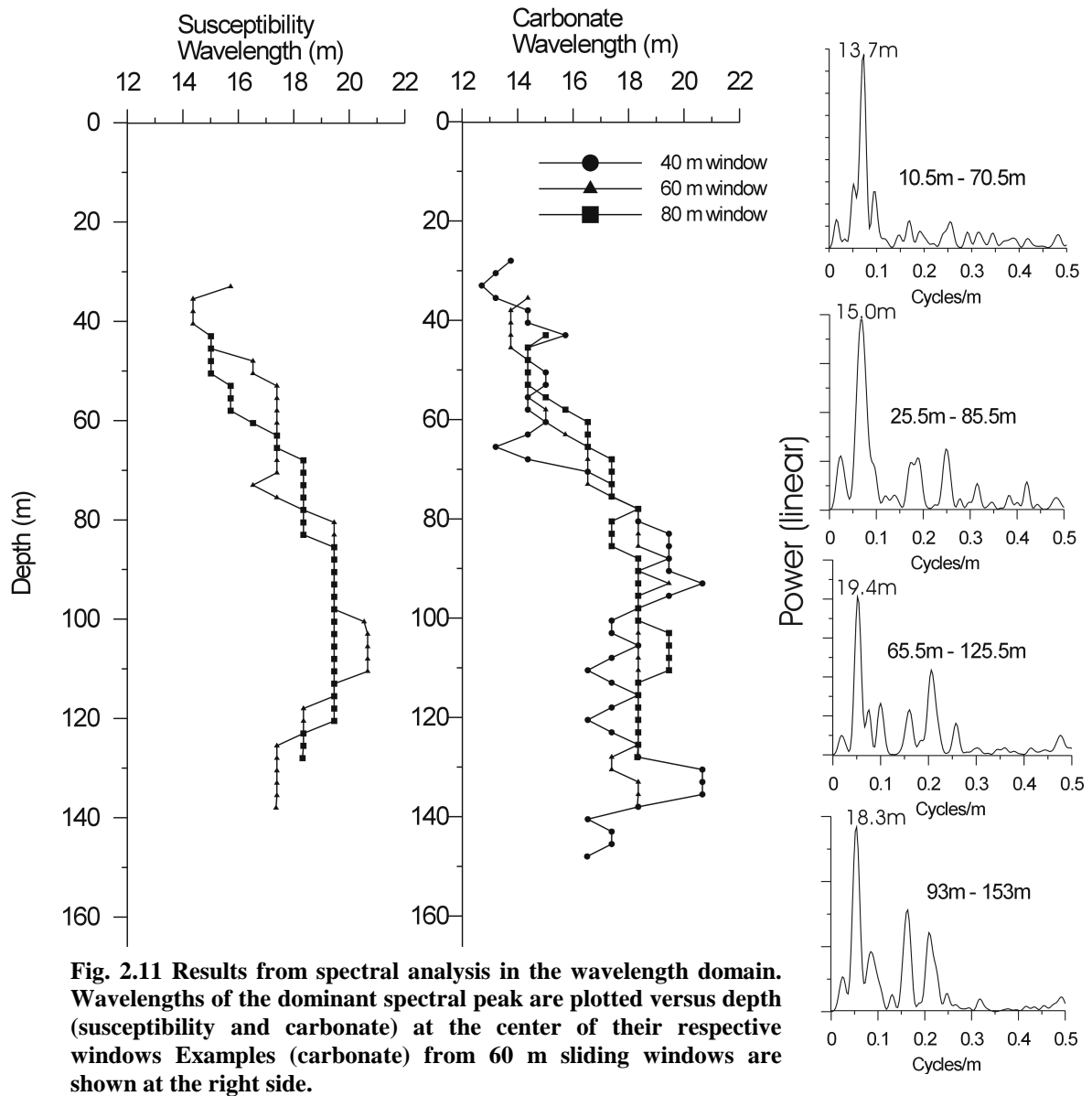


**Fig. 2.11 Results from spectral analysis in the wavelength domain. Wavelengths of the dominant spectral peak are plotted versus depth (susceptibility and carbonate) at the center of their respective windows. Examples (carbonate) from 60 m sliding windows are shown at the right side.**

software. The required preprocessing for this method included fitting of cubic-spline curve to the raw data and resampling at a constant interval of 5 cm using MATLAB tool box and later the data was smoothed by 5-point running average. To obtain a higher resolution of the spectra of sliding windows, the data was padded up with >5000 zeros. However the number of input cases was maintained same for all the windows.

For all the obtained spectra, the maximum power was found in the peak representing the maximum wavelength (Fig. 2.11). Carbonate gives more significant results than susceptibility and SIRM. The wavelengths are plotted at the center of their windows along the depth respectively. The results show a change in wavelengths between depths of 55 m and 75 m (Fig. 2.11) indicating a change in sedimentological conditions at a depth of about 65 m. Such change can be also seen in the grain size variation (will be shown in the coming chapters). For shorter sliding windows the transition interval becomes smaller indicating that the gradual shift of wavelengths between 55-75 m is a smearing effect caused by the window length. With the assumption that wavelengths represent the eccentricity cycle and are constant above 65m (14.5 m wavelength) and below 65 m (18.5 m) we can derive a discrete change for the rate of deposition from 15 cm/kyr (above 65 m) to 19 cm/kyr (below 65 m). However, it has to be mentioned that at 120-140 m a decrease of wavelengths towards the lower part of the core is indicated (especially in the susceptibility spectra).

### 2.3.8. Tuned age model

The simplest approach to determine an age model is a linear transformation of depth into time by using the safest tie points, i.e. B/M boundary and  $^{14}\text{C}$  dating. The corresponding Fourier spectrum (carbonate) of the complete sequence (Fig. 2.12a) shows the 95-kyr eccentricity peak, but only weak indication for precession and no reference to obliquity. A wavelength age model is obtained by using  $^{14}\text{C}$  as a tie point and rates of deposition from spectral analysis (15 cm/kyr for 0-65 m, 19 cm/kyr for 65-168 m). The obtained ages from the model are compared to the results of magnetostratigraphy. The magnetic tie points correspond to 107-116 ka (Blake Event), 785 ka (B/M boundary), and 909 ka (Jaramillo upper boundary). Results for Blake Event and B/M boundary match very well to the expected ages of 115 ka (Bleil and Gard 1989) and 780 ka (Cande and Kent 1995), respectively (Fig. 2.12a). However, for the upper Jaramillo boundary there is a clear underestimation of the expected age (990 ka; Cande and Kent 1995). This may be explained by a strongly lower sedimentation rate during the Matuyama Chron.

As mentioned above down-core curves indeed reveal a tendency towards shorter wavelengths at their lowermost end (Fig. 2.11). Unfortunately, Fourier spectra of sliding windows cannot be determined further down the core. From Figure 2.12b it is evident that the Fourier spectrum (carbonate) of the wavelength age model (using  $^{14}\text{C}$  as the tie point and 15.0 m/kyr and 19m/kyr sedimentation rate above and below 65 m respectively) shows no substantial improvement compared to the linear model. As an advanced option a tuned age model was derived by cubic spline interpolation based on tie points from

wavelength (sedimentation rates), radiocarbon dating and magnetic ages ('true' ages of Blake Event, B/M boundary, and Jaramillo upper boundary) (Fig. 2.13a). Spectral results of carbonate (Fig. 2.13b) clearly show well expressed eccentricity (95 kyr), obliquity (41 kyr),

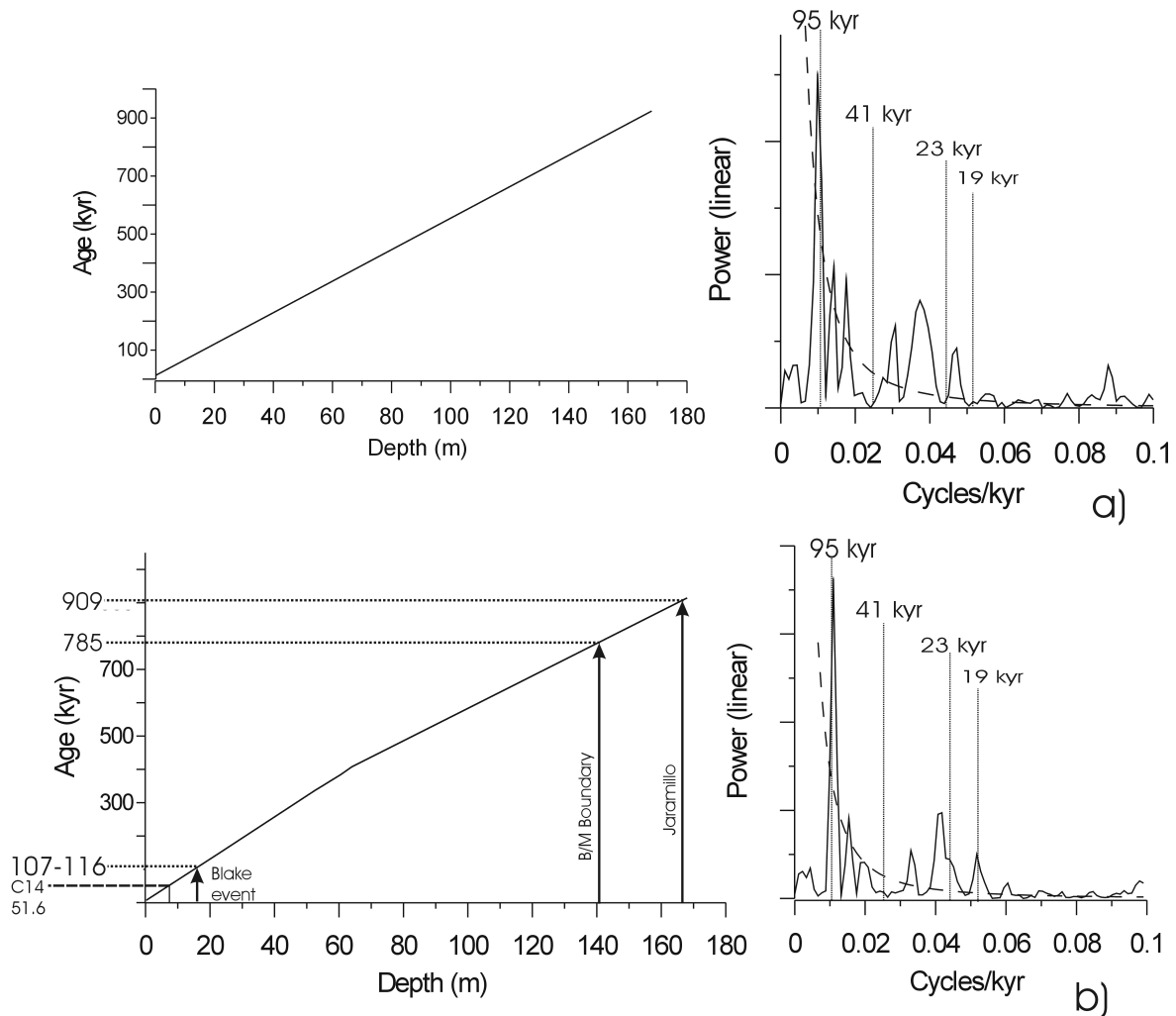


**Fig. 2.12 (a) Age model of linear depth-time transformation, and corresponding Fourier spectrum (whole-core carbonate). (b) Age model obtained from wavelength results with  $^{14}\text{C}$  age as a tie point. Results from magnetostratigraphy (reversals) are compared to this model (ages derived for Blake Event, B/M boundary, and Jaramillo are given). The corresponding Fourier spectrum (whole-core carbonate) is shown at the right side**

and precession (23 and 19 kyr) cycles but susceptibility (Fig. 2.13c) indicates only eccentricity and obliquity cycles. However the improved spectrum indicates that the interpretation of Jaramillo is justified.

As other approaches in deriving the age model, filtered curves and marine isotopic stages together with  $^{14}\text{C}$  and magnetic dates were used.

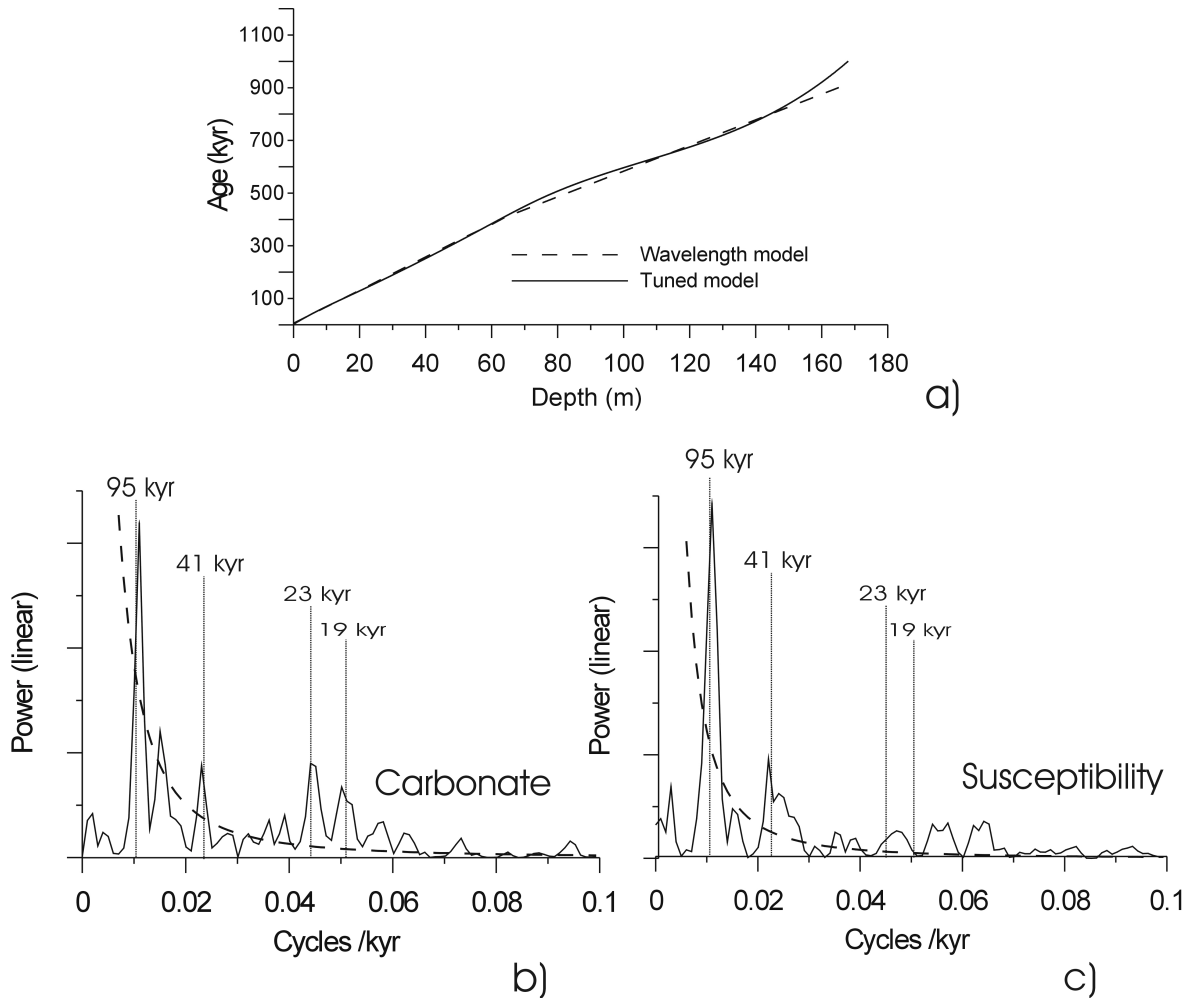


**Fig. 2.13 (a) Tuned age model (full line) by cubic spline interpolation of the following tie points obtained by radiocarbon dating (C14), magnetostratigraphy (MS), and wavelength results (WM): 7.3m/51.6ka (C14), 17.0m/115ka (MS), 55.0m/350ka (WM), 75.0m/480ka (WM), 141.5m/780ka (MS), 167.0m/990ka (MS). (b,c) Fourier spectra of whole-core carbonate and susceptibility time series using the tuned age model.**

As discussed above, Fourier analysis of wavelength domain indicate that the larger wavelength varies between 13 to 20 m along the depth and presumably represents Earth's eccentricity cycle. To resolve only the eccentricity cycle all along the core, a band pass filter with low and high cutoff of 11 m and 25 m was chosen for smoothing (Fig 2.14a). Bandpass filtering was done using REFLEX program (Sandmeier scientific software). Using  $^{14}\text{C}$  age as tie point and assuming that the time required for sedimentation between consecutive peaks of the smoothed curve is 95 kyr, the ages were determined for all depth with linear and cubic spline interpolations (Fig 2.14b). The age of first peak (8.5m) of the filtered curve is calculated using  $^{14}\text{C}$  date and assuming the same rate of deposition for depths between 8.5 m and 26.7 m.

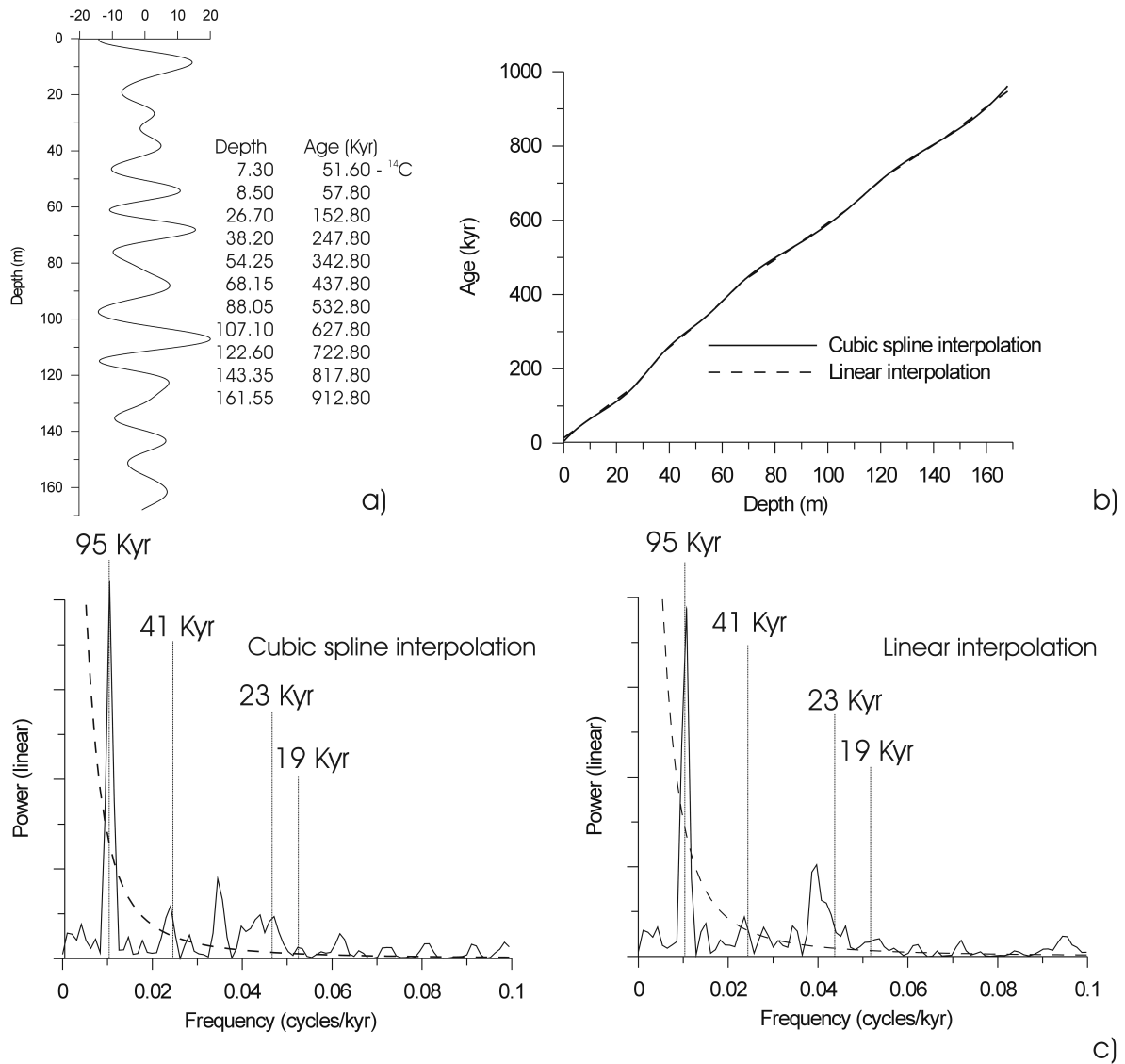


**Fig. 2.14** (a) Bandpass filtered curve of carbonate, the respective depths of the peaks and corresponding ages determined based on <sup>14</sup>C date (7.3m/51.6). (b) Age model obtained from bandpass curve and tie point <sup>14</sup>C (c) Spectra of carbonate using the age model for both cubic spline and linear ages

Spectral analysis was carried out for carbonate data using both the cubic spline and linear model (Fig 2.14c). Both the spectra show low power for 41 kyr cycle and a distortion of 23 kyr and 19 kyr cycles.

Susceptibility and carbonate curves roughly correspond with the marine oxygen isotope record. MIS 9, 11, 15, and 23 may be correlated to depths 55, 68, 122 and 165 m respectively (Fig. 2.10). Using these ages and <sup>14</sup>C age, an age frame was obtained for all depth with cubic spline and linear interpolations. Spectral analysis was carried out on carbonate data set with these ages respectively. Spectrum using cubic spline ages show

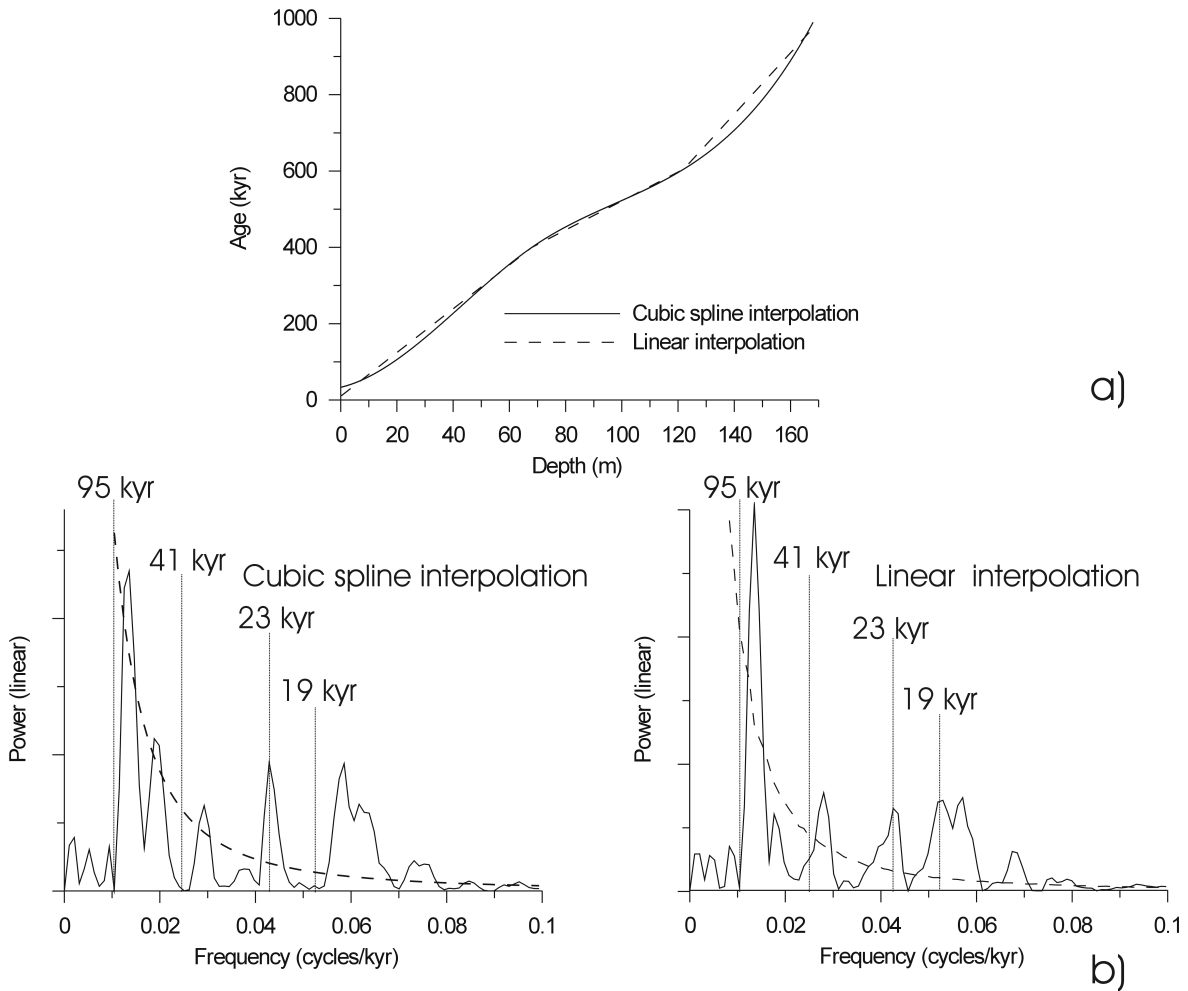


**Fig 2.15 (a) Age model obtained using cubic spline and linear interpolations with  $^{14}\text{C}$  and MIS as tie points : 7.3m/51.6ka , 55 m/325ka (MIS 9) , 68m/400ka (MIS11) , 122m/605ka (MIS15) 165m/950ka (MIS 23) (b) Spectra obtained with cubic spline and linear ages.**

distortion for all cycles except 23 kyr cycle (Fig. 2.15 a) but the spectrum of linear age show distortion for 95 and 41 kyr cycles (Fig. 2.15 a). As further approach to this model, magnetic polarities i.e. Blake event (17.0 m), B/M boundary (142 m) and Jaramillo (167.0 m) were added and interpolated (Fig. 2.16 a). The spectral results using the cubic spline and linear interpolation show more distortion which indicate unimprovement in the age model (Fig. 2.16b).

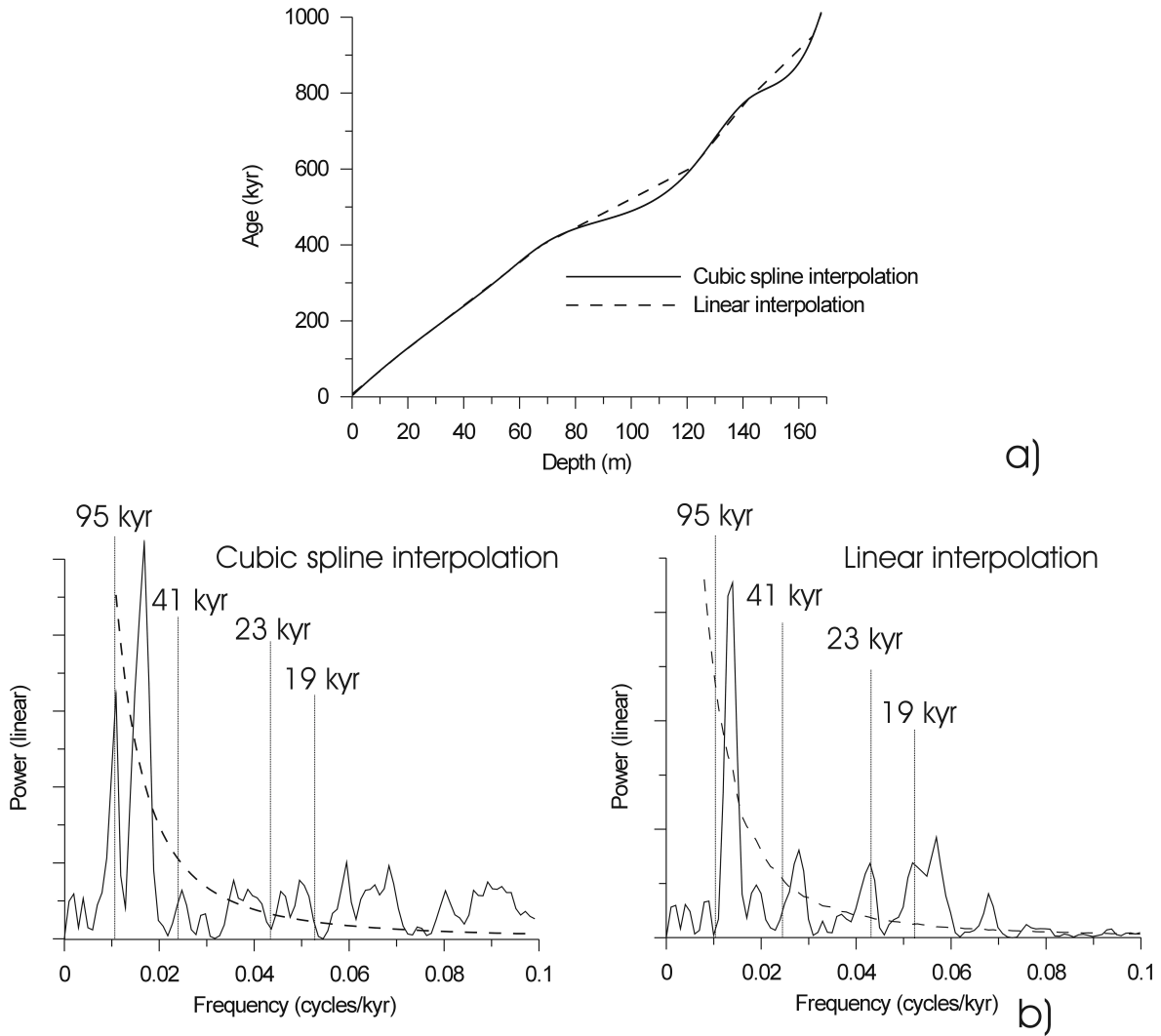


**Fig. 2.16** Age model using cubic spline and linear interpolations with tie points  $^{14}\text{C}$ , MIS and magnetostratigraphy ages (MS) : 7.3m/51.6ka ( $^{14}\text{C}$ ) , 17 m/111ka (MS) 55 m/325ka (MIS 9) , 68m/400ka (MIS11) , 122m/605ka (MIS15) 142 m/780ka (MS) 165m/950ka (MIS 23) 167 m/990ka (MS). (b) Spectra obtained using ages of cubic spline and linear interpolations

## 2.4 Palaeoclimatic proxies, multivariate statistics and time series analysis

### 2.4.1 Magnetic proxies

Magnetic properties of sediments are dominantly controlled by concentration, grain size and composition of constituent magnetic mineralogy. The sedimentation process is strongly dependent on the surrounding environmental changes. Magnetic properties may reflect or amplify these changes. Therefore magnetic measurements can be used as a rapid and a nondestructive method for detecting environmental changes. It was well demonstrated that magnetic parameters could be excellent proxies of past climatic variations (Banerjee, 1994, Banerjee et al. 1993, Thomson and Oldfield, 1986; King and Channell, 1991; Dekkers, 1997).

Prior to the magnetostratigraphy work natural remanent magnetization (NRM) and low field susceptibility ( $\chi$ ) were measured using a 2G SQUID magnetometer and a Bartington MS2B instrument, respectively. Subsequently laboratory remanences ARM (alternating field 100 mT with DC field of 0.5 mT), SIRM (2 T along +Z axis) and subsequently reverse IRM (300 mT along -Z axis) were imparted. For the samples from 0 to 110 m ARM, SIRM, IRM measurements were done on discrete samples using a Molspin spinner magnetometer (at University of Tuebingen) whereas for the lower part of the core (>110 m) a u-channel 2G SQUID magnetometer was used (at University of Davis, USA). The fields (100 mT, DC 0.5 mT) and instruments (2G degausser) used for imparting and measuring ARM were the same throughout the section. To adjust for systematic differences the lower part of the core (>110 m) was normalized to the upper part. Results of  $\chi$  and laboratory imparted remanences correspond well (Fig. 2.17, 2.19), suggesting that ferro(i)magnetic grains mainly control the  $\chi$  signal. As mentioned in the last chapter, there are mainly two types of samples, predominated by the maghemite and maghemite+magnetite respectively. For a total of 91 samples, an isothermal remanence was produced and thermally demagnetized to classify them into these groups. The maghemite group (50 samples) falls into zones with predominantly lower  $\chi$  values whereas the maghemite+magnetite group (41 samples) corresponds to predominantly higher  $\chi$  values. A number of 94% of maghemite samples have  $\chi < \chi_{\text{mean}}$  ( $\chi_{\text{mean}}$ : average of all 91 samples), and 80% of maghemite+magnetite have  $\chi > \chi_{\text{mean}}$  demonstrating the clear separation of these two groups. The depths where maghemite and maghemite+magnetite association occur are shown in Figure 2.18g. The difference in magnetic mineralogy seem to have a relation to the climatic conditions which will be discussed later. Carbonate free  $\chi$  ( $\chi_{\text{free}}$ ) is calculated from the measured  $\chi$  of the bulk

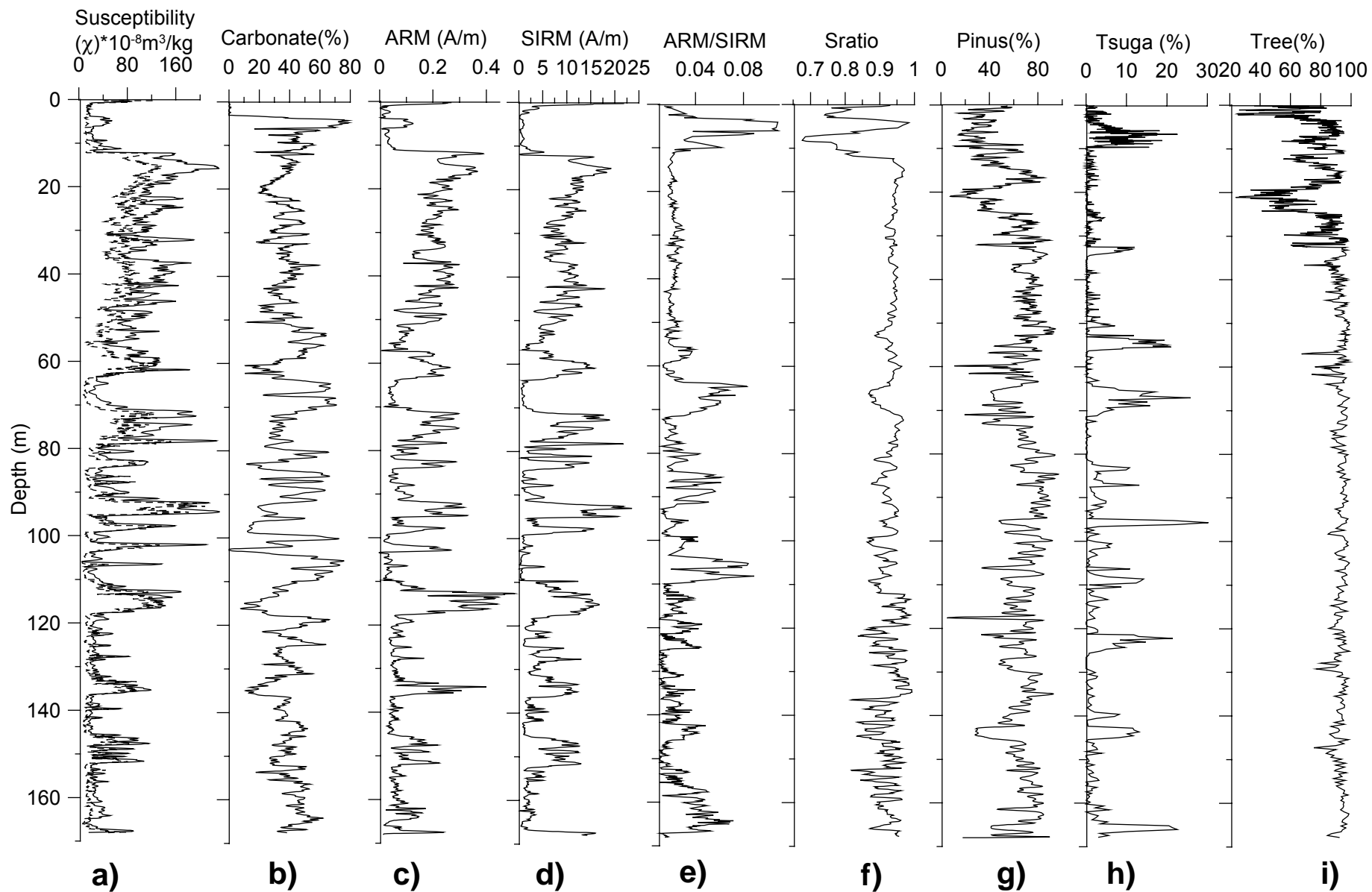


Fig. 2.17 Variations of magnetic and non-magnetic parameters. a) susceptibility, the dotted line is susceptibility without carbonate correction and the full line is carbonate corrected, b) variations of carbonate content. c) ARM. d) SIRM. e), ARM/SIRM ratio. f) S-ratio. g,h,i) pollen (*Pinus*, *Tsuga* and tree). A strong correspondence between magnetic parameters can be seen. Data provided by scientists of Nanjing Institute of Geography and Limnology, China.

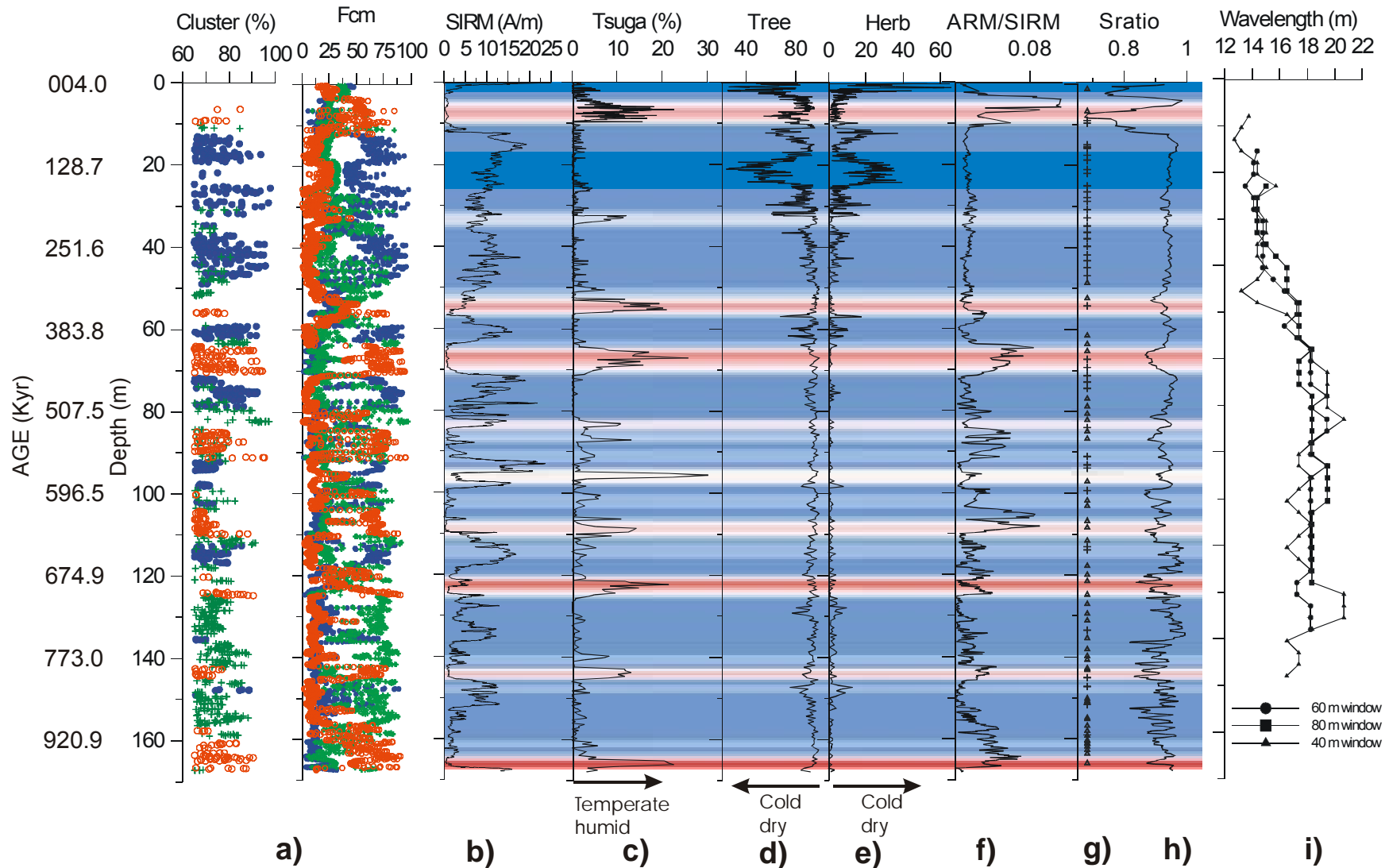


Fig. 2.18 a) Results of cluster analysis, red open circles, blue closed circles, and green + symbols indicate first, second and third clusters respectively, their membership probability is shown beside. b) Variations of SIRM. c, d, e) Pollen (*Tsuga* Total tree and herb). f) ARM/SIRM ratio. g) Magnetic mineralogy at various depths, the symbol '+' indicate maghemite with magnetite association and  $\Delta$  indicate only maghemite. h) S-ratio vs depth. i) wavelengths known from the Fourier spectral analysis of sliding windows of carbonate data set. A clear correlation between ARM/SIRM, first cluster and *Tsuga* can be seen. The ARM/SIRM is in accordance with identified mineralogy. The color code is given based on the *Tsuga* values. The higher values indicate deep red and lower values deep blue. The deepest blue is coded for lowest values of Total tree. A decrease in wavelengths of SIRM indicates a change in depositional system.

sample ( $\chi_{\text{bulk}}$ ) and carbonate% by  $\chi_{\text{free}} = (\chi_{\text{bulk}}) * (100/(100 - \text{carbonate}\%))$ . The carbonate free susceptibility curve is almost alike to the uncorrected curve of susceptibility (Fig. 2.17a), which strongly suggests that the highs and lows of the magnetic signal is not only a dilution effect caused by carbonate.

The ARM/SIRM ratio is often used as an indicator of magnetic grain sizes (higher values correspond to higher proportion of single domain grains). In this case the ratios seem to be more influenced by mixed mineralogy of maghemite and magnetite. High and low values are found at depths with dominance of maghemite and magnetite association respectively. It is interesting to note that the higher values of ARM/SIRM ratio show a close relation with Tsuga and first cluster of cluster analysis (will be discussed later in this chapter). S-ratios were calculated by  $S = ((\text{IRM}_{-0.3T}/\text{SIRM}) + 1)/2$  (Bloemendal et al., 1992) (indicates magnetic mineral composition) roughly correspond with the identified magnetic mineralogy. Significant low values are found above the depth of ~10 m. The results of SIRM, ARM/SIRM and S-ratio are shown in Figure 2.18 b,f,h.

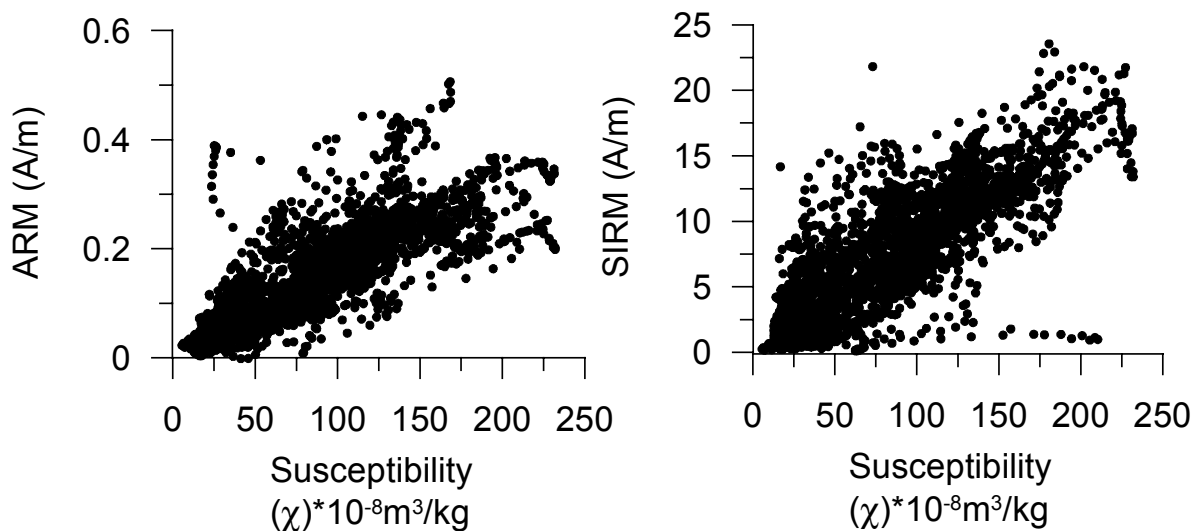


Fig. 2.19 Crossplot of susceptibility with ARM and SIRM, a linear correspondence can be observed between them.

## 2.4.2 Non-magnetic proxies

### *Variations of Carbonate*

Carbonate is a sensitive parameter in responding to climatic and tectonic influences and depends on lake hydrology and morphology. Climate controls the nature and rate of biogenic productivity, erosion and rate of flow into the lake. In lake Heqing the carbonate is largely of detrital origin as it is surrounded mainly by limestone rocks and carbonate

content is high (up to 80%). For carbonate analysis, the samples were grinded and treated with diluted HCl and the weight loss is considered as the total percentage of carbonate in the samples. The results are plotted against depth (Fig. 2.17b). For the major part of the sequence an anti-correlation between the carbonate and magnetic parameters (especially susceptibility, Fig. 2.17a,b) is observed. This correlation will be discussed in more detail further below.

### **Pollen analysis**

Pollen studies widely contributed to decipher palaeoclimatic conditions. A vast number of pollen grains can be found even in few grams of mud or peat samples, and they are virtually non-destructive. As pollen is transported by wind to large distance, the pollen falling on a given site reflects the vegetation not only at that investigated site, but also from the general vicinity. Categorizing different pollen and knowing the dominant type would give a broad idea of the regional environmental conditions along the geological time span. The samples were treated by acid alkaline method and approximately 400-600 pollen grains were counted using a Leitz microscope (Yang et al., 2000). Ten main pollen taxa were analysed including *Absies* and *Picea*, *Pinus*, *Tsuga*, *Quercus*, evergreen broadleaf taxa, *Rosa*, *Verberum*, *Artemisia* and *Gramineae*. Smoothed (5-point running average) results of four pollen results, *Pinus*, *Tsuga*, total tree pollen are shown in Figure 2.17g,h,l and herb in Figure 2.18e

### **Grain size analysis**

Grain size analysis can play an important role in indicating the lake level changes. Usually during low lake hydraulic conditions the grain sizes are typically higher and vice versa. The samples were measured with laser diffractometry at depths of 0 - 120 m with a resolution of 10 cm at the uppermost part. The laser diffractometry technique allows measuring the samples rapidly beginning from range of

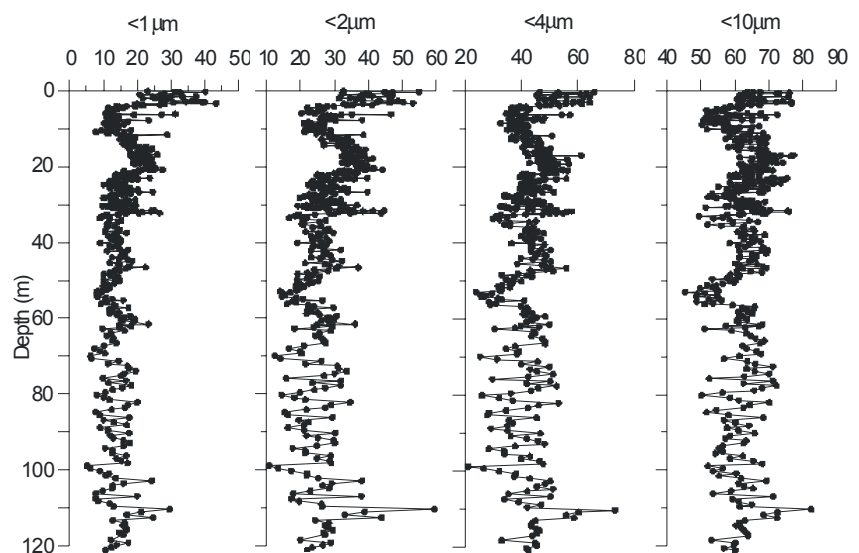


Fig.2.20 Results of grain size analysis, a clear change can be observed in all sizes at the depth of 55 m. Data provided by scientists of Nanjing Institute of Geography and Limnology.

of .02  $\mu\text{m}$  and with a precession of +/- 1%. The results show a significant decrease of smaller grain sizes at around 60 m. Above a depth of 50 m the small particle fraction increases again and reaches a higher level than below 60 m. Around 10 m depth again coarsening is observed and at the top ( $\leq 5$  m) again fining (Fig. 2.20).

### 2.4.3 Multivariate statistics

Multivariate statistics detect the pattern of relationships between several variables simultaneously. It is impossible to view a set of variables in a comprehensive way as they have several dimensions. Multivariate statistics can help to reduce the dimensionality of the data set to conceivable and plottable two or three dimensions. When dealing with variables along long stratigraphic sequences it is better to have high resolution and continuous data sets for better understanding. Heqing data set contains more than 12 variables which includes measured variables and calculated variables, suitable for statistical analysis.

The raw data sets of all variables were interpolated to regular depth intervals (5 cm) with cubic spline fitting using MATLAB software. In order to nullify the nonsystematic components of individual observations, simple five point running average was selected for smoothing. The smoothed data was used for the statistical and time series (will be discussed in next section) analysis.

#### **Correlation of carbonate and susceptibility**

The degree of linear relationship between two variables is called correlation coefficient and is usually represented by R. It is an important factor, which can indicate whether the variables are linked directly or inversely. It could be a tool to know the underlying geological processes. It is given by equation

$$R_{xy} = \frac{\sum_{i=1}^n (x_i - \bar{x})(y_i - \bar{y})}{(n-1)s_x s_y}$$

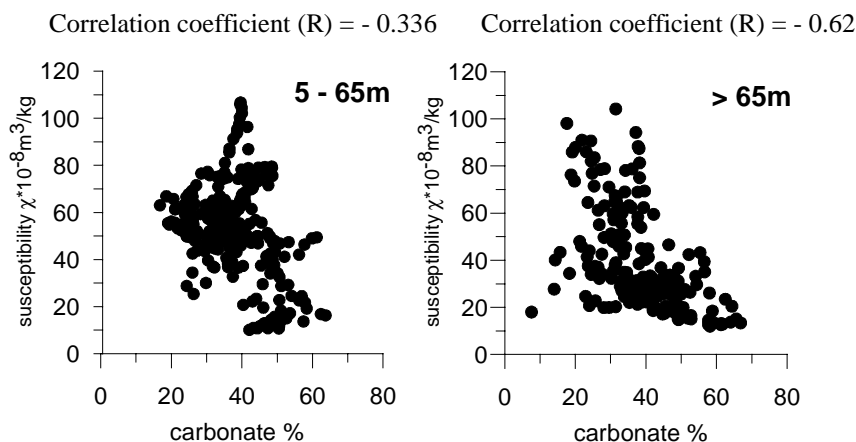


**Fig 2.21** Crossplot between carbonate corrected susceptibility ( $\chi$ ) and carbonate of upper and lower parts of the core.

where  $S$  is the standard deviation,  $x$  and  $y$  are the variables and  $\bar{X}$  and  $\bar{Y}$  are their mean values. The correlation coefficient ranges from 1 to  $-1$ , the extremes indicate strong correlation and is dimensionless. The values closer to zero are said to have less or almost no correlation. From the  $\chi$  (carbonate free) and carbonate variations (Fig. 2.17) it seems that the lower part of the core (below 65 m) has a more cyclic behaviour than the upper part. By so we can observe typically anti-correlation between them but at certain depths a positive correlation also exists. On a whole these differences obviously control strongly the numerical value of  $R$ . The overall bivariate plots (cross plot) between carbonate and  $\chi$  for depths 5-65 m and  $> 65$  m show almost no correlation in the upper part and some negative correlation ( $R = -0.62$ ) in the lower part (Fig.2.21). However this information is not sufficient (with respect to depth) for any further palaeoclimatic investigations. To resolve the correlation between carbonate and  $\chi$  correlation coefficient

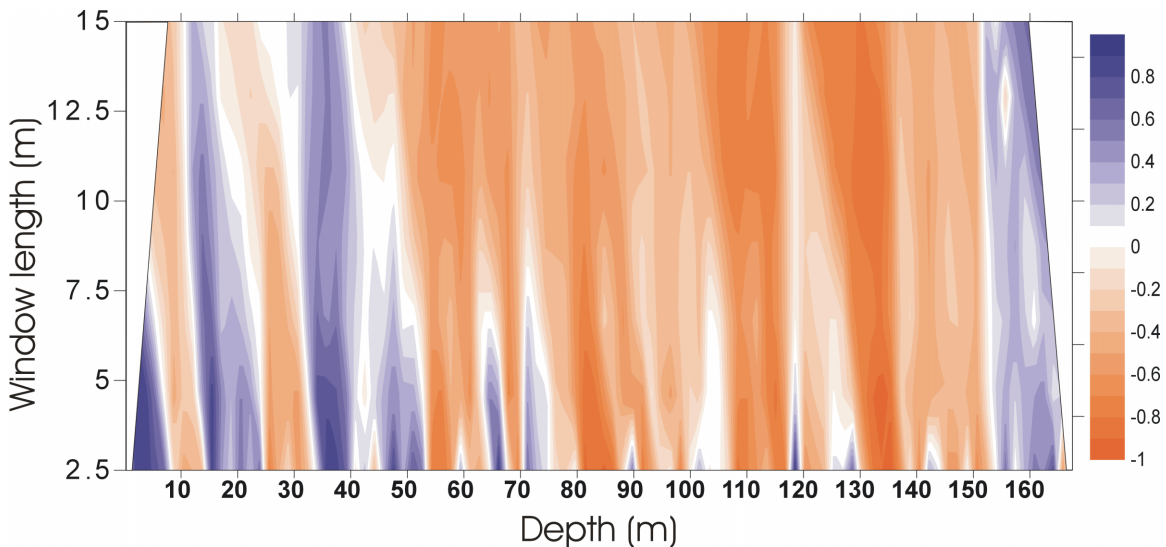


**Fig. 2.22** Correlation coefficients of sliding windows for different window lengths. The results are plotted at their center of their respective window lengths. Deep blue indicates strong positive and deep red indicates strong negative  $R$ . In the larger window lengths a clear distinction of correlation coefficient between upper part (50 m) and middle part (50 – 150 m) and lower part (>150 m).

$R$ ) was calculated for sliding windows with 5 cm interval of different window lengths using 2.5, 5, 7.5, 10, 12.5 and 15 m.  $R$ -values (center of windows) are contoured using kriging method along depth against the window lengths (Fig. 2.22). The results of smaller windows show systematic negative and positive correlation. For larger window lengths, mostly negative correlation exists below 55 m (except bottommost 10 m) whereas correlations are predominantly positive above, indicating a change in the depositional regime. The correlation of smaller window lengths (e.g. 2.5 m window) show a global climatic link, which will be discussed later in this chapter.

### Fuzzy C-means cluster analysis

Cluster analysis is a multivariate procedure that characterizes the set of objects (entries), and groups together in clusters, in a way that the profiles of objects in the same cluster are very similar and for different clusters are quite distinct. Cluster analysis involves decisions of the user concerning the calculation of clusters; the decisions can strongly influence the results of the classification. Care should be taken that groups (classes) are meaningful in some fashion and are not arbitrary or artificial. The discrepancies in units of various variables can distort the proximity calculations, which is the basis of clustering. Hence the first step before proceeding for cluster analysis is, normalizing the data to bring to same proportional scale. The key steps within cluster analysis are the measurement of distances between objects and to group the objects based upon the resultant distances (linkages). The distances provide a measure of similarity between objects and may be measured in a variety of ways, such as Euclidean and Manhattan metric distance. The linkage distances can be represented graphically or numerically. Graphically they are represented by icicle plot or a dendrogram. A dendrogram characterizes a set of input variables based on the dissimilarity coefficient between them.

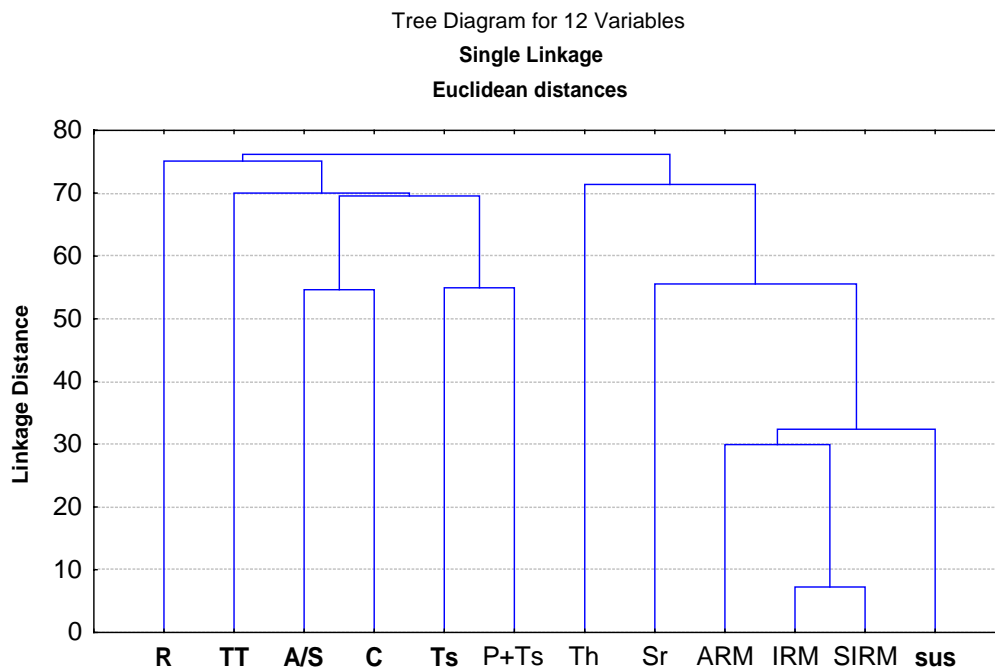


**Fig. 2.23** Dendrogram of all measured and calculated variables. R is correlation coefficient, TT is total tree pollen, A/S is the ratio between ARM and SIRM, C is the carbonate, P+Ts is *Picea* and *Tsuga* pollen, Th is total herb pollen, Sr is S-ratio, ARM, IRM, SIRM are the laboratory imparted remanences and sus is susceptibility (carbonate-free).

All the variables were first normalized by subtracting their mean and dividing by their standard deviations. Single linkage Euclidian distance (geometric distance in multidimensional space) is known between all the measured and calculated parameters and plotted as a dendrogram (Fig. 2.23). Selection of variables for fuzzy cluster analysis was based on the dendrogram. The higher the level of linkage distance between the

**Table 3. Combinations of different variables used for cluster analysis. Selected variables are marked by symbol x**

Variable	comb 1	comb 2	comb3	comb 4	comb 5	comb 6
ARM/SIRM	x	x	x	x	x	x
Sus	x		x	x		
carbonate		x	x		x	
R				x	x	x
Tsuga	x	x	x	x	x	x
Tree	x	x	x	x	x	x

variables, the more dissimilar they are (e.g. the variables IRM and SIRM in Figure 2.23

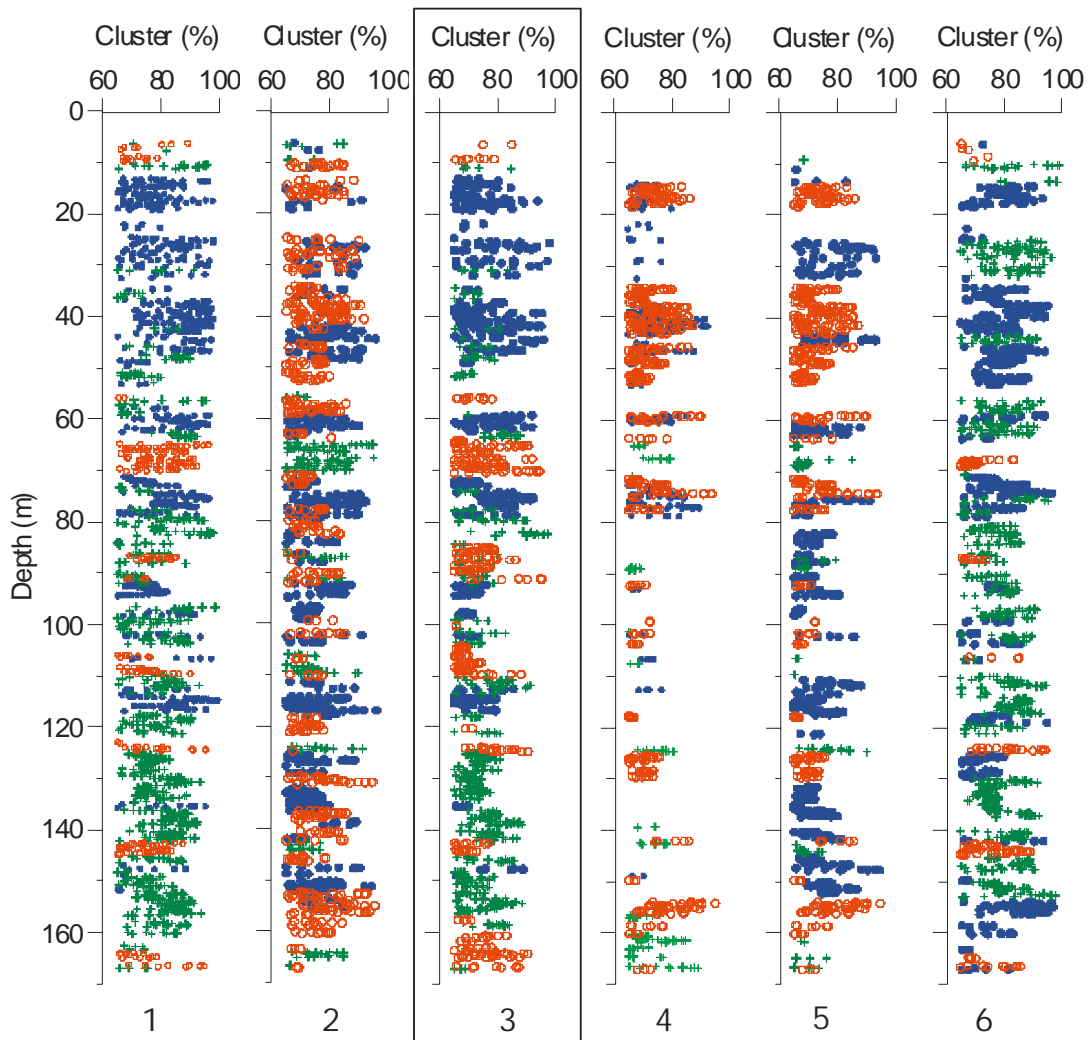


**Fig.2.24 Results of fuzzy C-mean cluster analysis for 3 clusters using different combinations as mentioned in table 3. Combinations 4,5,6 show clear distortion in the cluster grouping.**

have the lowest dissimilarity level).

For cluster analysis six variables (correlation coefficient, total tree pollen, carbonate, susceptibility, ARM/SIRM, and *Tsuga*) were chosen based on primarily longest Euclidian distance (means most dissimilar characteristics with respect to each other) and their response to regional and global climatic signal. Carbonate and  $\chi$  represent a global effect, however with different regional influence (as shown by R values). ARM/SIRM is an indicator for magnetic grain size variations which are probably caused by alteration of magnetite to maghemite (weathering during warmer and more humid conditions). Values of  $\chi$  are also dependent on this magneto mineralogical alteration. High *Tsuga* documents temperate-humid phases and low total tree related with high herb content is indicative for extreme cold-dry conditions. Fuzzy cluster analysis was performed using MATLAB software with six different combinations of variables (Table 3). From the obtained cluster results (for three-cluster case), >65 % of cluster memberships are plotted against depth (Fig 2.24). The results show a distortion for combinations where variable R is involved. The cluster results of all the combinations are shown in Figure 2.24. Combination 3 involving ARM/SIRM, susceptibility, carbonate, *Tsuga* and tree is considered to be most systematic and reliable for environmental interpretations. It is compared with the other parameters, which was already shown in Figure 2.18a. Combination 3 was also tested for four, five and six cluster cases. For all cluster cases, > 65% of the cluster memberships are plotted against depth with their respective positions of cluster centers are shown in Figure 2.25. The grouping of three and four cluster cases show similar behaviour, but the five and six cluster cases become complex. The three-cluster case was chosen for further interpretation, as it seems to be reliable and systematic. The results show a consistent grouping between the depths of 55 m to 125 m and a different pattern of grouping at rest of the depths. It is interesting to note that cluster1 (red in Figs. 2.24 and 2.25) does not appear between the depths 15 to 50 m and also cluster 3 is seldomly dominate at these depths (will be discussed further).

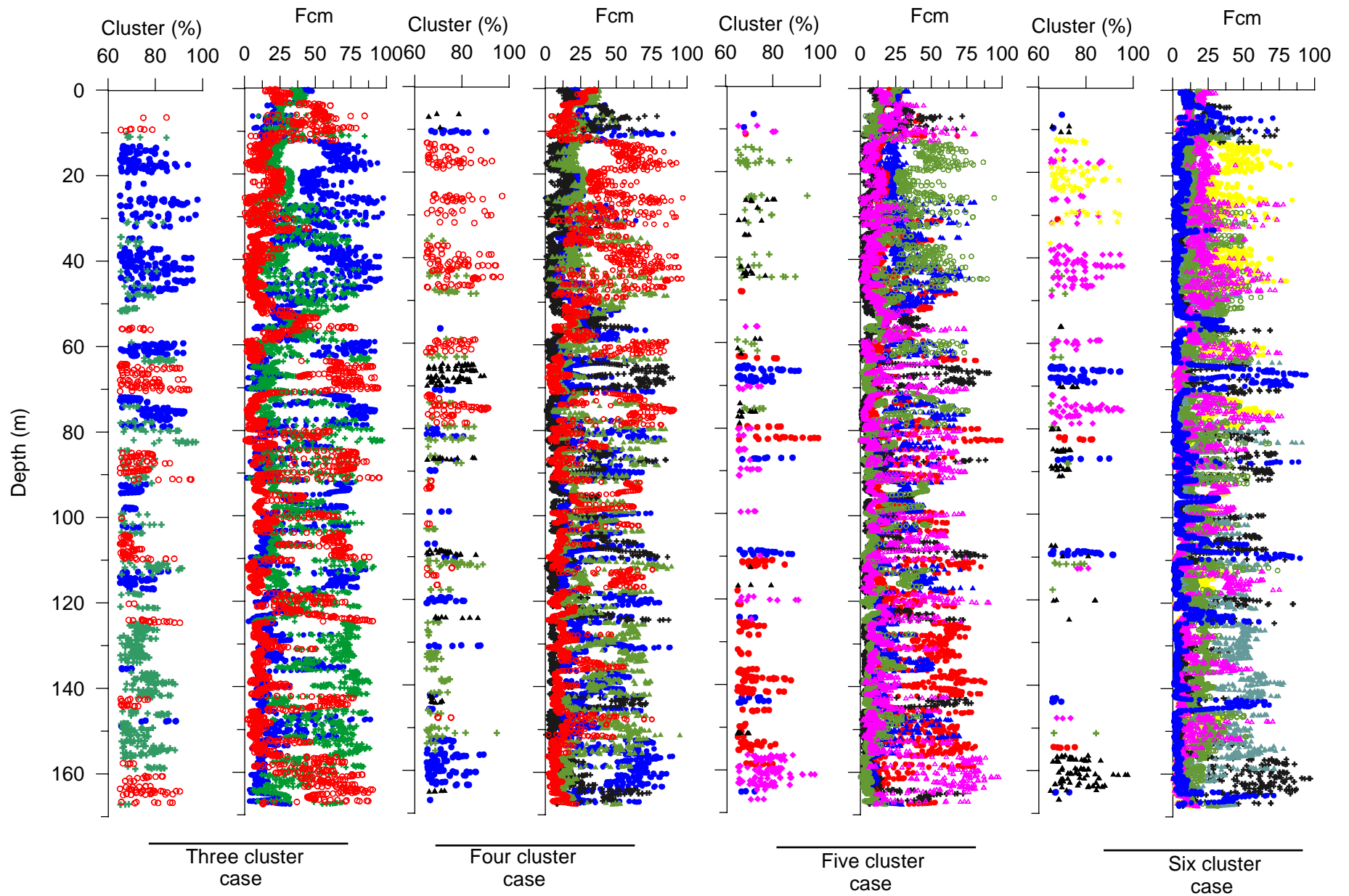


Fig. 2.25 Results of fuzzy C-mean cluster analysis for different cluster numbers and their corresponding membership probability% using combination 3, which involves ARM/SIRM, susceptibility, carbonate, *Tsuga* and total tree pollen.

## 2.4.4 Time series analysis

Time series analysis can be used for identifying the nature of the phenomenon represented by the sequence of observations, and predicting future values of the time series variable. It seems to be suitable for the study of stratigraphic data provided when the sequences are continuous and well dated. It is an important tool for palaeoclimatic investigations as it allows distinguishing the contribution associated with several processes through time. It has been vigorously used in quantitative geological interpretations for the past two decades (Diggel, 1990).

### **Spectral analysis**

Fourier analysis carried out on sliding windows in wavelength domain was used to calibrate the time axis of the Heqing sequence and in understanding the depositional system (discussed in the last chapter). Spectral analysis was also performed on whole

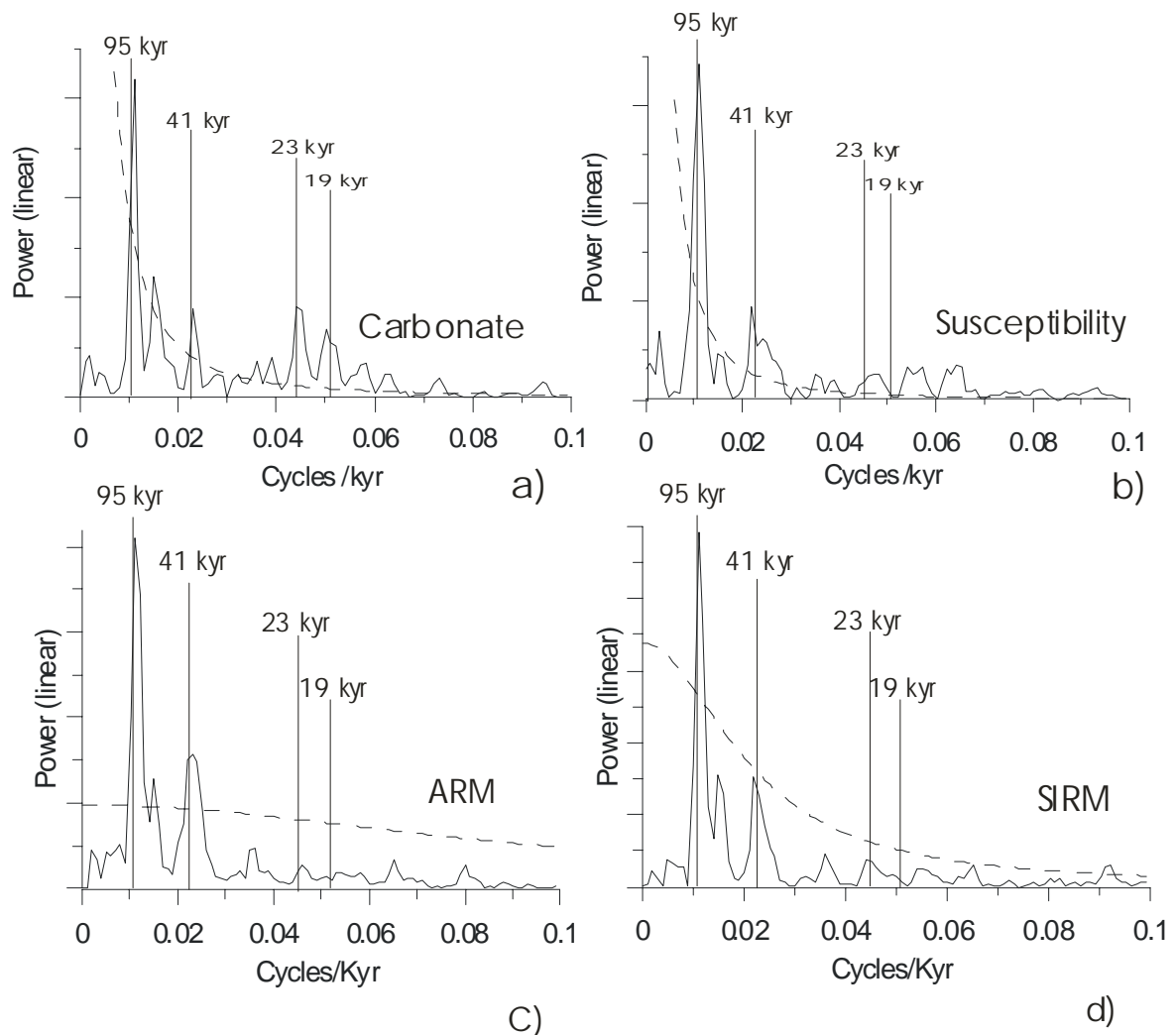


**Fig. 2.26 Spectral results of a) carbonate, b) susceptibility (carbonate free), c) anhysteretic remanent magnetization d) saturation isothermal remanent magnetization of whole-core time series using the tuned ages. Milankovitch cyclicities can be seen for all the parameters. The dashed line in all spectra indicates the 95% confidence level.**

core data sets of various parameters with calibrated ages (using unequally spaced time interval). Usually spectra of palaeoclimatic time series show decrease of spectral power

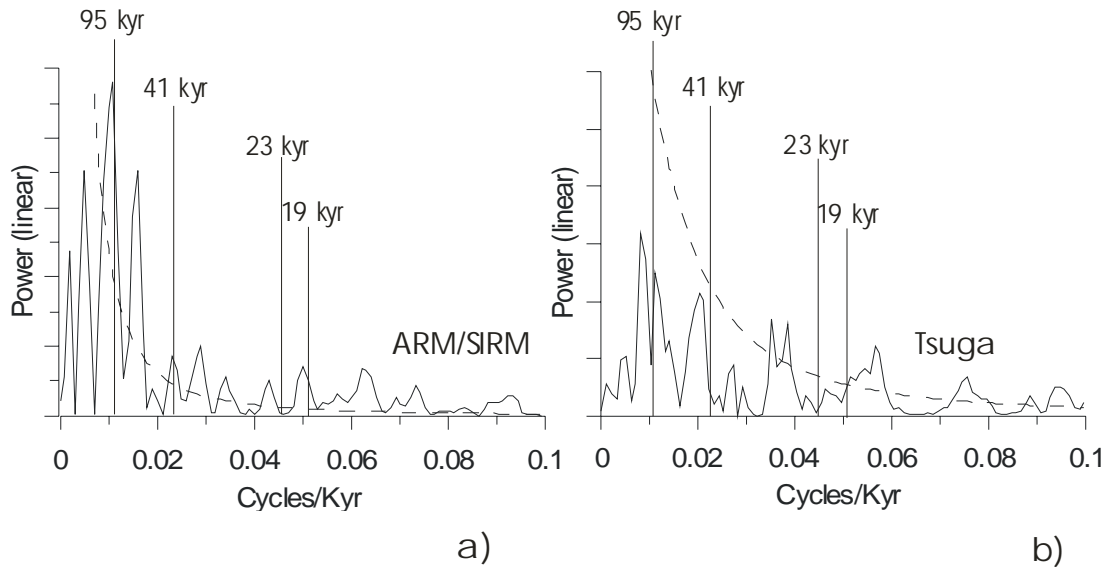


**Fig. 2.27 Spectral results of ARM/SIRM ratio and *Tsuga* pollen of the whole core. *Tsuga* do not represent any Milankovitch cyclicities. ARM/SIRM represent only 95 kyr cycle. Dotted line is the 95 % confidence level**

with increasing frequency, which is called red noise. The REDFIT program overcomes this problem by using a first-order

autoregressive model (for overview of the program see Schulz, and Mudelsee, 2002). The results of carbonate, show clear Milankovitch cyclicities, but  $\chi$ , ARM and SIRM demonstrate only the eccentricity and obliquity cycles. However it seems that the core has a strong tie to global climatic signal (Fig. 2.26a,b,c,d). The

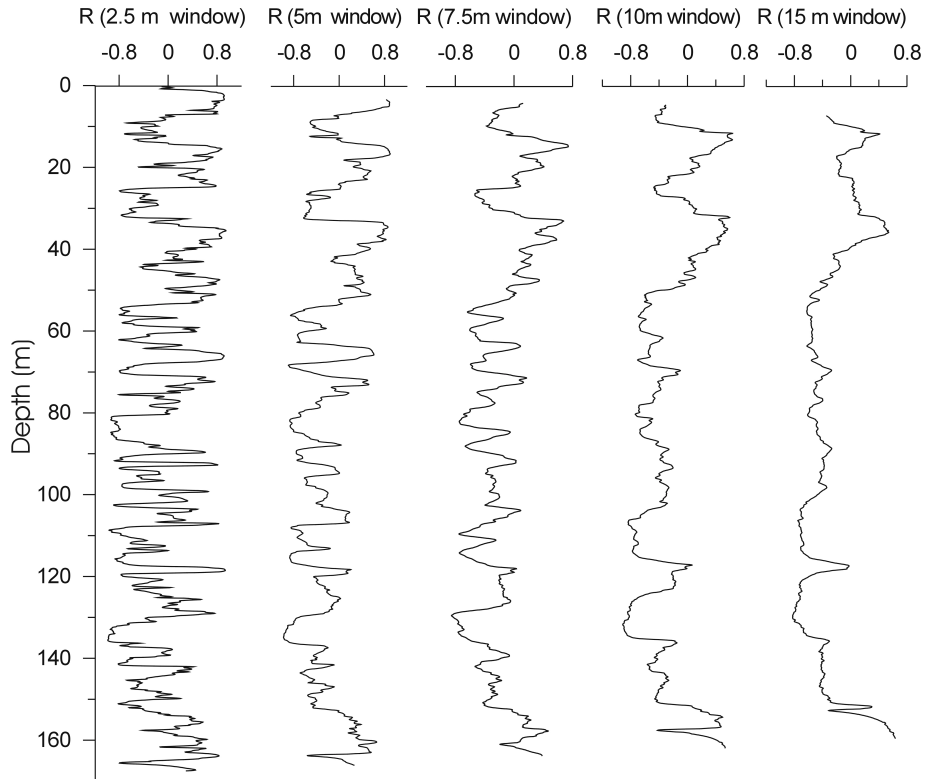


**Fig. 2.28 Correlation coefficients of carbonate and  $\chi$  (carbonate fee) for sliding windows of window lengths 2.5, 5, 7.5 10 and 15m.**

cyclicities are evidently above the 95 % confidence level, confirming that the assumed 95 kyr cycle for the age model (in the last section) was sensible. Spectral analysis performed on pollen (e.g. *Tsuga* in Fig. 2.27b) does not show any information of Milankovitch cyclicities but the spectrum of ARM/SIRM ratio shows a slight indication of eccentricity cycle. A justifying reason cannot be given for this behaviour. It could be that the pollen and the magnetic mineralogy records (ARM/SIRM represents magnetic grain size which will be discussed further) are more influenced by regional or local variations.

The R-values are plotted against depth in Figure 2.28. Surprisingly the R-values (correlation factor of  $\chi$  and carbonate) of smaller window lengths show a cyclic behaviour. Especially the R-values of 2.5 m window length respond well to Earth's obliquity and precession (Fig. 2.29). This indicates that  $\chi$  and carbonate correlation might have a link to

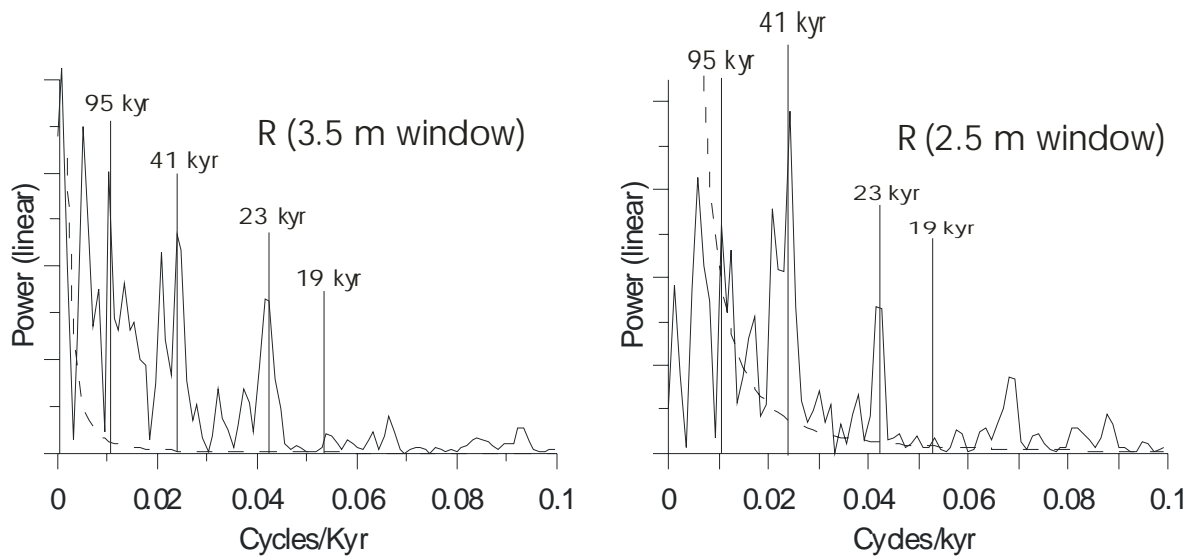


**Fig. 2.29** Spectral results on correlation coefficients of window lengths 3.5 m and 2.5 m. The results show clear Milankovitch cyclicities where the obliquity and precession are dominantly observed. The cyclicities are clearly above the 95% confidence level.

the global climatic signal. Further spectral analysis was also carried out for larger window lengths and the results show that the smaller periods (higher frequencies) are fading with an increase of window length. Based on these spectra, it may be concluded that smaller windows are mainly responding to small-scale climatic variations (2.5 window show clear 41 kyr and 23 kyr, cyclicities) and the bigger windows exhibit larger variations. Susceptibility, ARM, SIRM are controlled by both a regional and global signal with globally controlled variations of R. This might be a reason why  $\chi$ , ARM, SIRM do not show the precession cycle.

**Wavelet analysis**

Local variations of power within a time series can be analyzed using wavelet transform. The wavelet transform has been used in numerous studies in geophysics (especially it is mostly used in seismics). Since the last decade it has been also successfully used in climate investigations. By decomposing a time series into time-frequency space, the dominant variability and its variation with time can be determined. (Torrence and Compo 1997). Wavelet analysis measures the similarity with basic functions called wavelets. Wavelet transform can be explained by equation

$$\gamma(s, \tau) = \int f(t) \psi_{s, \tau}^*(t) dt$$

which shows how the function  $f(t)$  is decomposed into a set of basic functions  $\psi_{s, \tau}(t)$  called wavelets.  $\psi^*$  is complex conjugate of  $\psi$ . The variables  $s$  and  $\tau$  are scale and translation, which are the new dimensions after the wavelet transform. The inverse wavelet transform is given by the equation

$$f(t) = \iint \gamma(s, \tau) \psi_{s, \tau}(t) d\tau ds$$

The wavelets are generated from a single basic wavelet  $\psi(t)$ , the so-called mother wavelet, by scaling and translation.

$$\psi_{s, \tau} = \frac{1}{\sqrt{s}} \psi\left(\frac{t - \tau}{s}\right)$$

where  $s$  is the scale factor,  $\tau$  is the translation factor and the factor  $\sqrt{s}$  is for energy normalization across different scales.

To explore the local variations of power within the time series, susceptibility and carbonate data sets were subjected to wavelet transform using Matlab software. Morlet wavelet function was used for the analysis. Prior to the wavelet analysis the data of carbonate and susceptibility was sampled to equally time space and later was normalized using their

**Table 4. Details of spectral power of obliquity and precession between 350-750 ka**

	Obliquity	Precession
Carbonate	350-750 ka	500-700 ka
Susceptibility	500-750 ka	450-500 ka
	< 250 ka	550-620 ka

mean and standard deviation. Both wavelet results of carbonate and  $\chi$  data sets show similar power spectra. In both cases the maximum power is seen for the 95 kyr period and it is interesting to note that the highest power is concentrated between about 300 to 750 ka (i.e. 50 m to 140 m). It is observed that the smaller periods 41, 23, 19 kyr have much less power and are mainly confined to 450-800 ka (table 4, Fig. 2.30a,b).

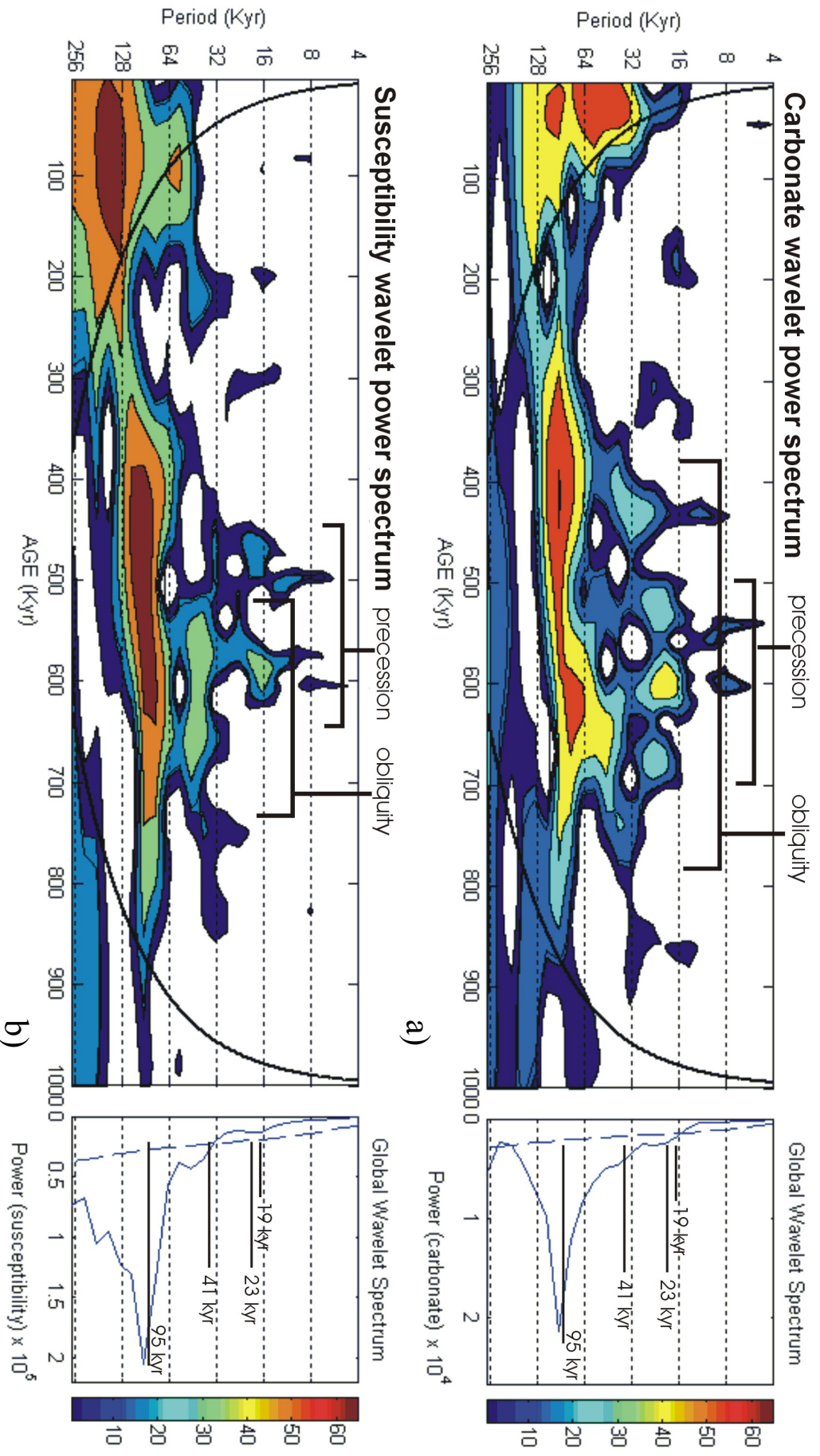
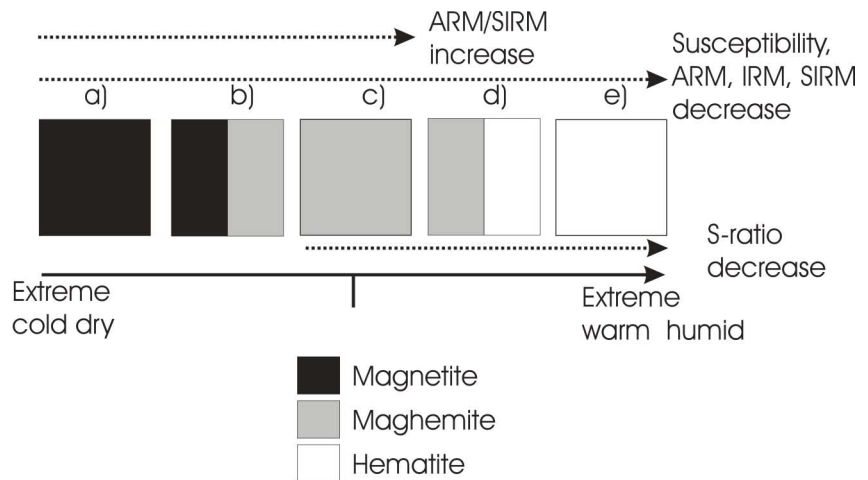


Fig. 2.30 Wavelet power spectra a) carbonate and b) susceptibility (carbonate-free). Both of them show the dominance of 95 kyr cycle. The total sum of the power of the spectrum is shown as global wavelet spectrum. The thick line indicates 95% confidence level. The color scales of the spectral power are shown at the far right .

## 2.4.5 Discussion and conclusions

From the pollen results *Picea-Tsuga* and *Pinus* were chosen to subdivide the core into zones (Yang et al., 2000) because they are dominant components growing in their own spectrum today with sensitive response to climate changes. Yang et al. (2000) make use of treeline pollen as well as other pollen taxa to infer palaeoclimatic changes in the region. The pollen analysis reveals alternations between temperate-humid (indicated by high *Pinus* and high *Tsuga*) and cold-dry climatic conditions (indicated by low *Tsuga* and low total tree). As the lake is surrounded by limestones and the carbonate content is very high the main input of carbonate is detrital. Microscope analysis reveal that the samples contain micro-crystals or pseudo-crystals suggesting that authigenic production of carbonate accompanies the carbonate of detrital origin. Usually carbonate content plays a major role in dilution of magnetic mineral concentration but this occurs mostly in marine environments. However, the carbonate content in Heqing basin does not play a dominant role in dilution of magnetic minerals

During cold and dry conditions, vegetation and soil formation are limited producing rapid terrigenous sedimentation, which causes input of larger magnetic particles. During warm and humid conditions vegetation and soil formation are enhanced restricting erosion, causing input of finer magnetic particles. It is confirmed that maghemite and magnetite are the predominant magnetic phases in the Heqing core with some contribution of hematite. Differences in magnetic mineralogy can be expected to be the dominating control factor of magnetic variations due to regional environmental conditions. The link of magnetic mineralogy to climate at Heqing basin could be explained with a scenario of magnetite alteration (low temperature oxidation) (Fig. 2.31). At room temperatures magnetite gradually oxidizes to maghemite which may further transform to hematite (Tang et al., 2003). The oxidation process occurs



**Fig. 2.31. Inferred scenario of the transformation processes from magnetite to maghemite and hematite with relation to climatic conditions. a) magnetite, b) magnetite+maghemite, c) maghemite d) maghemite+hematite e) hematite. The arrow from left to right indicates the increasing trend of temperature and climatic conditions from cold dry to warm humid.**

At room temperatures magnetite gradually oxidizes to maghemite which may further transform to hematite (Tang et al., 2003). The oxidation process occurs

at the surface by diffusion of Fe<sup>2+</sup> from crystal interior to surface and further Fe<sup>3+</sup> is formed (Dunlop and Özdemir, 1997). When the crystals are larger in dimension the particle interior may not be affected at all (Cui et al., 1994). As grain size of eroded particles is larger during cold-dry conditions the transformation process of magnetite to maghemite is expected to be relatively slower in cold dry conditions than in warm humid conditions.

The complete transformation process of magnetite to hematite from extreme cold dry to extreme warm humid conditions can be explained as follows, a) During extreme cold dry conditions coarse grained magnetite is eroded and deposited without significant alteration (rarely observed in the Heqing basin) (Fig. 2.31a). b) Magnetite is eroded in less coarse grain size and partially transformed to maghemite during cold dry conditions and exhibits magnetic mineralogy as magnetite+maghemite (Fig. 2.31b). c) In warm humid conditions the process of magnetization is advanced, allowing magnetite to be completely transformed to maghemite, demonstrating mineralogy as maghemite (Fig. 2.31c). d) In further warm and humid conditions the transformation process continues to form hematite indicating mineralogy as maghemite+hematite (Fig. 2.31d). e) In extreme warm and humid conditions the transformation is complete and hematite is formed (Fig. 2.31e). The cases b and c are most common in lake Heqing. It is interesting to note that, above the depth of ~65 m the mineralogy is more controlled by mixed mineralogy (maghemite and magnetite) which could be due to cold and dry climatic conditions. Also the pattern of  $\chi$  and carbonate variations are different in the upper and lower parts. More pronounced  $\chi$  fluctuations occur only in the lower part (below 65 m). In the upper part (12-65 m), the mean level of  $\chi$  is clearly higher ( $113 \times 10^{-8} \text{ m}^3 \text{ kg}^{-1}$ ) than in the lower part ( $45 \times 10^{-8} \text{ m}^3 \text{ kg}^{-1}$ ), arising from the additional occurrence of magnetite. As discussed earlier ARM/SIRM ratio is expected to be mainly controlled by the mineralogy. The low values may correspond to maghemite+magnetite and higher values point to maghemite with small portion of hematite. ARM/SIRM is strongly in accordance with the identified magnetic mineralogy at respective depths, hence it could be used as a high resolution magnetic mineralogy scale. ARM/SIRM may also indicate magnetic grain sizes, wherever magnetite content is relatively higher it could be expected that the magnetic grain sizes are relatively larger (from the above scenario a decreased effective magnetic grain size can be expected by inhomogeneous degree of maghemitization). Low values of ARM/SIRM between 10 to 65 m are well supported by the predominant occurrence of maghemite+magnetite. S-ratio is better for distinguishing hard component phases like hematite; lower values dominate in the presence of hematite. From the results, lowest values occur only at the uppermost part of the core (0-10 m). Significant decrease in S-ratio and increase in ARM/SIRM ratio above 10 m (~70 ka) could be explained by the presence of hematite-like phase and also

could indicate a strongly warm period. The indication of hematite phase comes from SIRM thermal demagnetization experiments.

Pollen is the most reliable direct proxy for regional climate in continental sequences. Point-to-point correlation of  $\chi$  and carbonate to pollen data is poor. However *Tsuga* (one of the tree pollen) is corresponding well with magnetic mineralogy. The total tree pollen taxa in general indicates forest conditions at the lake catchment. Remarkable fluctuations of the tree pollen level above 40 m (Fig. 2.17) demonstrate an opening and closing of forests. The drastic decrease at depths of 25 m may indicate most extreme cold-dry conditions prevailed during this period. It has to be mentioned that the total tree pollen usually respond to extreme conditions of climate (can resist to a larger temperature window). The increase in herb pollen at these depths (20 m) confirms that these observations are reliable. Higher values of *Tsuga* usually characterize temperate-humid conditions (at the areas of east Asia) and its strong accordance with higher values of ARM/SIRM is quite supportive to the above discussed magnetic mineralogy scenario. From pollen and magnetic mineralogy, temperate humid phases can be identified at 990-960 ka, 800-780 ka, 690-670 ka, 630-620 ka, 580-570 ka, 530-520 ka, 450-420, 360-340, 215-200 and 65-35 ka.

The correlation coefficient along the depth indicates a change in depositional system above  $\sim 55$  m. When the larger window lengths are taken into account (Fig. 2.22), it seems that R is in general controlled by rate of deposition. It is mainly positive during lower rates of deposition and negative during higher rates of deposition. It is evidential from the spectral analysis of wavelength domain i.e. the shorter wavelengths in the upper part of the core and tendency of decrease in the wavelengths at the bottommost part of the core are corresponding with strong positive correlations above 55 m and below 150 m (Fig 2.22). As discussed above the correlation coefficients of smaller windows lengths seem to represent small scale climatic fluctuations and unfortunately it is quite difficult to give a convincing explanation why it represents Milankovitch cyclicities.

The close link between ARM/SIRM and *Tsuga* with the clusters is certainly fascinating. Comparing pollen and magnetic parameters relation with the clusters, we may interpret that each cluster could represent a climate pattern. Categorizing the clusters it appears that the first cluster represents temperate/warm climate (corresponding to high *Tsuga*), the second illustrates relatively cold/dry climate (corresponding to lower *Tsuga*) and the third might indicate a moderate climate. One might expect that the positive correlation between carbonate and  $\chi$  of larger scale (larger windows) above the depths of 50 m would influence the cluster results but cluster analysis done on different combinations show almost the same cluster grouping pattern which confirms that the cluster results are trustworthy.

The spectral results of the whole core of carbonate,  $\chi$ , ARM, SIRM show dominant cycle as 95 kyr, which is supposed to be weak in terms of solar radiation. This behavior is seen also in many records around the world, convincing results coming from marine cores. Since the last three decades it has been suggested that this behaviour could be due to beat effect from the two main precession periodicities (Wigley 1976). Simplified glacial dynamics models and zonally symmetric model of global energy balance forced by orbital parameters can also have such power. Some researchers propose that the high power is due to the internal system (Imbrie et al. 1993), which is related to cryosphere-lithosphere. However a convincing reason could not be given for the high power of 95 kyr due to the difficulty that, the power is not constant all over the period and also have been found at time there was no ice sheet on the Earth (Berger, 1988). The spectral analysis on the pollen data shows insignificant results confirming that they are more confined to the regional climatic signal rather than the global signal. As

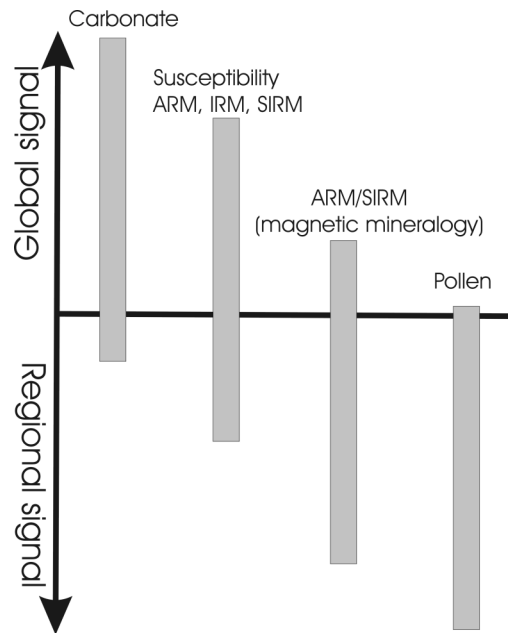


**Fig. 2.32 Inferred response of various parameters to global and regional climatic signal.**

discussed earlier the spectral results of magnetic parameters  $\chi$ , ARM, IRM, SIRM show a clear global signal. ARM/SIRM spectrum represents only Earth's eccentricity which might be due to slight influence of magnetic concentration variations which indirectly affect ARM/SIRM ratio (ARM/SIRM variations are related to magnetic grain size). Summarizing the above discussions it seems that the regional signal least influenced carbonate variations, moderately the magnetic concentration parameters  $\chi$ , ARM, SIRM, more the magnetic mineralogy (ARM/SIRM) and largest the pollen variations (Fig. 2.32). The wavelet power spectrum shows that the maximum power is concentrated between 50 to 140 m. At these depths most of the parameters show cyclic behaviour and also highest rates of deposition 18 to 19 m /kyr are observed from wavelength analysis. It may be interpreted that high rates of deposition could have played an important role in better recording of climatic signal.

The wavelengths and correlation coefficients show low lake level conditions above 65 m, which may be due to weakening of monsoons. The depths between 10 to 50 m (80 to 320 Ka) show low *Tsuga* and heterogeneous magnetic mineralogy and fall in same cluster group which demonstrates a cold and dry climatic conditions during this period at the SE margin of the Tibetan plateau. The winds coming from the southwest of India may have

carried moisture and latent heat due to evaporation and may have strengthened the monsoon. If the Tibetan plateau is colder, the sensibility decreases and one expects lower intensification of monsoon (Hagelberg and Mix, 1991; Clemens et al. 1991). They are several evidences that Marine Isotope Stage 11 (MIS 11) around 400 kyr BP (Loutre, 2003) may have been the longest and perhaps warmest interglacial period of the last 500,000 years

(McManus et al., 1999) with partial melting of Greenland ice sheet and possible complete or partial collapse of Antarctic ice sheets (Hearty et al., 1999; Scherer et al., 1998). Also Droxler et al. (1999) argue that the MIS12 to MIS 11 represents the highest amplitude deglaciation within the last several Ma

The calculation of insolation variations for this time period suggests that stable warm conditions existed (Berger et al., 1999). The corresponding orbital configurations and similar atmospheric greenhouse gas concentrations have led to the proposal that MIS 11 is a suitable, possibly the best, geological analogue for the natural development of Holocene and future climate. (Loutre, 2003). Some studies show that the sea level was 13-20 m higher than the present level during MIS 11 (Poli et al., 1999; Hearty et al., 1999; Scherer et al. 1998, Scherer 1999). The depths between 64 to 73 m (~ 400 - 465 ka) of Heqing core seem to resemble onset of MIS 11. At these depths, Tsuga, ARM/SIRM, S-ratios values and clusters seem to indicate stable warm humid conditions. Also at these depths the susceptibility and laboratory remanences demonstrate constantly lower values. A clear change in the pattern of magnetic, carbonate, grain size, pollen content variations and clusters at about 55 m is interesting; it could also be linked to a strong regional palaeoclimatic signal at about 360 ka. An upliftment phase of Tibetan plateau might be responsible (Hu et al. 1999) superimposed to the global signal during this period. The

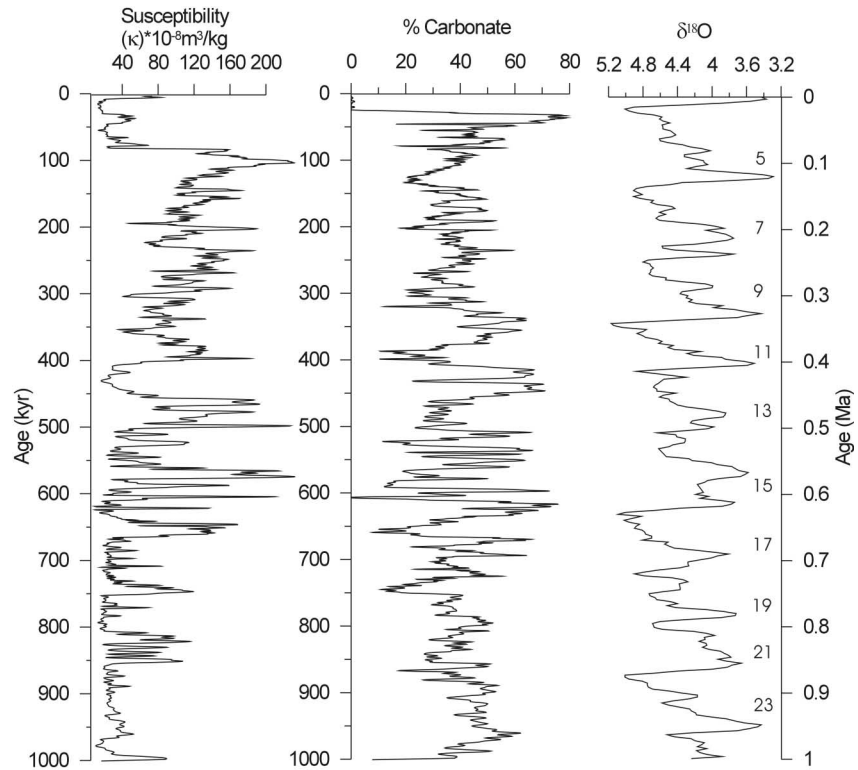


**Fig. 2.33. Magnetic susceptibility(carbonate free) and carbonate with tuned age and its relation with marine oxygen isotope record**

strong anomaly observed at the depths of ~ 65 m (discussed above as it resembles onset of MIS 11) might be a beginning phase of the clear changes occurred at 55 m. However it is difficult to verify whether the anomaly at 65 m and the changes in variations at 55 m are interlinked or they are individual events. Susceptibility and carbonate show a correlation with the marine oxygen isotope curve (Fig. 2.33) demonstrating that the core has a strong tie to the global climatic signal.

The top of the sequence between 0-12m, where  $\chi$  returns to very low values, is difficult to interpret. In the uppermost 3 m, carbonate content dramatically decreases to less than 5%. Meanwhile, coarser fluvial deposits replaced lacustrine sediments, and the ancient Heqing lake disappeared.

Summarizing the above discussions we may conclude that the results demonstrate that Heqing lake is a promising archive for studying long-term change of palaeoclimate and palaeoenvironment. The High-resolution magnetostratigraphy of Lake Heqing provides a reliable polarity sequence based on maghemite and magnetite; magnetite might be responsible for some disturbances in the results. B/M boundary can be easily distinguished at 141.5 m. Blake event is clearly recorded at the depth of 17.2 m. The bottom most samples show positive polarity indicating the Jaramillo subchrone. Both Blake event and Jaramillo are confirmed with tuned age model. Based on spectral analysis of carbonate, susceptibility and SIRM, constant sedimentation rates of 15 cm/kyr and 19 cm/kyr are estimated for 30–65 m and 65–120 m respectively; a tendency to lower rates is indicated below 120 m. The tuned age model provides the optimum transformation of depth into time which is determined by cubic spline interpolation of tie points from wavelength model, radiocarbon dating and magnetic ages. Conversion of depth into time is shown in table 5. Accordingly the Heqing core spans almost the complete past 1 Myr (5-1,001 ka). Spectral analysis shows clear Milankovitch cyclicities and the susceptibility, carbonate records shows a rough correlation with marine oxygen isotopes. This suggests that the climate record from the Heqing core has a strong and direct tie to the global climate changes. The strong anomaly of the magnetic and non-magnetic parameters at the depth of ~ 65 m (about 400 ka) and their clear changes at 55 m (about 360 ka) illustrates that a major climatic and/or tectonic event could have occurred, which may be regional or global, or both together. The pollen and magnetic mineralogy records of Heqing lake responds to regional and regional + global climatic changes respectively.

Table 5. Conversion of depth into time of Heqing core by tuned age model.

Depth (m)	Age (Ka)						
0.25	4	46	290.34	92	563.82	138	761.4
1	9.66	47	296.87	93	568.06	139	767.11
2	17.01	48	303.43	94	572.24	140	772.95
3	24.15	49	310.01	95	576.38	141	778.91
4	31.1	50	316.61	96	580.47	142	785
5	37.88	51	323.24	97	584.52	143	791.22
6	44.49	52	329.89	98	588.54	144	797.58
7	50.96	53	336.57	99	592.51	145	804.07
8	57.3	54	343.27	100	596.46	146	810.71
9	63.52	55	350	101	600.38	147	817.5
10	69.65	56	356.75	102	604.28	148	824.44
11	75.69	57	363.52	103	608.16	149	831.53
12	81.66	58	370.29	104	612.03	150	838.79
13	87.58	59	377.07	105	615.88	151	846.2
14	93.45	60	383.85	106	619.73	152	853.78
15	99.3	61	390.61	107	623.57	153	861.53
16	105.15	62	397.36	108	627.41	154	869.46
17	111	63	404.08	109	631.26	155	877.56
18	116.87	64	410.76	110	635.11	156	885.84
19	122.76	65	417.41	111	638.98	157	894.31
20	128.67	66	424	112	642.85	158	902.97
21	134.61	67	430.54	113	646.75	159	911.82
22	140.57	68	437.02	114	650.67	160	920.86
23	146.55	69	443.43	115	654.62	161	930.11
24	152.55	70	449.76	116	658.6	162	939.56
25	158.57	71	456.01	117	662.61	163	949.22
26	164.62	72	462.16	118	666.66	164	959.09
27	170.69	73	468.22	119	670.75	165	969.17
28	176.78	74	474.16	120	674.89	166	979.47
29	182.89	75	480	121	679.08	167	990
30	189.03	76	485.72	122	683.31	168	1000.75
31	195.19	77	491.32	123	687.61		
32	201.37	78	496.8	124	691.96		
33	207.57	79	502.18	125	696.38		
34	213.8	80	507.45	126	700.87		
35	220.05	81	512.62	127	705.43		
36	226.32	82	517.69	128	710.07		
37	232.62	83	522.66	129	714.78		
38	238.94	84	527.55	130	719.58		
39	245.28	85	532.35	131	724.46		
40	251.65	86	537.06	132	729.44		
41	258.04	87	541.7	133	734.51		
42	264.45	88	546.26	134	739.67		
43	270.89	89	550.75	135	744.94		
44	277.35	90	555.17	136	750.32		
45	283.83	91	559.52	137	755.8		

### 3. A study on Kathmandu basin

#### 3.1 Geological settings, lithology and sampling of Kathmandu basin

Kathmandu valley located in the central Nepal, is one of the large intermontane basins in the Lesser Himalayas with an average altitude of 1400m above sea level. The basin measures ~25 km NS and ~30 km EW covering an area of ~650 km<sup>2</sup>. The basin is flanked by mountain ranges of ~2500 m altitude. Bagmati river which was responsible for basin fill sediments, still exists. It cuts the Mahabharat Range in the south and drains into the Gangetic plane (Fig. 3.1a). The northern slope of the basin is mainly composed of gneiss

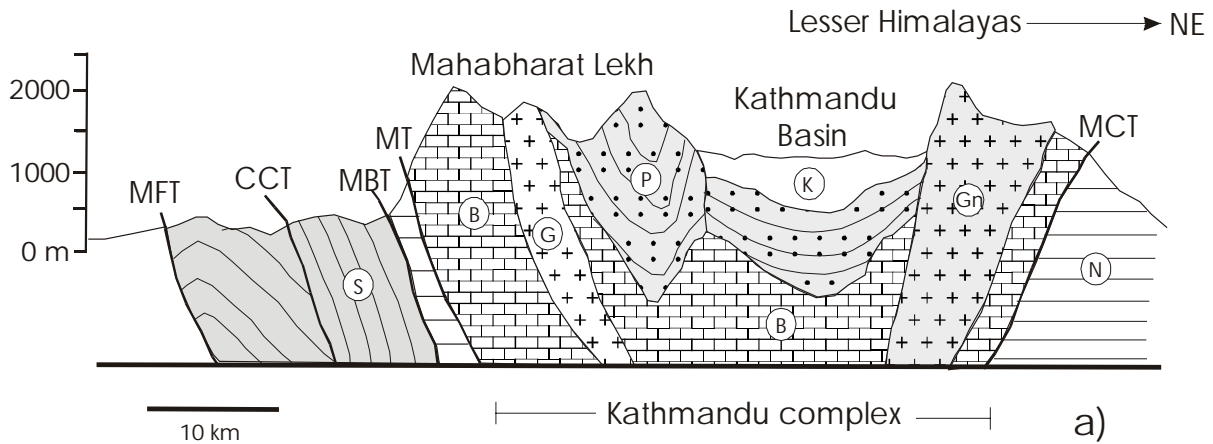
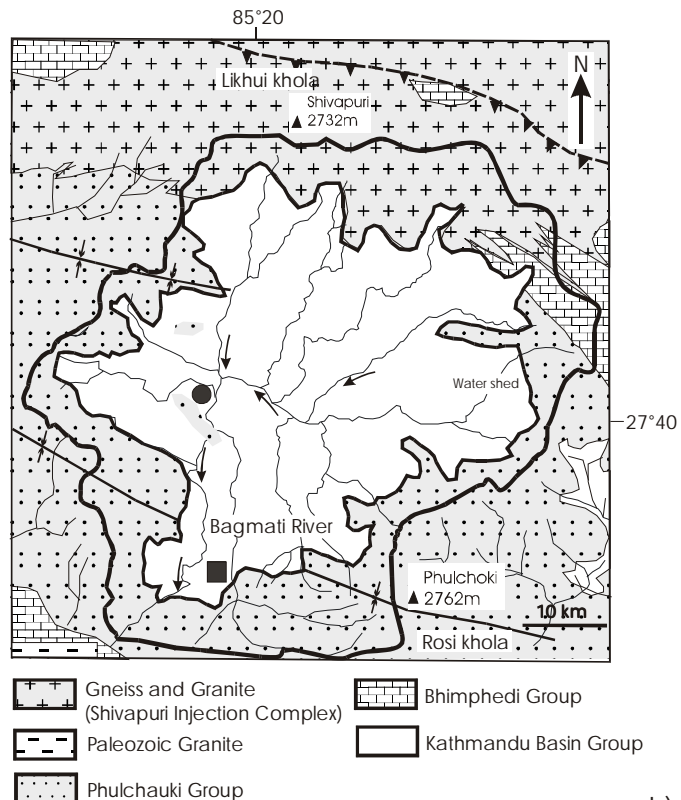


**Fig.3.1 a)** A schematic geological cross section in the Central Nepal Himalayas (modified after Stöcklin and Bhattarai, 1981). S: Shivalik group, B: Bhimphedi group, P: Phulcauki Group, N: Nawakot group, G: Granite, Gn: Gneiss complex, K: Kathmandu complex, MFT: Main Frontal Thrust, CCT: Central Churia Thrust, MBT: Main Boundary Thrust, MT: Mahabharat Thrust (Main Central Thrust : MCT).

**b)** Simplified geological map of Kathmandu valley region (modified from Stöcklin and Bhattarai, 1981). The arrows show the present flow direction of the river. The circle is the location of drill core JW3 (Sakai, 2001) and the square shows our sampling area (Lukundol village).



and granite, called the Shivapuri Group, while in the NW part of the valley Palaeozoic Tethyan rocks (Phulchauki Group) are outcropping, stretching to the south. The southern part of the Kathmandu basin is composed of the Shivapuri Group, and schists and marbles of the Bhimphedi Group are overlaid by the Phulchauki Group. Figure 3.1b shows a simplified geological map of Kathmandu basin and the location of the sampled section. The total thickness of the sediments is estimated to be about 600m (Moribayashi, 1980), based on gravity data. The expected time span of sedimentation is mid-Pliocene to Pleistocene.

The inconsistency in the usage of the formation names by earlier researchers working on this basin, have given rise to confusion in stratigraphic division of the lake. Sakai (2001) published a convincing proposal for a new stratigraphic division based on his several drill cores at different areas of the basin and correlating it with previous work (Table 6). From the new stratigraphic division, our study area is confined to Itaiti formation and Lukundol formation (marked in Table 6). In the southern part of the basin (Lukundol village), a sequence of about 120 m was sampled (Lukundol Fm.). Approximately 70 m of gravel and debris overlies this sequence (Itaiti Fm.). A detailed lithology of the sampled section can be seen in Figure 3.2. The sampled formation can be divided into two parts. The topmost part is mainly comprised by repetition of a fining upward sequence of gravel, fine sand and silty clay with carbonaceous mud in the ascending order. Mainly mud, silty clay, clay beds intercalating with lignite beds and a few sand beds represent the bottom part of the formation. For sampling the weathered layer was removed about 2 cm deep using a pick

**Table 6. Stratigraphic position of the sampled Lukundol Fm section and its correlation with the newly proposed stratigraphy (Sakai, 2001) and other workers. The black bar shows our sampled stratigraphic position.**

Yoshida and Igarashi (1984) Yoshida and Gautam (1988)		Dongol (1985, 1987)	Shrestha et al (1998)	Sakai (2001)	Sakai (2001)			
					Southern part	Central parts		
Patan Fm		Kalimati Clays	Gokarna Fm Takha Fm Kalimati Fm & Chapagaon Fm	Lukundol Formation	Upper member	Itaiti Fm		
Thimi Fm								
Gokarna Fm								
Borogaon Terrece deposits		Champi lthari Gravel			Lukundol Fm & Kobgaon Fm		Middle member	Lukundol Fm
Chapagaon Terrece deposits								
Pyanggaon Terrece deposits								
Lukundol Formation	VII	Nakhu Khola Mudstone & Kaseri-Nayankhandi Lignite	Lukundol Fm & Kobgaon Fm	Lower member		Tarebhir Fm		
	VI							
	V							
	IV							
	III							
	II	Tarebhir Basal Gravel	Basal Boulder bed	Lower member	Tarebhir Fm			
	I					Bagmati Fm		

axe and then oriented samples (in total 750) were collected in 10 cm<sup>3</sup> plastic boxes at an interval of 10 cm, using a self-designed corer. Additionally a number of 128 samples were taken for pollen analysis (several grams) with an interval of 50 cm. Sampling could not be done at a few places due to inaccessibility and un-exposure of the formation. Yoshida and Gautam (1988) has done magnetostratigraphic work in this area, but with much lower sampling resolution.

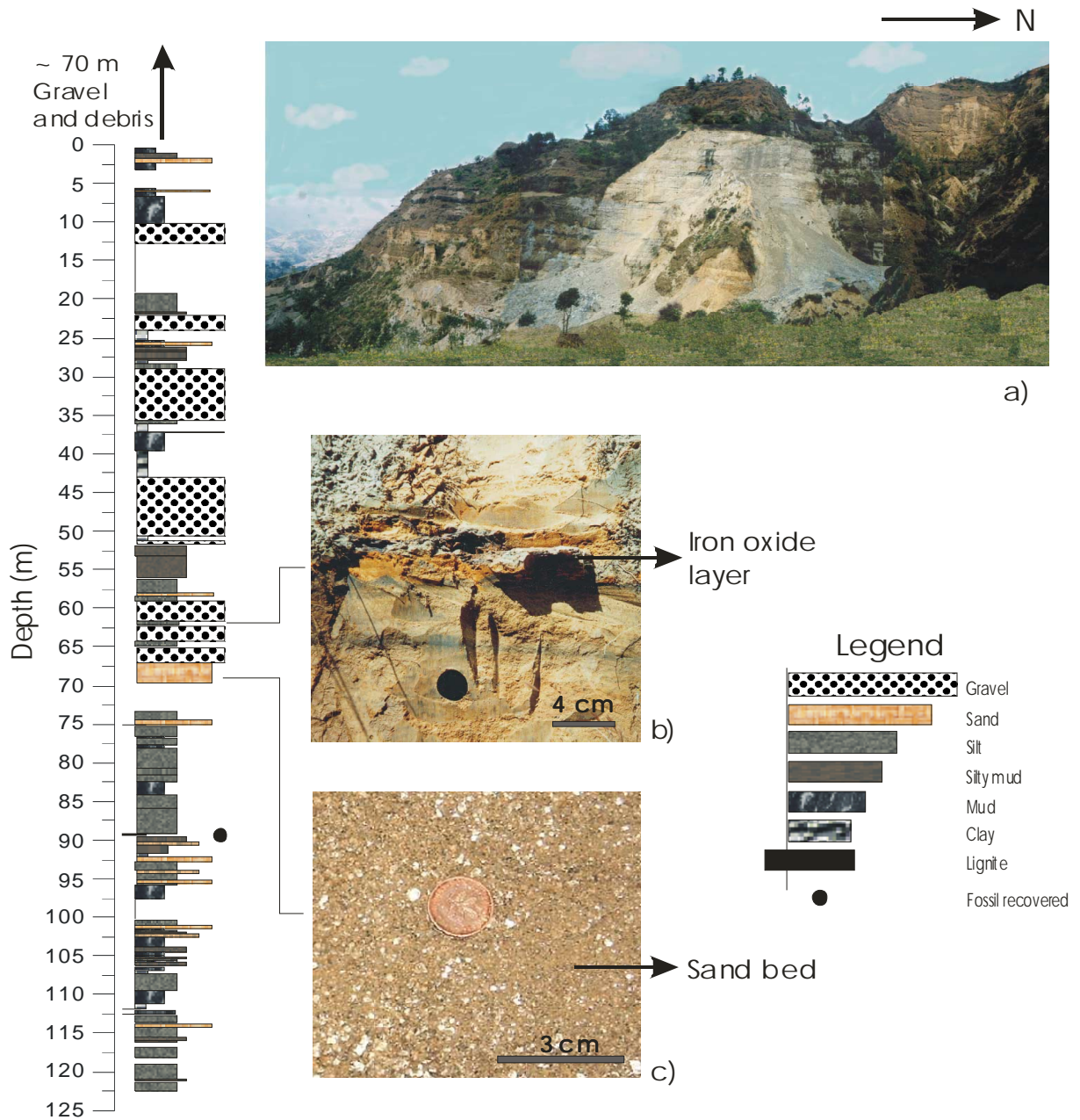


**Fig. 3.2** A detailed lithostratigraphy section of the sampled section (Lukundol formation). (a) Exposure of the Lukundol formation, (b) highly oxidized iron oxide (possibly limonite), (c) sand bed rich in mica.

## 3.2 Dating and palaeoclimate at Kathmandu basin

### 3.2.1 Dating

#### ***Magnetic mineralogy and Magnetostratigraphy***

Low temperature susceptibility measurements were done on selected samples by using a KLY-3 kappabridge and CS-3 temperature unit. Verwey transition is observed in some samples (Fig. 3.3a) indicating the presence of multidomain magnetite which is likely of detrital origin. High-temperature susceptibility measurements up to 700 °C are dominated by secondary formation of magnetite during heating and are not indicative for the initial magnetic mineralogy.

A number of 64 samples were chosen for IRM acquisition (using a MMPM9 pulse magnetizer). The results show two types of behaviour. For the majority of the samples >90% of the saturation is acquired around 250-350 mT and nearly complete saturation is reached at about 550-700 mT for most samples (Fig. 3.3b). After IRM acquisition, back field demagnetization was done along the same axis. Remanence coercive force ( $H_{cr}$ ) is between 35-60 mT for almost all the samples (Fig.3.3b). Both acquisition and backfield measurements indicate a relatively soft magnetic component (magnetite, titanomagnetite, maghemite or greigite). Some samples which have relatively lower NRM and susceptibility ( $\chi$ ) acquire saturation magnetization at about 1 T and have relatively higher  $H_{cr}$  values.

After IRM acquisition, a set of samples showing higher and lower susceptibilities were selected for thermal demagnetization (using MMTM18 furnace). The results show that the samples have a mixed magnetic mineralogy (Fig. 3.3b). Almost all the samples contain magnetite (maximum unblocking ~ 580°C) and hematite (maximum at ~ 680°C) (Fig. 3.3b) but their concentrations differ. A significant decrease in magnetization is observed between the temperatures 300 to 400°C for almost all the samples indicate presence of maghemite. The samples that have relatively higher  $\chi$  values show a dominance of magnetite whereas the samples with low  $\chi$  show the dominance of hematite.

A few samples were chosen for ARM acquisition (varying the AF field with constant biasing DC field of 0.1 mT using a 2G ARM magnetizer 615). After acquisition, the samples were demagnetized along the same axis. Two types of behaviour could be distinguished, i.e. a relatively soft component with an intersection point of acquisition and AF-demagnetization curves around 25 mT and a harder component with an intersection at 55-60 mT (Fig. 3.3c). The mean susceptibility is  $304 \cdot 10^{-8} \text{ m}^3/\text{kg}$  for lower coercive component and  $87 \cdot 10^{-8} \text{ m}^3/\text{kg}$  for higher coercive component.

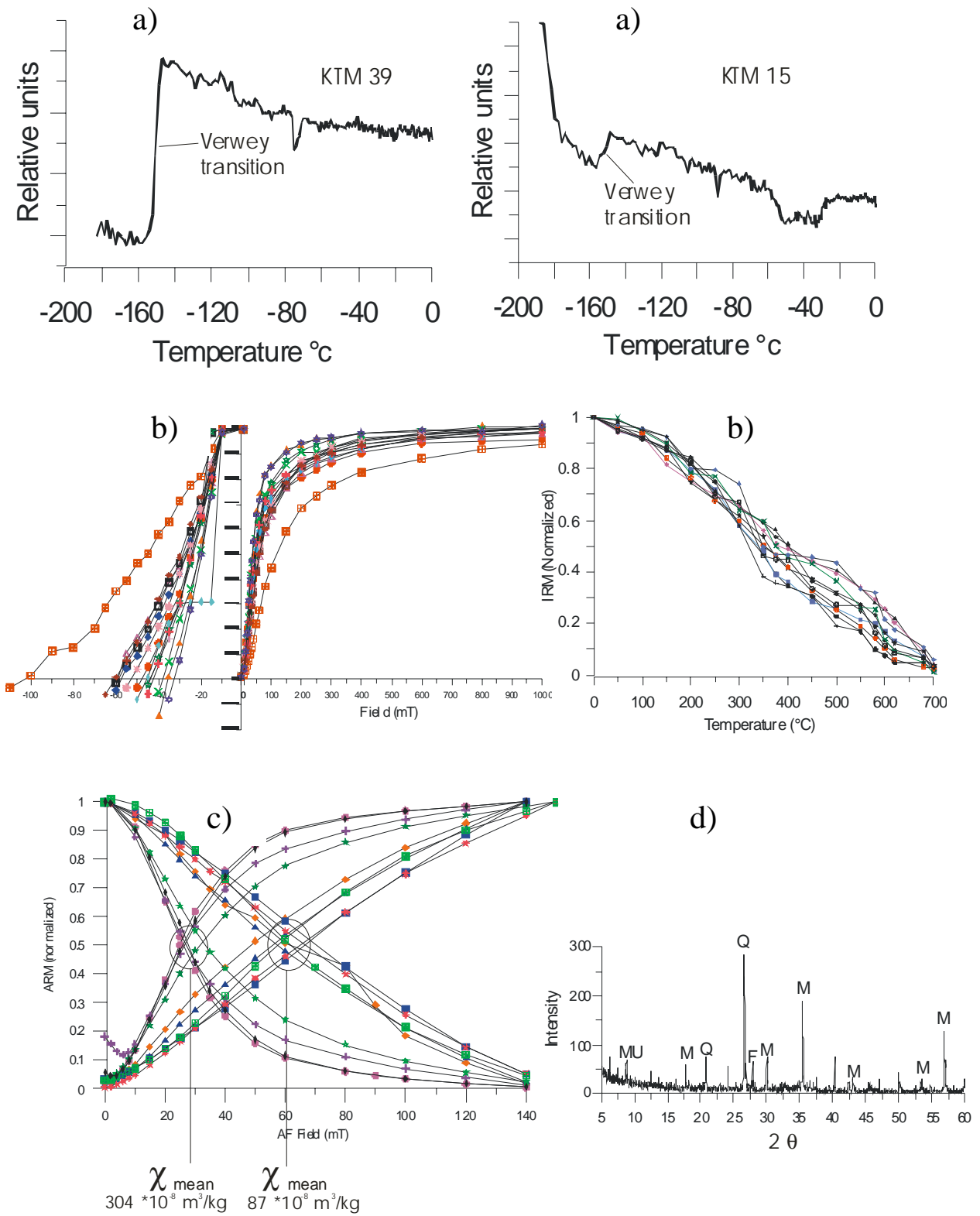


**Fig. 3.3 (a) Thermomagnetic analysis of low temperature variations of magnetic susceptibility for raw samples (b) Results of stepwise IRM acquisition, backfield along the same axis of acquisition and SIRM Thermal Demagnetization (c) ARM acquisition with an AF of 100 mT and biasing field of 0.1mT DC field and its demagnetization, the crossover points represent the coercivities showing two components (their  $\chi_{\text{mean}}$  is shown below) (d) Results of X-Ray diffraction on magnetic extract, showing M- Magnetite, MU- Muscovite, F- Feldspar, Q- Quartz.**

Magnetic extracts were prepared for few samples and XRD was performed with a Philips Bragg-Brentano diffractometer equipped with a secondary monochromator. The results show only magnetite among the magnetic minerals (Fig. 3.3d). The reason could be that the harder component could not be extracted efficiently and thus it was below the detection limit. Also the other expected magnetic minerals such as greigite(?), or maghemite (?) are below the detection limit.

Remanent magnetization was measured using a 2G RF SQUID magnetometer equipped with a degausser. About 40% of the samples showed a weak NRM ( $< 1.5$  mA/m). More than 350 samples with relatively stronger remanence were selected for alternating field demagnetization (AFD). About 30% of the results could not be used for determination of the characteristic remanent magnetization (ChRM) due to erratic behaviour. Most of the samples show the presence of two components (Fig. 3.4). Usually a softer component was removed at 10-15 mT showing a present field direction (Fig. 3.5a). The soft component may be carried by coarser

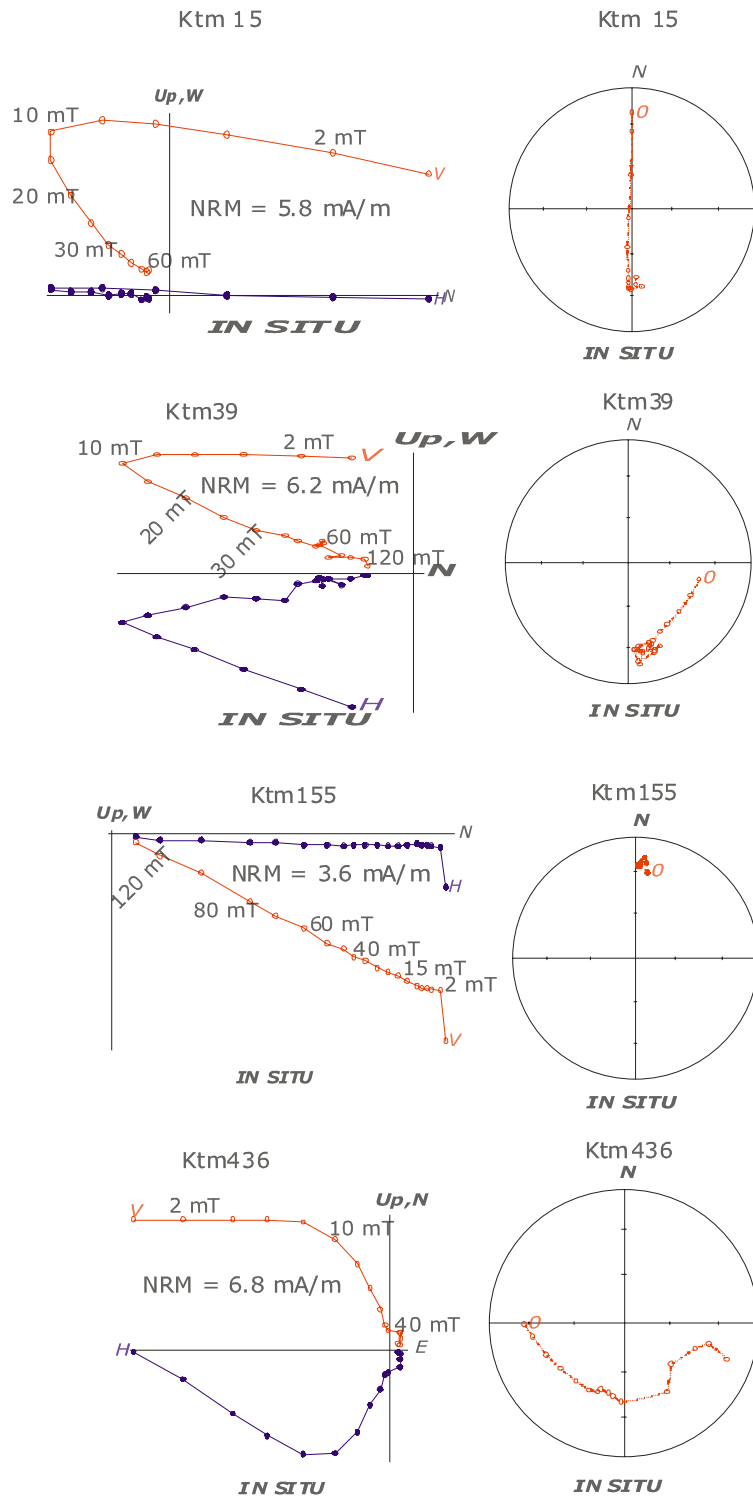


**Fig. 3.4 Results of alternating field demagnetisation for representative samples.**

grained magnetite. The second component is quite stable and is considered to be the ChRM. In most of the samples the ChRM directs towards the origin. The directions of ChRM were determined from straight demagnetization paths. NRM is reduced less than ~10% at an AF field of 70mT (~ 5% at >100 mT). In the peak AF fields above 100mT, most of the samples showed unstable behaviour. Few samples were selected for thermal demagnetization. Their remanence directions show similar results as for AFD. Some samples acquired a gyrometric remanent magnetization (GRM) at AF fields of >35mT. These samples were not used for magnetostratigraphy. The samples which acquired GRM may contain small portions of greigite ( $Fe_3S_4$ ) (Hu et al., 1998). Normal and reverse polarity directions are not antiparallel (Fig. 3.5b) indicating that the components could not be completely separated (also when 5° bedding dip is corrected) but sufficient for magnetostratigraphy. In Figure 3.5 the ChRM declinations and inclinations are plotted against their stratigraphic position. Remanence directions were not corrected for bedding as the layers are dipping only slightly (~ 5°). A systematic change in polarity transition is observed along the depth, which strongly suggests that the obtained ChRM is primary. Four magnetic transitions were observed in the polarity sequence, i.e. Brunhes/Matuyama boundary, Jaramillo (upper and lower boundaries) and possibly Cobb Mountain or Olduvai (upper boundary). ChRM declinations and inclinations are also plotted against depth excluding the gravel beds in Figure 3.6.

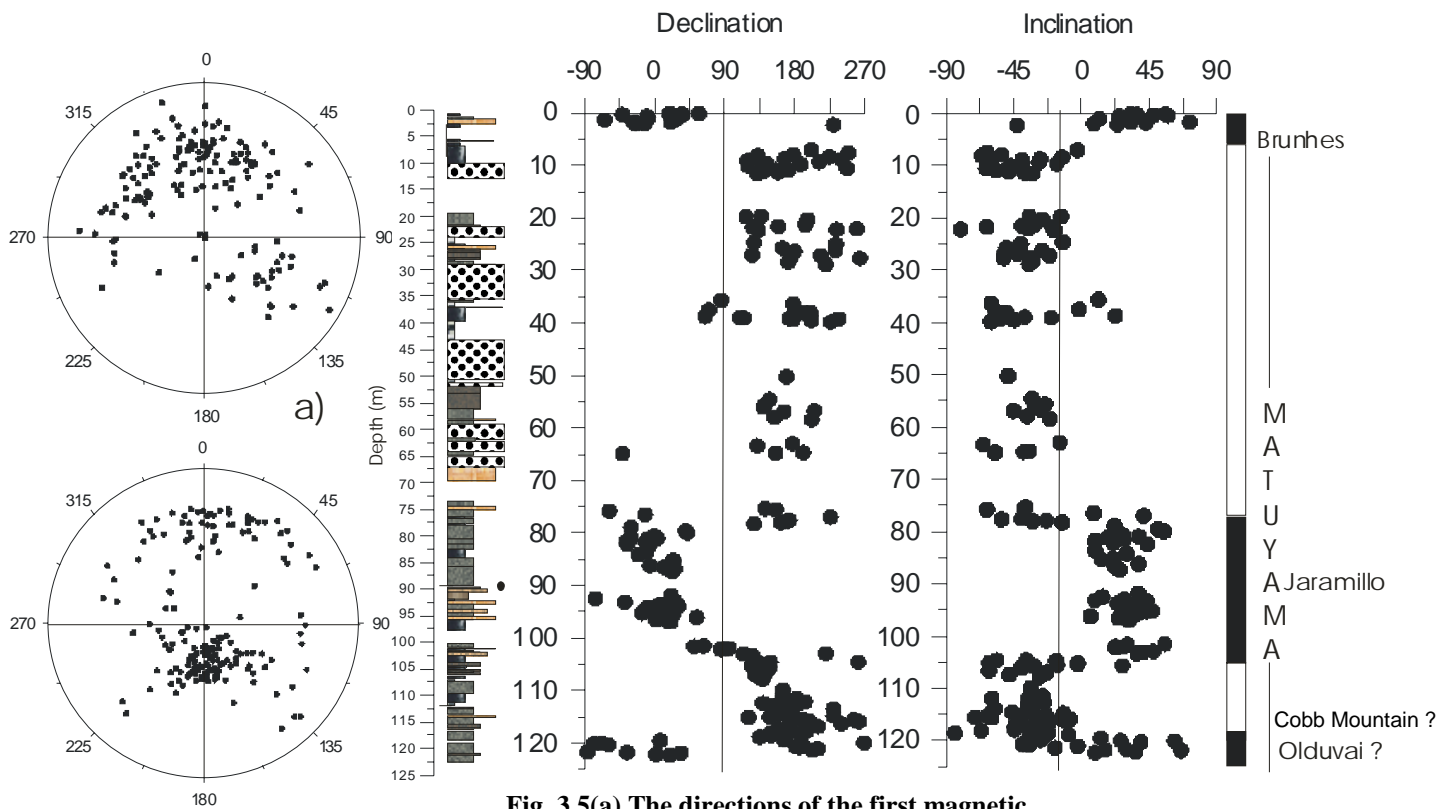


**Fig. 3.5(a) The directions of the first magnetic component (b) The directions of the second magnetic component. (c) Declination and inclination of ChRM verses depth with geomagnetic polarity time scale.**

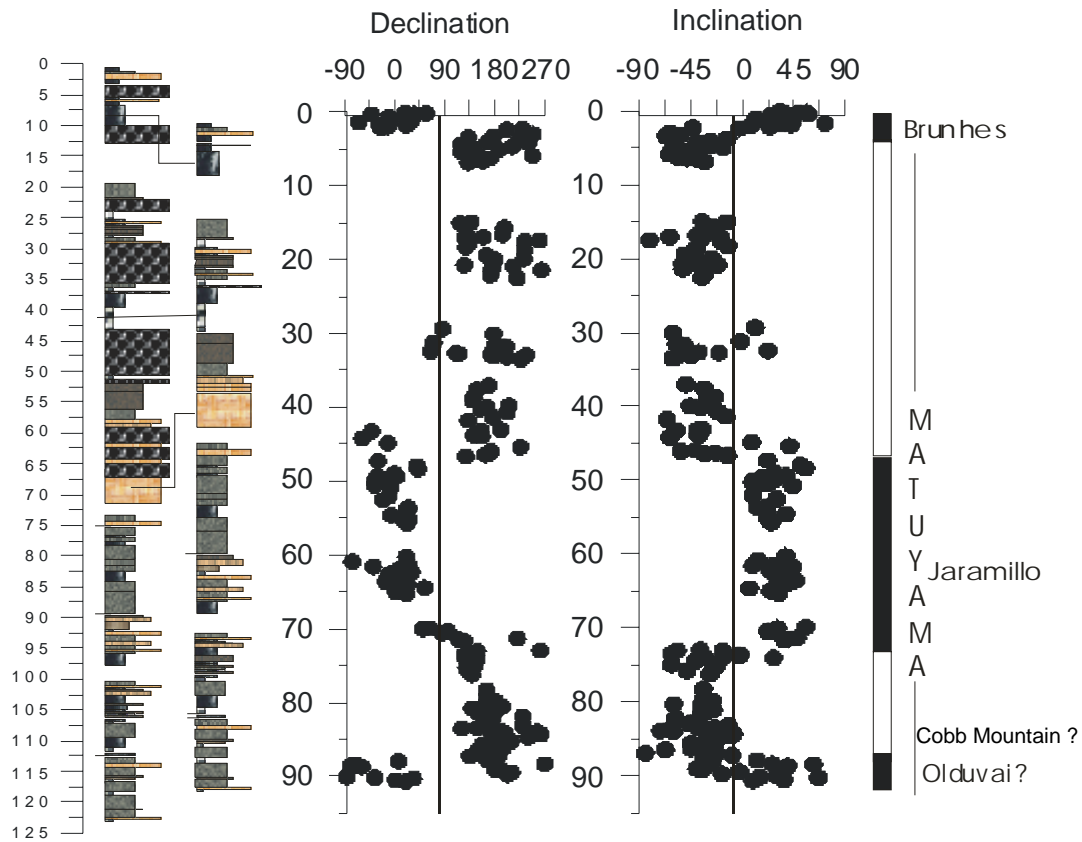


**Fig. 3.6. Declination and inclination of ChRM versus depth with geomagnetic polarity time scale excluding gravel beds.**

### ***Radiometric dating***

The deposition of the sampled section occurred between about ~0.7 Ma and ~1.1 or 1.8 Ma ago. This age window excludes the application of C-14 dating, because the C-14 clock is “dead” after about 60000 years. Other radiometric methods were checked for their applicability (A. Rocholl).

#### *U-Th disequilibrium method.*

As a most appealing alternative to C-14 dating, the U-Th disequilibrium method was envisaged. Given high U/Th ratios, closed system conditions and grain sizes sufficiently large to allow for physical separation from the matrix, this method is capable of dating minerals, especially carbonates, in the “age window” of a few to 500 000 years. In a first step, the sediments deposited in the uppermost part of the KTM basin were investigated in the field with the aim to find minerals that are potentially datable by U-Th disequilibrium. Unfortunately it became clear that exclusively clastic material had been deposited. No precipitates (such like carbonates) and no biogenic carbonate (such like shells of snails or

mussels) were observed in the upper part. If ever present, such shells were probably destroyed during the relatively violent transport and sedimentation of the clastic material. Second, the sediments available to sampling were friable and wet, i.e. they had not been sufficiently compacted and cemented by diagenesis to form a chemically closed system (a basic condition for any radiometric method). Both observations are true for the complete sedimentary succession and exclude the application of U-Th disequilibrium dating of the KTM sediments.

#### *Fission track dating*

Under favorable circumstances, *authigenic* apatite may form within the lacustrine environment and can theoretically be dated by fission track. A basic condition is its discrimination from *allochthonic* apatite derived from eroded country rock and transported together with the clastic freight. The discrimination between both types of apatite may be performed on the basis of chemical composition, grain shape and habitus and coexisting mineral phases. Also, it may be anticipated that, due to its relatively high density, *allochthonic* apatite is lacking in fine-grained sediments. Fourteen fine-grained were studied, partly carbon-rich horizons microscopically under the binocular and analysed by X-ray diffraction. In addition, four samples were separated by heavy liquid separation. In none of the investigated samples apatite was detected.

#### *U-Pb dating*

Theoretically, conventional U-Pb dating may successfully be applied to young samples, if uranium concentrations and U/Pb ratios are sufficiently high. Uranium is soluble under oxidizing conditions but becomes immobile when entering reducing environments. Therefore, carbon-rich sediments (clays and lignites) were considered as best "candidates" for the U-Pb dating approach, because (i) they reflect reducing conditions and (ii) are capable of fixing uranium and lead to organic molecules. We have determined the trace-element and Pb-isotopic compositions of seven fine-grained pairs of C-rich and adjacent C-poor or C-free horizons by means of ICP-MS. It was found that the uranium concentrations and the U/Pb ratios in the C-bearing sediments are not systematically increased (relative to the C-free horizons) to allow for U-Pb dating (Table 1). Possible explanations include (1) low abundances of dissolved U (to be trapped and concentrated by the organic material) in the sedimentary waters; (2) a too rapid deposition of the clastic and organic material to allow for U adsorption; (3) post-depositional Pb redistribution by diagenetic fluids; (4) intermingled clay minerals and other fine-grained silicates dominating the U-Pb budget. The latter two possibilities are supported by the fact that Pb isotopes are indistinguishable between carbon-rich and carbon-poor layers in spite of variable and different U/Pb ratios.

In summary, the combination of sedimentation age, sedimentation environment, mineral/chemical composition and still continuing diagenetic processes preclude the application of radiometric methods to date the KTM sediments.

### ***Amino acid dating***

In one of the intercalated lignite beds at the bottom part of the section (depth 88m), two fossils (elephant tooth) were recovered, which allowed the application of the amino-acid method (Oches and William, 1995).

The D/L ratios (ratio of D-form to L-form amino acids) for the most important amino acids are: D/L-Aspartic Acid = 0.70, D/L-Glutamic Acid = 0.55, D/L-Valine = 0.54, D/L-Phenylalanine = 0.85 , Alloisoleucine/Isoleucine = 0.67. They reflect the degree of racemization that has occurred in the sample during the entire period since the original formation of the tooth and include the effects of both, age and temperature history of the sample. There are three possible interpretations:

1. Assuming a slightly elevated post-burial temperature history, effective temperatures were similar to known standard samples in Hungary (for samples that weren't heated due to deep burial), thereby making the tooth possibly around 0.8 Ma old.
2. Assuming no significant elevation in temperature, effective temperatures were close to known standard samples in Czech Republic sites, thereby making the tooth considerably older than the B/M boundary, possibly close to 1.0 Ma.
3. Assuming that temperatures were significantly elevated during the period of lignite formation, the sample could be relatively young, with the high D/L and A/I ratios reflecting the elevated post-burial temperatures. However, this is unlikely because of the dominantly reverse polarity at the top of the section.

Summarizing from amino acid dating, the part of the section where the fossil was recovered has an age between 0.8 to 1.0 Ma. This is in good agreement with the magnetostratigraphic result.

## 3.3 Palaeoclimatic proxies

### 3.3.1 Pollen

All samples were prepared with HF, acetolysis solution and separated with  $ZnCl_2$  liquid treatment. Among analyzed 143 samples, 77 samples contained fossils (pollen analysis of Kathmandu part was done by Yaeko Igarashi, department of geology and mineralogy, Hokkaido University, Sapporo, Japan). Total numbers of pollen in each sample were 132 to 3883. Percentages of each taxa of pollen were calculated based on the total sum. Undeterminable taxa were included in non-arboreal pollen count. Samples taken between 42m and 65m in depth did not contain any pollen and spores. The pollen results are plotted against their stratigraphic position in Figure 3.7 According to the characteristics of the arboreal pollen assemblage the Lukundol Formation was divided into 14 pollen zones. The pollen assemblage of each zone was compared with the present flora and vegetation in central Nepal (Malla et al., 1976, Malla, 1986; Manandhar, 2002; Polunin and Stainton, 1984) and climate was inferred from characteristics of the pollen assemblage and ecology of some key genera included in the pollen assemblage based on the assumption that Pleistocene plants had climatic requirements similar to those of the modern ones.

In many cases we cannot discriminate species by pollen morphology, but we can discriminate genus. For example, genus *Pinus* includes alpine pine and species which grow in subtropical regions. However, all species of genus *Quercus* grow in places higher than 1500m a.s.l. Tree *Picea*, *Abies*, *Tsuga*, *Salix*, *Sorbus*, Ericaceae and *Ephedra* which grow from cool temperate to subalpine zones (2000 m to 4000 m a.s.l.) are indicators for a colder climate than at the modern Kathmandu Basin. Tree *Quercus*, *Juglans*, *Ulmus*, *Eleagnus*, *Ilex*, *Betula*, *Symplocos*, *Buxus*, *Corylus*, *Carpinus*, *Berberis*, *Osmanthus* and *Lonicera* which mainly distribute from warm temperate to cool temperate zones (1300m to 3000m a.s.l.) are indicators of cool climate. On the other hand, *Pinus*, *Alnus*, *Castanopsis* and *Jasminum* occur from subtropical to cool temperate zones. However, entomophilous *Castanopsis* is considerably important to show warm temperate climate when it occurred with the other temperate plant groups. Concerning non-arboreal pollen and spores, the high ratio of non-arboreal pollen shows steppe vegetation under dry climatic and/or grand condition. The high frequency of fern spores is inferred to indicate moist climate, though fern growth might have been affected by local conditions. Aquatics such as *Typha*, *Trapa* and Algae (*Pediastrum* and *Botryococcus*) indicate moist climate and/or existence of bogs and/or open water.

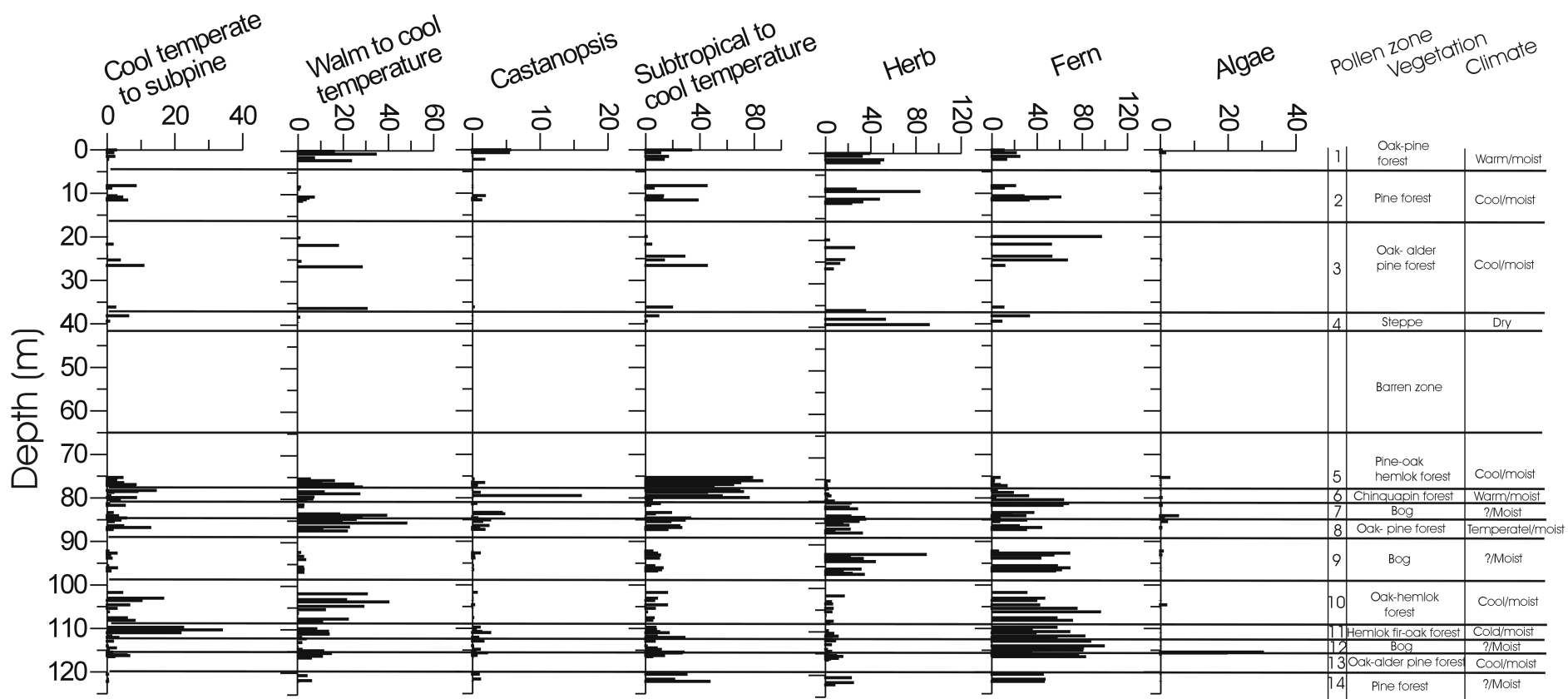


Fig. 3.7 Pollen results showing ratios of main components in the total pollen and spores along the depth.

Vegetation and climate of each pollen zone period was reconstructed as follows in ascending order (Fig. 3.7). Zone 14 period (120-123 m): The high percentage of *Pinus*, *Trapa* and fern show that pine forest was developed around open water under moist climate. Zone 13 period (115-120 m): Vegetation was open forest mainly composed of *Quercus*, *Pinus* and *Alnus*. High percentages of algae (*Botryococcus* and *Pediastrum*) and fern coexisted with *Typha* indicating the existence of open water under cool/moist climate. Zone 12 period (112-115 m): Low percentage of arboreal pollen and dominant fern show the expansion of bog under moist climatic conditions. Zone 11 period (109-112 m): This period was characterized by dominant *Tsuga*, *Abies* and *Quercus* coexisted by *Alnus*, *Ulmus* and *Juglans*. *Trapa* and dominant by fern occurred. Hemlock-fir-oak forest of cool temperate to subalpine was developed under cold/moist climate. Zone 10 period (99-109 m): Forest components were dominant *Quercus* and *Tsuga* coexisted by *Ilex*, *Alnus*, *Juglans* and *Ulmus*. Fern was also dominant. Oak hemlock forest was distributed under cool/moist climate. Zone 9 period (89-90 m): Low occurrence of arboreal pollen except for *Pinus* and occurrence of *Typha* and dominant fern indicate the expansion of bog under moist climate. Zone 8 period (84.5-89 m): *Quercus* and *Pinus* were dominant. At the same time *Castanopsis* occurred predominantly. *Trapa*, *Typha* and *Botryococcus* were contained. Oak-pine forest was established under temperate/moist climatic conditions. Zone 7 period (84-84.5 m): Arboreal pollen percentage was low. One of bog elements *Persicaria* and fern are yielded in high rate. Bog was developed under moist climate. Zone 6 period (78-81 m): This zone was characterized by high ratio of *Castanopsis* (16%), *Pinus* and fern. Chinquapin forest existed under warm/moist climate. Zone 5 period (65-78 m): *Pinus*, *Quercus* and *Tsuga* were dominant. Percentages of herb and fern were extremely low. Closed pine-oak-hemlock forest flourished under cool/moist climate. Zone 4 period (38-42 m): This zone was characterized by dominant non-arboreal pollen such as *Artemisia*, *Gramineae* and *Chenopodiaceae* which indicate dry climate. Vegetation might be steppe. Zone 3 period (17-38 m): Dominant *Quercus*, *Alnus*, *Pinus* and fern occurred with *Betula* and *Picea*. Oak-alder-pine forest prevailed under cool/moist climate. Zone 2 period (5-12 m): Forest consisted of dominantly *Pinus* with relatively predominant *Quercus* and *Tsuga*. *Gramineae*, *Persicaria* and fern occurred predominantly. Pine forest was distributed under cool/moist climate. Zone 1 period (0-5 m): *Quercus*, *Pinus* and *Gramineae* dominated with relatively high *Castanopsis*. Oak-pine forest prevailed under warm/moist climate.

### 3.3.2 Total Organic Carbon

Carbonate content was measured on samples from each horizon for a preliminary check. When the beds were thicker, several samples per horizon were taken. Few milligrams of

material was crushed and treated with HCl. The percentage of weight loss is treated as percentage of total carbonate in the sample. Carbonate content is <0.01% throughout the section. After treatment of the samples with HCl, the samples were dried out and TOC (total organic carbon) as well as TN (total nitrogen) were measured with an elemental analyser (Vario EL). The results of TOC (Fig. 3.8b) roughly show an anti-correlation with the magnetic concentration signal.

### 3.3.3 Magnetic parameters

Low field susceptibility measurements were done for all samples using a KLY-2 kappabridge (Agico). ARM was imparted with a 2G 615 device (maximum AF field 100 mT, biasing DC field 0.1 mT). After ARM acquisition, SIRM was induced with a pulse magnetiser (MMPM9), at a field of 2.0 T. Reverse IRM(-0.3T) was induced afterwards in a field of 300 mT. S-ratio was calculated from these measurements using the formula  $S = ((-IRM - 0.3T / SIRM) + 1) / 2$  (Bloemendal et al., 1992). Variations of the NRM, susceptibility and the laboratory imparted remanences (ARM, IRM, SIRM) show quite good correlation all along the section. The correlation strongly suggests that the magnetic mineralogy is mainly ferrimagnetic. The results are shown in Figure 3.8. Roughly high and low magnetic values are observed below the depth of 50m. The highest magnetic concentration signal is observed at the depth of 60m to 70m. Thus we may interpret higher magnetic concentration in terms of colder climate probably related to relatively higher magnetic content vice versa, a lower magnetic concentration signal and high amounts of hematite (lower S ratio) characterizes warmer climate (Reynolds, 1995) (Fig. 3.9). Based on the pollen data, it is observed that magnetic concentration signal is in tendency higher during cold/dry stages compared to warmer stages. It is also observed that the presence of higher coercivity phases is more significant for the samples with lower magnetic concentration.

Susceptibility can be correctly approximated by a second order symmetric tensor, which facilitates the measurements of anisotropy of magnetic susceptibility (AMS). The AMS is the physical property of rocks, used for determining the magnetic fabric and structural studies. (Owens and Bamford 1976, Hrouda 1982, Lowrie 1989 Rochette 1992). AMS arises due to the magnetic fabric of the sample, due to alignment of non-spherical particles of preferred orientations of crystallographic axes. AMS measurements are normally represented as an ellipsoid of magnetic susceptibility defined by the length and

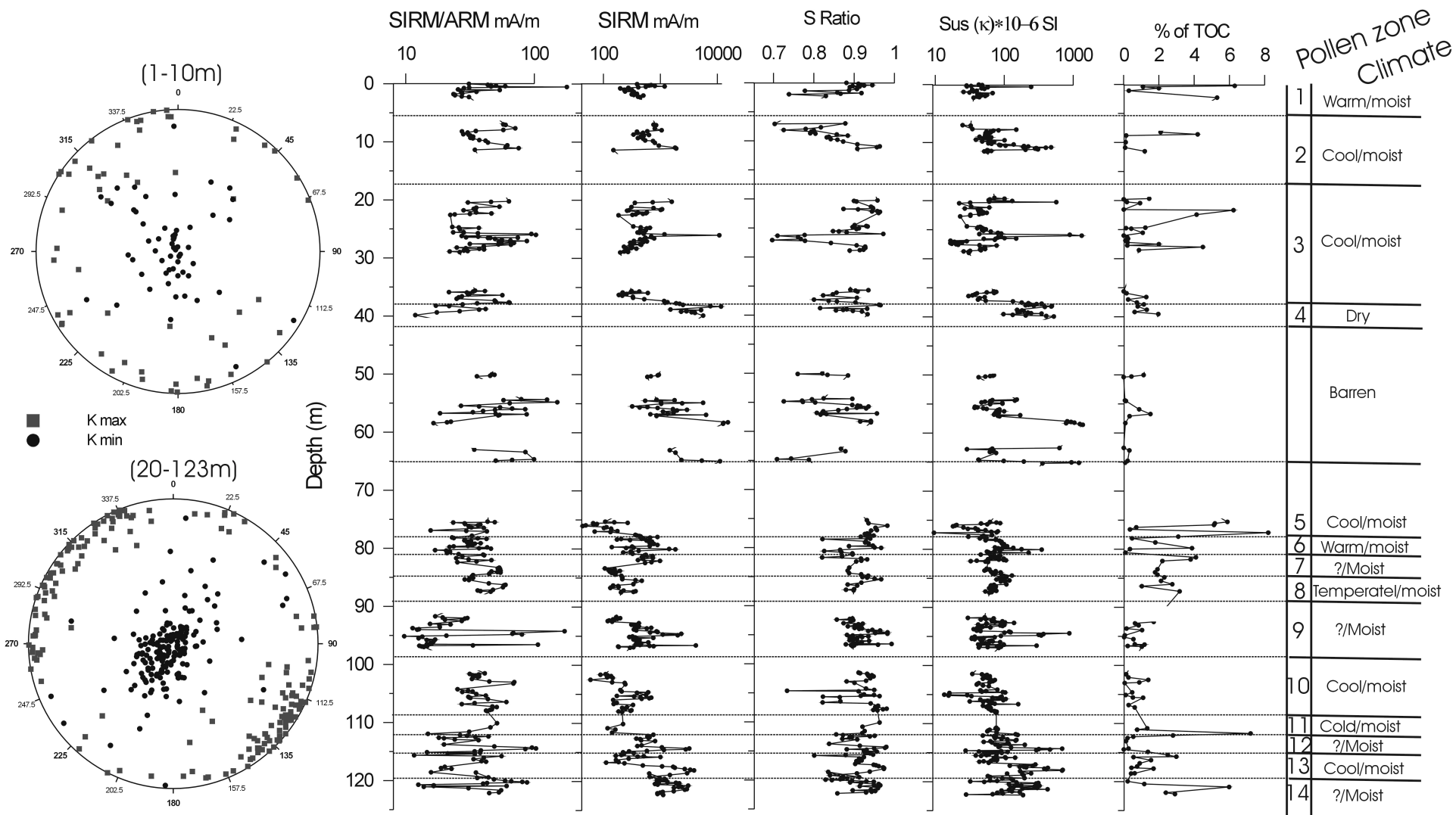


**Fig. 3.8 (a) Results of anisotropy of magnetic susceptibility from 0-10 m and 20-123 m. (b) Variations of magnetic and non-magnetic parameters and their correlation with the climate obtained from pollen record.**

orientations of the three principle axes,  $\kappa_1 > \kappa_2 > \kappa_3$  i.e, the three eigenvectors of susceptibility tensor.  $\kappa_1$  ( $\kappa_{\max}$ ) is maximum susceptibility which is the axis of easy magnetisation,  $\kappa_3$  ( $\kappa_{\min}$ ) is minimum susceptibility which is the axis of the hard magnetization,  $\kappa_2$  ( $\kappa_{\text{int}}$ ) relative to  $\kappa_1$  and  $\kappa_2$  which is used to define whether the fabric is characterised by a lineation (prolate) or a foliation (oblate). The anisotropy parameters most often used are the mean susceptibility  $K_m = (\kappa_1 + \kappa_2 + \kappa_3)/3$  and the standard anisotropy ratios  $L = \kappa_1 / \kappa_2$ ,  $F = \kappa_2 / \kappa_3$  and  $P = \kappa_1 / \kappa_3$  which are the lineation, foliation, and degree of anisotropy. The AMS ellipsoid is coaxial to the petrofabric, the  $\kappa_3$  axis is perpendicular to the bedding plane in sedimentary environments.

As the magnetic parameters are related to the depositional process, it is important to know the sediment depositional system and the direction of deposition. Here in our study we interpret AMS results mainly in terms of sediment flow direction More than 230 samples from various depths were measured on a KLY-2 kappabridge using 15 directions. The directions of maximum ( $\kappa_1$ ) and minimum axes ( $\kappa_3$ ) are plotted in Figure 3.8a. The direction of  $\kappa_3$  values which represent the bedding plane show a clearly better grouping in the bottom part (20 – 123 m) of the section than in the upper part (0 - 10m) of the section. The directions of  $\kappa_1$  shows a NW-SE lineation in the bottom part and is more scattered in the upper part. The sedimentary fabric is primarily influenced by the depositional system and stresses. The results illustrate high scatter in the upper part of the section, which is discussed further.

### 3.4 Discussion

Magnetostratigraphy reveals four polarity changes but only 9 samples represent the fourth (oldest) transition at the depth of 121m, out of which the bottommost 5 samples are consecutive. Further sampling could not be carried out as the formation is unexposed beyond this depth at the sampling area. Whether this transition is Cobb Mountain or the upper boundary of the Olduvai subchrone cannot be confirmed. Nevertheless, polarity stratigraphy together with amino acid dating result in a reasonable age model for the sampled section. Lithologically, finer grain beds are predominant in the lower part of the section (75-123 m), demonstrating that the lake was quite deep during this period. Also the lithology of drill cores of Sakai (2002) also show mostly fine grain sediments during this

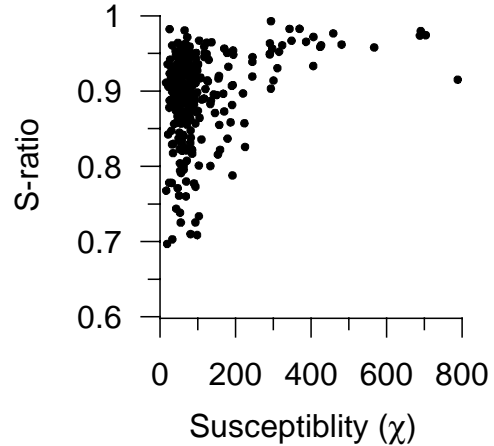


**Fig. 3.9 Cross plot between susceptibility and S-ratio**

period. It is worth to note that an unconsolidated sand bed of about 3 m (~ 0.9 Ma) rich in mica and tiny fossils was found at the depth of 68m (Fig. 3.2c). This bed is extensively distributed all over the lake (Katel et al., 1996), suggesting that the lake level decreased during this period. A highly weathered iron oxide layer in a silt bed (possibly limonite) with a thickness of ~ 1cm was found at the depth of 62 m also indicating the shallowness of the lake and the hydrolysis condition (Fig. 3.2b). Pollen analysis shows that significant dry climate prevailed at this depth, which will be discussed further. Sakai et al. (2002) concluded that the lake level started increasing after the sand bed deposition in the central part of the lake. But in our study area, sequential gravel and fine grained beds (mainly mud and clay) are observed after this sand bed deposition. The sudden change in the depositional system (derived from lithology) at ~0.8 Ma could be either due to a major climatic event or a strong tectonic stress from the Mahabharath lekh. The AMS results (will be discussed further) show that deposition of the fine grains are always in the same direction (NW) but this deposition is disturbed by the sudden input of the gravel beds from the southern part of the basin (Phulchoki group), which might be due to release of high tectonic stress. Also no gravel beds were reported in the drill core of JW-3 (Sakai, 2001). About 70 m thick gravel and debris (Itaiti Fm., not shown in the Fig. 3.2) overlying the sampled section suggest that the southern part of the lake has come to an extinct at this stage. Very fine grain size and good consolidation of the sediments below the depth of 105m suggest that the basin was deep and a relatively slow rate of deposition prevailed during this stage. The slow deposition could be interpreted either by a calm environment or because the sediment could not reach the southern part of the lake due to the upliftment of Mahabarath range. AMS shows that the maximum susceptibility axis is mainly NW to SE almost in all parts of the section, suggesting that the sediment flow direction was mainly from NW of the lake (for calm flow regime). This strongly suggests that the lake regained its usual sedimentation behaviour after sudden deposition of the gravel beds (mainly from the southern side of the lake). In the bottom part  $\kappa_{\min}$  directions are deviating slightly (~ 10°) from the vertical direction, which can be related to tilting after deposition. The northward tilting of about 5° to 10° of the formation (Fig. 3.2a) corresponds to the tilt of the  $\kappa_{\min}$  axis. The directions of the AMS of the topmost part of the section is more scattered which can be explained due to disturbance caused by tectonic stress after deposition. According to the rock magnetic results the softer component (magnetite) is more dominant where the magnetic concentration signal is higher. Higher concentration signal indicates colder stages in this case. The amount of TOC is directly proportional to existence of plant life at their respective depths. Whenever there is more vegetation, the erosion is relatively lower causing reduced erosion and less input of magnetic material into the lake. TOC and magnetic results show a rough anti-correlation supporting that the magnetic concentration signal is lower in warmer stages and higher in colder stages. The

magnetic results are not in point-to-point accordance with the pollen data (direct proxy) but in general they show a similar trend. Vegetation and climate was reconstructed using pollen (Fig. 3.7). During 5 to 14 periods bog appeared repeatedly especially distinct colder/moist climate than at modern Kathmandu Basin occurred during Zone 11 period. The vegetation was cool temperate to subalpine forest mainly consisting of *Tsuga*, *Abies* and *Quercus*. Warmer/moist climate occurred during Zone 6 and 1 periods. Vegetation was chinquapin forest and oak-pine forest respectively. Except for these periods climate was cooler and more moist than in the modern Kathmandu Basin. It might be caused by moist climate influenced by Indian monsoon and/or by dam up streams because of tectonic movement. The barren zone above might be explained by two factors. Firstly, climate was very dry, so growing of plants was restricted. Second, sediments of the barren zone are sand or pale colored silt, which do not contain any organic matter. It is assumed that the lake or bog reduced by inflow of coarse material from surrounding mountains by tectonic movement. Vegetation was destroyed and the basin became barren land. Afterwards steppe occurred in the basin during Zone 4 period. Vegetation, which shows drier climate, was found from Zone LK-9 in Member IV of Lukundol Formation (Igarashi et al., 1988, Yoshida and Igarashi, 1984.). Both dry periods might represent the same period.

### 3.5 Conclusions

- a) Magnetostratigraphy dates the section into ~ 0.75 – 1.1/1.8 Ma supported by amino-acid dating.
- b) AMS results reveal that a calm depositional environment existed below the depth of 70 m and major tectonic stress occurred during <0.8 Ma which was the cause of changes in depositional system of the lake.
- c) The magnetic parameters show a relatively higher concentration signal during colder periods and show a rough anti-correlation with the TOC results. Combining the interpretations of TOC, pollen, magnetic parameters we expect that the coldest and driest period occurred around 0.9 Ma.

## 4. General conclusions

As mentioned earlier, at SE Tibetan plateau and south of Chinese loess plateau very few palaeoclimatic records are obtained up till now. Heqing core fills this gap and turns out to be a unique continental archive for long-term palaeoenvironmental evolution. Calibrating ages of continuous sequences using  $^{14}\text{C}$ , magnetostratigraphy and wavelength model could be a promising technique. The ages obtained for Heqing core provides an optimal age frame in this area. Heqing core shows clearly the orbital cyclicities and regional events. Pollen records indicate strong temperate humid and cold dry periods documented by increased *Tsuga* and decrease of total tree pollen respectively. Magnetic mineralogy corresponds well with pollen. From pollen and magnetic mineralogy, temperate humid phases can be identified at 990-960 ka (strong indication), 800-780 ka (moderate), 690-670 ka (strong), 630-620 ka (moderate), 580-570 ka (moderate), 530-520 ka (weak), 450-420 (strong), 360-340 (strong), 215-200 (weak) and 65-35 ka (strong). A strong cold dry period is indicated at 160-110 ka. Surprisingly, the correlation coefficient (R) of susceptibility and carbonate shows a cyclic behaviour and demonstrates clear orbital cyclicities. Fuzzy c-means cluster analysis show a systematic grouping and each group represent a climatic pattern. The cyclic behaviour of carbonate and magnetic concentration parameters between 55 to 155 m (350 ka to 910 ka) and the concentration of maximum power between 350 ka to 800 ka (55 m – 145 m) of wavelet spectra demonstrates that the core is less controlled by regional climatic influence during this period. The decrease in rate of deposition above 65 m (~400 ka) may be due to weakening of monsoons or/and tectonic influences.

The features observed for Kathmandu basin are less significant than for the Heqing core. The section overlaps the time span between 700 ka to 1 Ma. The topmost 10 m clearly show a change in sedimentation regime, which might be contemporaneous with the temperate humid period of 800-780 ka seen in the Heqing core (Fig. 4.1)

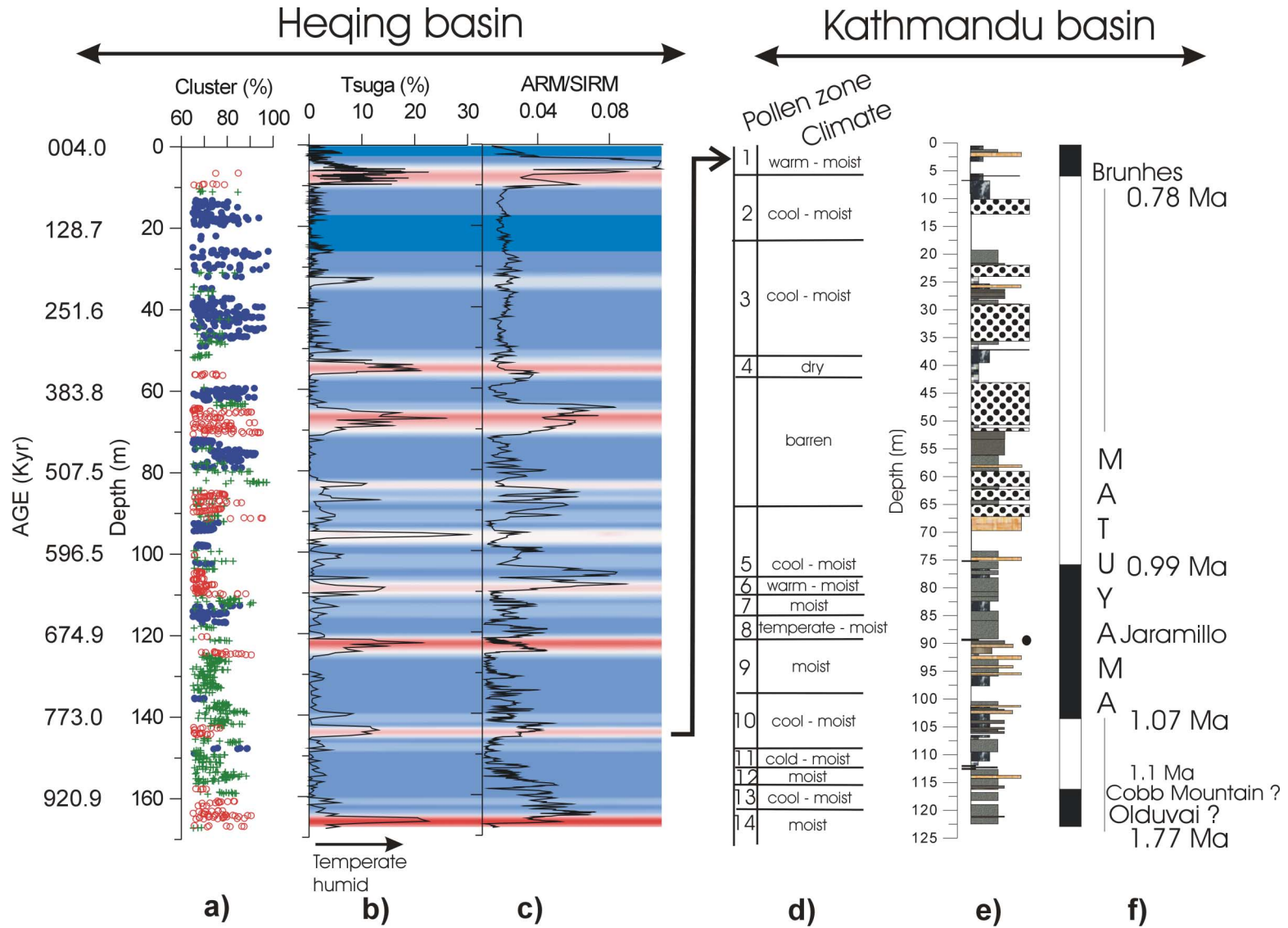


**Fig. 4.1** a,b,c represent cluster results (three cluster case), Tsuga and ARM/SIRM of Heqing basin. d,e,f are the climatic conditions along the depth derived from pollen, litholog, and geomagnetic polarity time scale of Kathmandu basin. The arrow shows the possible correspondence between the two basins.

## 5. References

- Banerjee, S. K., 1994. Contributions of fine particle magnetism to reading the global palaeoclimate record. *Jour of applied physics*, 75, 5925-5930
- Banerjee, S.K., Hunt, C.P. and Liu, X.M., 1993. Separation of local signals from the regional paleomonsoon record of the Chinese loess plateau: A Rock magnetic approach. *Geophysical Research Letters*, 20 (9), 843-846.
- Berger, A. 1988. Milankovitch theory and climate. *Reviews of geophysics* 26(4), 624-657.
- Berger, A., 1978. Long-term variations of daily insolation and Quaternary climatic changes. *J. of Atmospheric. Sciences* 35, 2362-2367.
- Berger, A., and Loutre, M.F., 1991. Insolation values for the climate of the last 10 million years. *Quat. Sci. Rev.*, 10, 297-317.
- Berger, A., Li, X.S., Loutre, M.F, 1999. Modelling northern hemisphere ice volume over the last 3 Ma. *Quaternary Science Reviews*, 18, 1-11
- Berger, A., Loutre, M.F., 1994. Astronomical forcing through geological time. *Spec. publs int. ass. Sediment.* 19, 15-24.
- Bleil, U. and Gard, G., 1989. Chronology and correlation of Quaternary magnetostratigraphy and nanofossil biostratigraphy in Norwegian-Greenland Sea sediments. *Geol. Rundschau*, 78, 1173-1187.
- Bloemendal, J., and Menocal, P., 1989. Evidence for a change in the periodicity of tropical climate cycles at 2.4 Myr from whole-core magnetic susceptibility measurements, *Nature*, 342, 897-900.
- Bloemendal, J., King, J. W., Hall, F.R., Doh, S.J, 1992. Rock magnetism of late Neogene and Pleistocene deep-sea sediments: Relationship to sediment source, Diagenetic processes and sediment lithology. *J. of Geophys Res.*, 97, 4361-4375.
- Burbank, D.W. and Johnson, G.D., 1982. Intermontane basin development in the past 4 Myr in the north-west Himalaya, *Nature* 298, 432-436.
- Burbank, D.W. and Johnson, G.D., 1983. The late Cenozoic chronologic and stratigraphic development of Kashmir intermontane basin, Northwestern Himalaya. *Palaeogeography, Palaeoclimatology, Palaeoecology* 43, 205-235.
- Cadet, D.L and Reverdin, G., 1981. The Monsoon over the Indian Ocean during Summer 1975. Part I: Mean Fields. *Monthly Weather Review* 109, 1, 148–158.
- Cadet, D.L., and Reverdin, G., 1981. Water vapor transport over the Indian Ocean during Summer 1975. *Tellus* 476-487.
- Cande, S.C. and Kent, D.V., 1995. Revised calibration of geomagnetic polarity timescale for the late Cretaceous and Cenozoic. *J. Geophys. Res.*, 100, 6093-6095.

- Clemens, S., 1999. An astronomical tuning strategy for Pliocene sections: implications for global-scale correlation and phase relationships. *Philos. Trans. R. Soc. London A, Math. Phys. Sci.* 357, 1949-1973.
- Clemens, S., Warren, P., Murry, D., Shimmield G., Weedon G. 1991. Forcing mechanism of Indian ocean monsoon. *Nature* 353, 720-725.
- Clemens, S.C. and Prell, W.L., 1991a. Late Quaternary forcing of Indian Ocean summer-monsoon winds: A comparison of Fourier model and general circulation model results. *J. Geophys. Res.* 96, 22683-22700.
- Clemens, S.C. and Prell, W.L., 1991b. One-million year record of summer-monsoon winds and continental aridity from the Owen Ridge (Site 722B), northwest Arabian Sea. *Ocean Drill. Program, Sci. Results*, 117, 365-388.
- Clemens, S.C., and Prell, W.L., 1990. Late Pleistocene variability of Arabian Sea summer monsoon winds and continental aridity: eolian records from the lithogenic component of deep-sea sediments. *Paleoceanography* 5, 109-145.
- Clemens, S.C., Murray, D.W., Prell, W.L., 1996. Nonstationary phase of the Plio-Pleistocene Asian monsoon. *Science* 274, 943-948.
- Clemens, S.C., Prell, W.L., Murray, D., Shimmield, G., Weedon, G., 1991. Forcing mechanisms of the Indian Ocean monsoon. *Nature* 353, 720-725.
- Cui, Y., Cerosub, K.L., Roberts, A.P., 1994. The effect of low-temperature oxidation on large multi-domain magnetite. *Geophys. Res. Lett.* 21, 757-760.
- Dekkers, M.J., 1997. Environmental magnetism: an introduction. *Geology and Mijnbouw*. 76, 163-182.
- Diggle, P.J., 1990. *Time series : A biostatistical introduction* (ed). Clarendon press, oxford.
- Doxler, A.W., Poore, R.Z., Burckle, L., 2003. Earth's climate and orbital eccentricity: the marine isotope stage 11 question (ed). *AGU Geophysical union Monograph*, 137, 240 pp
- Dunlop, D.J. and Özdemir, O., 1997. *Rock magnetism: fundamentals and frontiers*. Cambridge University Press, 573 pp
- Dunlop, D.J., 1972. Magnetic mineralogy of unheated and heated red sediments by coercivity spectrum analysis. *Geophysical soc. of royal astronomical soc.* 27, 37-55.
- Geiss, C.E. and Banerjee, S.K., 1997. A multiparameter rock magnetic record of the 1st glacial-interglacial palaeoclimate from south central Illinois, USA. *Earth and planetary scie. lett.* 152, 203-216.
- Hagelberg, T. and Mix, A.C., 1991. Long term monsoon regulators. *Nature* 353, 703-704.
- Hahn, D.G. and Manabe, S., 1975. The role of mountains in the South Asian monsoon circulation. *Journal of Atmospheric Sciences* 32, 1515-1541.

- Hastenrath, S., 1985. *Climate and Circulation of the Tropics*. Reidel, Dordrecht, The Netherlands.
- Hays, J.D., Imbrie, J., Shackleton, N.J., 1976. Variations in the Earth's orbit: pacemaker of the ice ages. *Science* 194, 1121-1132.
- Hearty, P.J., Kindler, P., Cheng, G., Edwards, R.L., 1999. A 20 m middle Pleistocene sea level highstand (Bermuda and the Bahamas) due to partial collapse of Antarctic ice. *Geology* 27, 375-378.
- Herbert, T. D., 1992. Paleomagnetic calibration of Milankovitch cyclicity in lower cretaceous sediments, *Earth Planet. Sci. Lett.* 112, 15-28.
- Hoffmann, V., 1992. Greigite ( $\text{Fe}_2\text{S}_4$ ). Magnetic properties and first domain observations, *Phys. Earth Planet. Inter.* 70, 288-301.
- House, M.R., 1985. A new approach to an absolute time scale from measurements of orbital cycles and sedimentary microrhythms. *Nature* 315, 721-725.
- Hrouda, F., 1982. Magnetic anisotropy of rocks and its application in geology and geophysics. *Geophys. surve.* 5, 37-82.
- Hsu, J., 1978. On the paleobotanical evidence for continental drift and Himalayan uplift. *Paleobotany* 25, 131-142.
- Hu, S., Appel, E., Hoffmann, V., Schmahl, W., Wang, S., 1998a. Gyromagnetic remanence acquired by greigite during static three axis AF demagnetisation. *Geophys. J. Int.* 134, 831-842.
- Hu, S., Appel, E., Wang, S., Wu., J., Xue, B., Wang, Y., Qian, J. & Xiang, L., 1999. A magnetic study on lacustrine sediments from Zoige Basin, Eastern Tibetan Plateau, China: Magnetostratigraphy and environmental implications, *Phys. Chem. Earth (A)* 24 (9), 811-816.
- Igarashi, Y., Yoshida, M., And Tabata, H., 1988. History of vegetation and climate in the kathmandu valley. *Proceedings of Indian national science academy* 54, A4, 550-563.
- Imbrie, J and Imbrie, K.P. 1979. *Ice ages. Solving the mystery* (ed). Enslow publ., short hills, NJ.
- Imbrie, J., Boyle, E.A., Clemens, S.C., Duffy, A., Howard, W.R., Kukla, G., Kutzbach, J and others., 1993. On the structure and origin of major glaciation cycles. 2. The 100, 000 year cycle. *Paleoceanography* 8 (6), 699-735.
- Katel, T. P., Upereti, B.N., Pokharel, G. S., 1996. Engineering properties of fine-grained soils of Kathmandu Valley, Nepal. *J. of Nepal Geol. Soc.* 13, 121-138.
- Kent, D.V., 1973. Post-depositional remanent magnetization in deep sea sediment. *Nature* 246, 32-34.
- Kent, D.V., 1995. Orbital tuning of geomagnetic polarity time-scales. *Phil. Trans. R. Soc. Lond. A* 357, 1995-2007.

- King, J.W., and Channell, J.E.T., 1991. Sedimentary magnetism, environmental-magnetism, and magnetostratigraphy. *Rev. of Geophys.* 29, 358-370.
- Kukla, G. and Clerk, V., 1996. Plio-Pleistocene megacycles: record of climate and tectonics, *Palaeogeogr. Palaeoclimat. Palaeoecol.* 120, 171-194.
- Kukla, G., Heller, F., Liu, X.M., Xu, T.C., Liu, T.S., An, Z.S., 1988. Pleistocene climates in China dated by magnetic susceptibility. *Geology* 16, 811-814.
- Laskar, J., Joutel, F., Boudin, F., 1993. Orbital, precessional, and insolation quantities for the Earth from -20 Myr to +10 Myr. *Astron. Astrophys.* 270, 522-533.
- Loutre, M.F., 2003. Clues from MIS 11 to predict future climate – A modeling point of view. *Earth and planetary sci. lett.* 212, 213-224.
- Lowrie, W., 1989. Magnetic polarity time scales and reversal frequency. Lowes, F.J (ed), *Geomagnetism and palaeomagnetism*, Kluwer academic publishers, Netherlands.
- Lowrie, W., Channell, J.E.T., Alvarez, W. 1980. A review of magnetic stratigraphy. *Investigations in cretaceous pelagic carbonate rocks. J. of Geophys. Res.* 85 (B7) 3597-3605.
- Malla, S. B., Shresta, A. B., Rajbhandari, S.B, Shresta, T. B., Adhikari, P. M., Adhikari, S. R., 1976. Flora of langtang and cross section vegetation survey (Central zone). *Bulletin of Department of medical plants, Kathmandu*, 269 pp.
- Malla, S.B., 1986. Flora of Kathmandu valley. *Bulletin of Department of medical plants, Kathmadu*.
- Manandhar,. N. P., 2002. *Plants and People of Nepal*. Alice Joyc, American Library Association 636 pp.
- Mayer, H. and Appel, E., 1999. Milankovitch cyclicity and rock-magnetic signatures of palaeoclimatic change in the Early Cretaceous Biancone Formation of Southern Alps, Italy. *Cretaceous Research* 20, 189-214.
- McManus, J.F. Oppo, D.W., Cullen, J.L., 1999. A 0.5 million-year record of millennial-scale climate variability in the north Atlantic. *Science* 283, 971-975.
- Mix, A.C., Pisias, N.G., Rugh, W., Wilson, J., Morey, A., Hagelberg, T.K., 1995. Benthic foraminifer stable isotope record from Site 849 (0-5 Ma); local and global climate changes. *Proceedings of the Ocean Drilling Program, Scientific Results*, 138, 371-412.
- Moribayashi. S and Maruo Y., 1980. Basement topography of the Kathmandu valley Nepal- An application of gravitational method to the survey of a tectonic basin in the Himalayas. *J. of Japan soc. Engineering Geol.* 21, 30-37.
- Morley, J.J., and Heusser, L.E., 1997. Role of orbital forcing in East Asian monsoon climates during the last 350 kyr: evidence from terrestrial and marine climate proxies from core RC14-99. *Paleoceanography*, 12, 483-494.

- Oches, E., William M., 1995. Amino acid geochronology applied to the correlation and dating of central European loess deposits. *Quaternary Science Reviews* 14, 7/8, 767-782.
- Ogg, J.G., 1995. Magnetic polarity time scale of the phanerozoic. Ahrens, T.J (ed): *Global Earth physics: A handbook of physical constants*, AGU reference shelf, 1, 240-270.
- Oldfield, F., 1991. Environmental magnetism: A personal perspective. *Quaternary Science Reviews* 10, 73-85.
- Oldfield, F., Hunt, A., Jones, M.D.H., Chester, R., Dearing, J.A., Olsson, L., Prospero, J.M., 1985. Magnetic differentiation of atmospheric dusts. *Nature* 317, 516-518.
- Owens, W. H., and Bamford, D., 1976. Magnetic, seismic and other anisotropic properties of rock fabrics *Philos. Trans. R. soc London*, ser A 283, 55-68.
- Poli, M., Thunell, R., Rio, D., 1999. Millennial-scale climate variability during marine isotope stages 11-12: the western northern Atlantic deep water record. AGU 1999 Fall meeting, Dec 13-17, 1999, San Francisco, California, *Eos, Transactions* 80 No 46, 1999, F556.
- Polunin, O. and Stainton, A., 1984. *Gentianaceae: In Flowers of the Himalaya*. Oxford University Press, Oxford. 265-275.
- Prell, W.L. and Kutzbach, J.E., 1992. Sensitivity of the Indian Monsoon to forcing parameters and implications for its evolution. *Nature* 360, 647-652.
- Prell, W.L., 1984a. Monsoonal climate of the Arabian Sea during the late Quaternary: a response to changing solar radiation. In Berger, A.L., Imbrie, J., Hays, J., Kukla, G., and Saltzman, B.. *Milankovitch and Climate* (Ed.) (Pt. 1): Dordrecht (D. Reidel), 349-366.
- Prell, W.L., 1984b. Variation of monsoonal upwelling: a response to changing solar radiation. In Hansen, J.E., and Takahashi, T., *Climatic Processes and Climate Sensitivity* (Ed.). *Geophys. Monogr., Am. Geophys. Union, Maurice Ewing Ser* 29, 48-57.
- Prell, W.L., Murray, D.W., Clemens, S.C., Anderson, D.M., 1992. Evolution and variability of the Indian Ocean Summer Monsoon: evidence from the western Arabian Sea drilling program. In Duncan, R.A., Rea, D.K., Kidd, R.B., von Rad, U., and Weissel, J.K. (Ed), *Synthesis of results from scientific drilling in the Indian Ocean*. AGU monograph 70, 447-469.
- Raymo, M.E., 1994. The Himalayas, organic carbon burial, and climate in the Miocene. *Paleoceanography* 9, 399-404.
- Raymo, M.E., Ruddiman, W.F., Froelich, P.N., 1988. Influence of late Cenozoic mountain building on ocean geochemical cycles. *Geology* 16, 649-653.
- Raymon, M. E. and Ruddiman, W. F., 1992. Tectonic forcing of late Cenozoic climate. *Nature* 359, 117-122.

- Reynolds, R. L. and King, J. W. 1995. Magnetic records of climate change. *Rev. Geophys.* 33, American Geophysical Union.
- Rocheete, P., Jackson, M., Aubourg, C. 1992. Rockmagnetism and the interpretation of anisotropy of magnetic susceptibility. *Rev. of Geophy* 30, 209-226.
- Ruddiman, W.F., 1997. *Tectonic Uplift and Climate Change* (Ed). Plenum Press, New York. 515 pp.
- Ruddiman, W.F., 1997. *Tectonic Uplift and Climate Change: New York (Plenum)* (Ed.).
- Ruddiman, W.F., Kutzbach, J.E., 1989. Forcing of late cenozoic northern hemisphere climate by plateau uplift in southern Asia and the American west. *J. of Geophys. Res.* 94, 18409-18427.
- Ruddiman, W.F., Raymo, M.E., Martinson, D.G., Clement, B.M., Backman, J., 1989. Pleistocene evolution: Northern hemisphere ice sheets and north Atlantic deep-water circulation. *Paleoceanography* 4, 353-412.
- Ruddiman, W.F., Raymon, M., McIntyre, A., 1986. Matuyama 41,000 year cycles; North Atlantic ocean and northern hemisphere ice sheets, *Earth Planet. Sci. Lett.* 80, 117-128.
- Sakai, H., Fujii, R., Kuwahara, Y., 2002. Changes in depositional system of the palaeo-Kathmandu lake caused by uplift of the Nepal lesser Himalayas. *J. of Asian Earth Sciences* 20, 3, 267-276.
- Sakai. H., 2001. Stratigraphic division and sedimentary facies of the kathmandu basin sediments *J. of Nepal Geol. soc.*, 25, 19-32.
- Sani, H.S., Waraich, R.S., Malhotra, N.K., Nagpaul, K.K., Sharma, K.K., 1979. Cooling and uplift rates and dating of thrusts from kinnaur Himachal Pradesh, Himalaya. *Himalayan Geology* 9, 546-567.
- Scherer, R.P. 1999. Quaternary collapse of the west Antarctic ice sheet: MIS 11 Yes but was it a unique event? AGU 1999 fall meeting, Dec 13-17, 1999, San Francisco, California, *Eos, Transactions* 80, 46, 1999, F556.
- Scherer, R.P., Aldahan, A., Tulaezy, K.S., Possderi, G., Gngelhardt, H., Kamb, B. 1998. Pleistocene collapse of the west Antarctic ice sheet. *Science* 281, 82-85.
- Schultz, H., Van Rad, U., Erlenkeuser, H., 1998. Correlation between Arabian Sea and Greenland climate oscillations of the past 110,000 years. *Nature* 393, 54-57.
- Schulz, M., and Mudelsee, M., 2002. REDFIT: estimating red-noise spectra directly from unevenly spaced paleoclimatic time series, *Computers and Geosci.* 28, 421-26.
- Schulz, M., Stattegger, K., 1997. SPECTRUM: Spectral analysis of unevenly spaced palaeoclimatic time series. *Computers and Geosci.* 23, 929-945.
- Schwarzacher, W., 1993. Cyclostratigraphy and the Milankovitch theory, *Developments in Sedimentology* 52, Elsevier Amsterdam, 225 pp.

- Stöcklin, J., and Bhattarai, K. D., 1981, Geological map of Kathmandu area and central Mahabharat Range (1:25,0000). Department of Mines and Geology, His Majesty's government of Nepal.
- Tang, J., Myers, M., Bosnick, K.A., Brus, L.E. 2003. Magnetite Fe<sub>3</sub>O<sub>4</sub> nanocrystals: spectroscopic observation of aqueous oxidation kinetics. *J. Phys. Chem. B* 107, 7501-7506.
- Thomson, R., Oldfield, F., 1986. *Environmental Magnetism* (Ed). Allen and Unwin, London, UK, 235 pp.
- Thouveny, N., De Beaulieu, J., Bonifay, E., Creer, K.M., Gulot, J., Icole, M., Johnson, S., Jouzel, J., Reille, M., Williams, T. & Williamson, D., 1994. Climate variations in Europe over the past 140 kyr deduced from rock magnetism, *Nature* 371, 503-506.
- Torrence, C., and G. P. Compo, 1998. A practical guide to wavelet analysis. *Bull. Amer. Met. Soc.* 79, 61-78.
- Verosub, K.L and Roberts, A.P., 1995. Environmental magnetism : Past, present, and future. *J. of Geophys. Res.* 100 B2, 2175-2192.
- Verosub, K.L. & Banerjee, S.K., 1977. Geomagnetic excursion and their paleomagnetic record, *Rev. Geophys. Space Phys.* 15, 145-155.
- Wang, S.M., Hu, S., Appel E., Ma, X.H., Hoffmann, V., Sun, Z.M., Yang, X.D., Ma, Y. Pan, H.X., 1999. Incursion of sea water into Gucheng lake detected by magnetic, biologic and chemical data, *Phys. Chem. Earth (A)* 24/9, 805-809.
- Wigley, T.M.L., 1976. Spectral analysis and the astronomical theory of climatic change, *Nature* 264, 629-631.
- Williams, D.F., Peck, J., Karabanov, E.B., Prokopenko, A.A., Kravchinsky, V., King, J., Kuzmin, M.I., 1997. Lake Baikal record of continental climate response to orbital insolation during the past 5 million years. *Science* 278, 1114-1117.
- Yang, X., Wang, S., Tong, G., Jiang, X., 2000. Vegetational and climatic responses to tectonic uplift in the Heqing Basin of Yunnan Province during the past 1.0 Ma. *Acta Micropaleontologica Sinica* 17(2), 207-217.
- Yoshida, M and Gautam, P., 1988. Magnetostratigraphy of Plio-Pleistocene lacustrine deposits in the Kathmandu valley central Nepal. *Proceedings of Indian National Science Academy* 54, A3, 410-417.
- Yoshida, M. and Igarashi, Y., 1984. Neogene to Quaternary lacustrine sediments in the Kathmandu valley, Nepal. *J. Nepal Geol Soc.*, 4, 73-100.

**Name** : Srinivasa Rao

**Surname** : Goddu

**Date of Birth** : 23-12-1973

**Place of Birth** : Visakhapatnam, India

**Nationality** : Indian

**Education** : **1980 – 1992** Schooling and Intermediate in Visakhapatnam, Andhra Pradesh, India.

**1992 – 1995** Bsc (Mathematics, Physics and Chemistry), Mrs A.V.N College, Visakhapatnam.

**1995 – 1998** Msc (Tech) Geophysics, Department of Geophysics, Andhra University, Visakhapatnam.

**1998 – 2000** Junior Research Fellow, Indian Institute of Geomagnetism, Magnetic observatory, Visakhapatnam.

**2001 - 2003** Scientific employee of Eberhard-Karls-University Tübingen. Working in a project (Himlakes AP-34/15-1) funded by DFG, Germany.

**1/2001 – Present** PhD student, in Institute of Geosciences, University of Tuebingen under the supervision of Prof. Dr. Erwin Appel.